



Università degli Studi di Padova

DIPARTIMENTO DI INGEGNERIA INDUSTRIALE
Corso di Laurea Magistrale in Ingegneria Aerospaziale

TESI DI LAUREA MAGISTRALE

**Direct numerical simulation of the flow inside devices for
hydraulic plastics separation**

Laureando:
Marco Magli
Matricola 1152487

Relatore:
Prof. Francesco Picano
Correlatori:
Prof. Luca Brandt
Dott. Marco Edoardo Rosti

..Extensive use of plastic per se is not the sole cause of the problem, it is the decision made about how to design, use and dispose of plastic items that result in waste and litter. Plastic pollution is caused by human actions.

Richard Thompson

Professor in Marine Science

Riassunto del lavoro

Al giorno d'oggi, vi sono molti problemi a livello globale che devono essere gestiti in maniera corretta. Tra i temi più attuali vi rientra l'eco-sostenibilità e le condizioni di vita sempre peggiori che bisogna sostenere. Il tasso di crescita della popolazione sta diminuendo negli anni, ma rimane comunque positivo e ciò fa sì che la popolazione mondiale continui ad aumentare. Di conseguenza anche la quantità di rifiuti che viene generata quotidianamente è in aumento. Bisogna perciò ricorrere a tecniche di gestione e riciclaggio dei rifiuti sempre più efficienti, per evitare di arrivare ad un collasso.

Una nuova tecnica di riciclaggio

Di tutti i materiali che vengono raccolti per essere smaltiti, una rilevante quota è occupata dalle materie plastiche. Esse hanno i più disparati usi e molti vantaggi, dall'uso domestico all'uso industriale. Di contro, sono inquinanti se lasciate nell'ambiente e devono essere gestite in maniera opportuna. Infatti con il termine *plastica* si intende la generica famiglia dei polimeri, costituita da composti diversi tra loro come *PET*, *PVC* e *PC*. Questi vengono raccolti indistintamente in un ammasso omogeneo, ma il processo di riciclo viene attuato per singolo tipo di materiale, e quindi la massa di plastica dev'essere suddivisa nei singoli polimeri.

Processi per fare ciò, ce ne sono diversi e più o meno efficienti, come processi meccanici, elettrostatici o ottici. All'*Università La Sapienza di Roma*, con lo scopo di effettuare tale *separazione della plastica*, è stato progettato e sviluppato un dispositivo che gestisce un flusso di acqua con immerse particelle di polimeri differenti, visibile in figura 2.1 a pagina 12. Tale apparato è formato da due parti identiche, costituite da una ripetizione di 8 semi-cilindri. Esse vengono unite sfalsate tra loro, come si vede nell'immagine (b) sempre di figura 2.1 a pagina 12, per avere una sezione orizzontale di ingresso L_1 , diversa da quella di uscita L_2 . Da quest'unione si generano otto identiche camere, dove il flusso, in ciascuna, entra dal lato sinistro ed esce da quello destro. Tale *flusso multifase* è introdotto da 8 fori di ingresso, ed esce dal

dispositivo da altrettanti fori di uscita, alcuni dei quali però possono essere mantenuti chiusi per poter variare le condizioni di deflusso.

Il flusso è composto da due fasi. La prima è costituita da sola acqua, mentre la seconda è composta da particelle di *PVC*, *PET* e *PC*, di forma variabile tra granulare, semi-cilindrica, a fiocchi o casuale. La dimensione del loro diametro è variabile tra i 2.5 mm e i 4.5 mm .

Dato che il dispositivo è stato creato in plexiglas, sono state scattate delle istantanee del movimento delle particelle lungo la serpentina. Inoltre, immergendo nel fluido anche dei *tracer*, è stato possibile rappresentare anche il movimento del fluido. Infatti, attraverso la tecnica *Particle Tracking Velocimetry*, è stato possibile risalire all'andamento delle velocità di entrambe le fasi del flusso reale, e fare delle relative considerazioni.

Da questi risultati ottenuti sperimentalmente, è cominciato il lavoro di questa tesi. L'obiettivo è stato infatti quello di realizzare un modello numerico che ben rappresenti il fenomeno reale, per poi andare a variare alcuni parametri del problema, con lo scopo di caratterizzare in modo analitico il comportamento sia della fase liquida che di quella solida.

Il modello numerico

Il fenomeno illustrato si sviluppa tridimensionalmente, e per modellarlo è stato utilizzato un modello numerico già sviluppato. Il codice di calcolo che lo implementa, realizzato con il linguaggio *Fortran*, è stato sviluppato in una collaborazione tra l'*Università degli Studi di Padova*, *KTH Mechanics* di Stoccolma e *TU-Delft*, iniziata nel 2011. Tale software può utilizzare fino a 10 000 processori in parallelo. Attraverso l'*Immersed Boundary Method* è possibile ottenere un'elevatissima accuratezza nella modellazione di flussi multi-fase. Le equazioni di Navier-Stokes vengono discretizzate in una griglia Euleriana ed implementate attraverso l'uso di una *Particle Resolved - Direct Numerical Simulation (PR-DNS)*. La discretizzazione invece della fase solida, è attuata attraverso una griglia Lagrangiana mobile, solidale con le particelle. Ulteriori dettagli si trovano in Ardekani 2019.

Per poter simulare il fenomeno, si è implementata la geometria nel codice andando a definire quali punti della griglia cartesiana possono essere percorsi dal flusso, e sui quali invece vi è il solido di parete. Le equazioni implementate sono adimensionali e come unità di misura, viene usato il diametro di particella. Scegliendo di simulare particelle reali con diametro di 3 mm , si sono assegnate le due dimensioni del dominio raffigurate in figura 2.1 a pagina 12, riscalandole le dimensioni reali del dispositivo. Per definire la lunghezza della terza dimensione si sono effettuate alcune simulazioni di partenza, con un valore arbitrario di tale dimensione. Attraverso uno studio di correlazione

della velocità orizzontale, è stata assegnata al dominio una profondità pari a 8 volte il diametro di particella.

Dopo questa fase preliminare si è potuto procedere a lanciare una serie di simulazioni.

Analisi svolte

Una volta che le dimensioni del dominio sono state definite, si sono potute lanciare le simulazioni di interesse. Con il tipo di fenomeno in esame, i parametri interessanti da esaminare sono diversi. A causa però, dell'elevato costo computazionale che possiede una *DNS*, il campo di studio è stato ristretto a due aspetti importanti, utili per iniziare i test numerici su un problema noto solo sperimentalmente. In particolare, si sono esaminate tre differenti geometrie visibili in figura 4.1 a pagina 50, differenziabili in base al valore del rapporto $\frac{L_1}{L_2}$. Per ognuna, sono state lanciate diverse simulazioni, ognuna con una densità diversa delle particelle: $1050 \frac{kg}{m^3}$, $1100 \frac{kg}{m^3}$, $1150 \frac{kg}{m^3}$, $1200 \frac{kg}{m^3}$, $1250 \frac{kg}{m^3}$.

Da ciascuna simulazione si ottengono infine, ad intervalli di step prefissati, sia i *campi istantanei* delle velocità lungo i tre assi principali, sia le *posizioni* del centro di ciascuna particella. Su questi risultati si sono fatte delle analisi attraverso la creazione di alcuni algoritmi, sia in codice *Fortran* che in linguaggio *Matlab*.

Nella prima parte di questo lavoro, per ogni geometria si è lanciata una simulazione con la sola fase fluida. Da questa, si sono mediati i campi istantanei nel tempo e nella direzione perpendicolare alla sezione, ottenendo i campi mediati per le velocità, mostrati in figura 4.4 a pagina 57. La media, effettuata in tale modo, è stata fatta anche per tutte le successive medie. Si è provveduto poi a rappresentare, nelle figure 4.6 a pagina 61 e 4.7 a pagina 62, gli *stress di Reynolds* medi e l'*energia cinetica turbolenta*.

Durante l'esecuzione di queste tre simulazioni, è stato monitorato il gradiente di pressione per ciascuna. Esso infatti all'inizio risulta avere un andamento casuale, per poi assestarsi con oscillazioni intorno ad un valore medio, figura 4.8 a pagina 65. Quando ciò avviene, il flusso si è sviluppato, e si possono perciò immettere le particelle nel flusso.

Per le simulazioni con particelle, sono state inizializzate, in posizioni arbitrarie, 100 particelle della stessa densità. Per ogni densità, e per ogni geometria, si è lanciata una diversa simulazione. Per poter ottenere risultati confrontabili, le si sono fatte girare finché il tempo simulato di ciascuna fosse circa lo stesso e pari a 35s.

Si è fatta una prima media delle velocità della fase fluida, in figura 4.9 a

pagina 66, per poterla confrontare con il flusso a singola fase. Da questo confronto è risultato che il fluido si comporta mediamente allo stesso modo, e quindi non viene influenzato dalle particelle in maniera rilevante. Dopodiché è stato esaminato il comportamento delle particelle sotto diversi aspetti.

Per tutte le densità e geometrie, si sono raffigurate, nelle figure 4.10 a pagina 68, 4.11 a pagina 68 e 4.12 a pagina 69, le traiettorie di tutte le particelle, lungo 5 camere. In questo modo si è potuto osservare qualitativamente che al decrescere del rapporto $\frac{L_1}{L_2}$, la camera diventa meno capace di fermare le particelle, ed esse tendono a fluire nelle camere successive. Per la geometria con $\frac{L_1}{L_2} = 2$, si nota una grande differenza nel comportamento delle particelle al variare della densità. Infatti particelle più pesanti, tendono a sedimentarsi nelle prime camere. Tale differenza si perde però nelle altre due geometrie.

Per comprendere efficacemente il comportamento delle particelle, si è poi raffigurato, in figura 4.13 a pagina 71, la traiettoria di una sola particella per tutti i casi simulati. Oltre alle differenze appena affermate, si sono potute delineare più chiaramente due zone di ricircolo in ogni camera, di dimensione più o meno grande, che influiscono sulla sedimentazione della fase solida.

Dopodiché si sono andate ad eseguire delle analisi quantitative sui dati ottenuti dalle simulazioni.

Controllando l'ultima camera in cui ciascuna particella era posizionata a fine simulazione, è stato possibile realizzare degli istogrammi che evidenziano la sedimentazione delle particelle in ogni camera. Per sole tre densità, allo scopo di chiarezza visiva, si è rappresentata la percentuale di particelle intrappolate rispetto al totale che entra nella camera. Questi istogrammi sono visibili nelle figure 4.14 a pagina 73, 4.15 a pagina 73 e 4.16 a pagina 74. Si possono notare, sotto un altro punto di vista, i comportamenti già riassunti. Per la geometria con rapporto $\frac{L_1}{L_2} = 2$, molte particelle si sedimentano nelle prime camere, e ciò aumenta all'aumentare della densità. Tale andamento è meno marcato per la geometria con rapporto $\frac{L_1}{L_2} = 1$ e le particelle riescono ad avanzare maggiormente. Infine per la geometria con rapporto $\frac{L_1}{L_2} = 0.5$, l'effetto della differenza di densità si perde, e molte particelle riescono ad arrivare fino all'ultima camera, ed anche ad uscire dal condotto simulato.

Successivamente si sono andati a fare dei confronti dal punto di vista statistico. Si sono raffigurate le *Probability Density Functions (PDF's)* della velocità orizzontale delle particelle, per ogni geometria e per la minore e maggiore densità, figure 4.17 a pagina 75, 4.18 a pagina 76 e 4.19 a pagina 76. Si sono creati degli intervalli di velocità di 0.5 nel range tra la minima e la massima velocità riscontrata, e si sono conteggiate le occorrenze delle velocità del centro di tutte le particelle, per tutti gli istanti di tempo salvati durante la simulazione.

Si nota come per la densità maggiore le velocità ricadano maggiormente in un intorno dello zero. Significa perciò, che lungo il deflusso, tendono a fermarsi in una delle camere, e quindi la velocità media tenderà ad annullarsi sempre di più, se si continuasse a far girare le simulazioni. Tale effetto si perde però per la geometria con rapporto $\frac{L_1}{L_2} = 0.5$, dato che le due distribuzioni risultano essere molto simili.

Andando ad integrare, in maniera discretizzata, la distribuzione di probabilità, nell'intervallo di velocità considerato, si ottiene un'unico valore di velocità media associabile a ciascuna combinazione *geometria-densità*. Questo è un modo veloce per classificare le diverse geometrie in base all'efficienza di separazione. Più tale velocità sarà elevata, più vuol dire che le particelle continuano a fluire nel condotto non sedimentandosi. Andando a dividere la lunghezza di una camera per tale velocità, si ottiene il *tempo di stazionamento* medio per una data combinazione. Maggiore è tale valore, maggior tempo le particelle stazioneranno nelle diverse camere.

Per effettuare un confronto delle probabilità, si sono raffigurate anche le *PDF's* delle velocità orizzontali della fase fluida, figure 4.20 a pagina 77, 4.21 a pagina 78 e 4.22 a pagina 78. Si nota come la distribuzione non sia influenzata in modo evidente né dalla densità e né dalla geometria considerata.

Infine, si sono andati a mediare nel tempo, i campi istantanei di velocità delle particelle ottenendo l'andamento medio in figura 4.23 a pagina 81. Anche qui per ogni geometria si è assunta la densità minore e quella maggiore. Si è osservata una distribuzione omogenea delle particelle in tutto il dominio. Si nota solo una ristretta zona dove non c'è mai transizione di particelle. Essa inoltre aumenta al calare del rapporto $\frac{L_1}{L_2}$.

Con questo lavoro si è potuto innanzitutto, convalidare il modello numerico confrontandolo con i risultati dell'esperimento reale. Dopodiché si sono andati ad evidenziare e caratterizzare alcuni comportamenti che avvengono al variare della densità e della configurazione della geometria.

Su queste basi, potranno essere svolte ulteriori analisi, dato che i parametri che possono essere variati sono molti. In particolare si può affermare che una geometria con rapporto $\frac{L_1}{L_2} = 2$, è efficiente e ben funzionante. Future simulazioni possono utilizzare geometrie con rapporto in un intorno di tale valore. Dopodiché, si potrebbe ad esempio passare a simulare particelle non sferiche e con un diametro maggiore o minore.

Grazie all'uso di una *DNS*, si possono perciò simulare fenomeni reali in modo molto preciso e dettagliato. Risulta perciò essere uno strumento molto valido per scopi di ricerca.

L'insieme di tutte queste combinazioni, simulate in questo lavoro e che potranno essere testate in futuri lavori, potrà perciò andare a simulare in ma-

niera sempre migliore il fenomeno reale. Tali studi, potranno quindi portare ad un miglioramento del dispositivo, per poter separare i diversi componenti polimerici in modo più distinto.

Abstract

Nowadays, recycling is a must and when some products are used up, they become waste. A great part of this is plastic waste, that causes pollution, and environmental degradation. When they arrive in the recycling plant, they are split out in different types as *PVC*, *PET*, or *PC*. To make it possible, some processes, more or less onerous, have to occur. An innovative device developed at the *Sapienza - University of Rome*, carries out the separation of the plastics through a fluid dynamics process.

These polymers are chopped and they are immersed in water, this mix is a multiphase flow. The shape of the device used is a serpentine and the mixed fluid flows around these curves. At the end of this apparatus, one type of plastic is yet immersed in the flow, while the other one is settled in the chambers.

The purpose of this thesis is, first of all, to create a working numerical fluid dynamics simulation that models this phenomenon. This is possible through the use of an existent code, which has been adapted to this problem. With this work, some parameters of the system have been changed, which are the geometry of the chamber and the density of the particles. With several simulations, different behaviours of the multiphase flow turn out. The different geometries, that have been simulated, are characterized by a ratio between two lengths, that identifies a certain configuration. The efficiency of the chamber moves with this ratio, and the greater it is, the more effective the plastics separation becomes.

Considering efficient geometry, as well as for density, the trend of efficiency is monotonic. Particles with greater density are more easily settled in the chambers. Lighter particles continue to flow into some other chambers, but almost all the particles are trapped in the device.

With the numerical model created and verified in this work, some other aspects of this phenomenon have to be studied. Much more simulations will be done, in order to better understand the different behaviours of the flow and improve the existent device.

Acknowledgements

First of all, I would like to thank my thesis main advisor, Prof. Francesco Picano of the Department of Industrial Engineering at the University of Padova. When I went into his office to ask for a thesis argument, to develop abroad, he gave me several interesting options. Furthermore, he was always available to answer any question in a fast and detailed way, with his dedication to the fluid dynamics.

Then, I would like to thank Prof. Luca Brandt of the Department of Mechanics at the Royal Institute of Technology. He welcomed me in his research team, giving me a workstation and some initial advice to promptly start my work.

I would also like to acknowledge Dott. Marco Edoardo Rosti of the KTH Mechanics department. With his passion and expertise, he helped me step by step to understand the code and to address my analyses in the right way. Also, thanks for his patience in regards to my many questions and doubts, which I expressed to him almost every single day.

Computer time provided by SNIC (*Swedish National Infrastructure for Computing*) is also gratefully appreciated.

Now, I would like to thank other people who have been fundamental to my work in these past several years. Most importantly, thanks to my parents who have always supported and encouraged me, in all my choices. With their help, I was able to follow my passion in every aspect of life. Another person whose support I like to recognize is my girlfriend for her motivation and for always being there for me. Then, I also must thank her family for accepting me into their family. Moreover, I would like to thank all these people for the help and support for this last difficult year.

Thanks to my extended family and some friends that were there in all these years. In particular, thanks to University buddies and to a friend who has always been there, and he supported me in this last period.

Finally, thank anyone who knows me,

Marco Magli

Contents

1	Introduction	1
1.1	Recycling and partition	2
1.2	The numerical model	3
1.3	Turbulence in multiphase flows	4
1.4	Analyses	8
2	Plastic separation	9
2.1	The duty to separate	9
2.2	The separation device	12
2.3	Functioning	13
2.4	Analysis	18
2.5	Results	21
2.6	Conclusions	23
2.7	Next works	24
3	IBM and the numerical model	25
3.1	The complexity of fluid dynamics	25
3.2	Numerical approaches	26
3.3	Multiphase flows	28
3.3.1	Preliminary introductions	28
3.3.2	Slurry transport	30
3.3.3	Properties of the phases	30
3.4	IBM	38
3.4.1	The Navier-Stokes equations	39
3.4.2	The equations of the model	41
3.4.3	Volume penalization	43
3.4.4	Discrete forcing method for moving particles	45
4	Analyses	49
4.1	Setup of the model	49
4.1.1	Configuration model	49

4.1.2	Simulations parameters	54
4.2	Single-phase flow	55
4.2.1	Mean velocities	56
4.2.2	Reynolds stress and kinetic energy	59
4.3	Multiphase flow	64
4.3.1	Pressure gradient	64
4.3.2	Fluid phase	65
4.3.3	Particles tracking	67
4.3.4	Tracking of one particle	70
4.3.5	Particles settling	72
4.3.6	Statistical comparisons	74
4.3.7	Solid phase	80
4.4	Summary	82
5	Conclusions	83
	Bibliography	85

List of Figures

1.1	Comparison between laminar and turbulent flow	6
1.2	Time variation of the turbulent velocity of a fixed point	7
2.1	Separation device and characteristic dimensions	12
2.2	Configuration of the experiment with all the devices	16
2.3	Real image of a chamber and binarization process	19
2.4	Module of the average flow velocity in all the chambers	20
2.5	Horizontal and vertical velocities, and turbulent kinetic energy in chamber C3	21
2.6	Percentage of plastic particles, settled in different chambers and expelled from the device	22
2.7	Trend of horizontal and vertical velocity at the input of cham- ber C2	23
3.1	No filtering and different filtering of a LES simulation	28
3.2	Simplified example of a homogeneous liquid-solid flow	30
3.3	Graph of the zone of dilute and dense flow for glass particles in an air flow	35
3.4	Forces and pressure acting on a infinitesimally small moving fluid element	40
3.5	Schematic representation of a discretized multiphase flow	43
3.6	Schematic representation of a staggered grid	44
4.1	Representation of three different geometries used in flow sim- ulations, with different ratio $\frac{L_1}{L_2}$	50
4.2	Correlation coefficient graphs for the three points of each ge- ometry	53
4.3	Mean field of the velocity v and w , for the geometry with $\frac{L_1}{L_2} = 2$. Adapted from Moroni, Lupo, et al. 2017	56
4.4	Mean fields for the velocities v and w for the three geometries analysed	57

4.5	Turbulent kinetic energy for the case #2 and #7 in Moroni, Lupo, et al. 2017	60
4.6	Components τ_{22} and τ_{33} of the Reynolds stress tensor	61
4.7	Components τ_{32} and turbulent kinetic energy	62
4.8	Trend over time of the pressure gradient for the three geometries	65
4.9	Mean fields for the velocities v and w of the fluid phase, for the three geometries analysed	66
4.10	Particle trajectories of different densities, in the geometry with $\frac{L_1}{L_2} = 2$	68
4.11	Particle trajectories of different densities, in the geometry with $\frac{L_1}{L_2} = 1$	68
4.12	Particle trajectories of different densities, in the geometry with $\frac{L_1}{L_2} = 0.5$	69
4.13	For each geometry, the trajectory of only one particle is tracked for all the five density.	71
4.14	Number and percentages of settled particles in the geometry with $\frac{L_1}{L_2} = 2$	73
4.15	Number and percentages of settled particles in the geometry with $\frac{L_1}{L_2} = 1$	73
4.16	Number and percentages of settled particles in the geometry with $\frac{L_1}{L_2} = 0.5$	74
4.17	PDF's of the particles velocities in the geometry with $\frac{L_1}{L_2} = 2$	75
4.18	PDF's of the particles velocities in the geometry with $\frac{L_1}{L_2} = 1$	76
4.19	PDF's of the particles velocities in the geometry with $\frac{L_1}{L_2} = 0.5$	76
4.20	PDF's of the fluid velocities in the geometry with $\frac{L_1}{L_2} = 2$	77
4.21	PDF's of the fluid velocities in the geometry with $\frac{L_1}{L_2} = 1$	78
4.22	PDF's of the fluid velocities in the geometry with $\frac{L_1}{L_2} = 0.5$	78
4.23	Average v -velocities of the solid phase for the three different geometries and for different densities	81

Chapter 1

Introduction

Despite the growth rate of the world population is decreasing, however, it remains positive. This means that the number of inhabitants of our planet is constantly increasing. This rapid growth creates a strong environmental impact and life conditions less and less tolerable. In fact, the dossier presented to the *United Nations* in 2015 and drafted by the former prime minister of New Zealand established that 2030 will be the last year to stop the climate changes and to save the Earth. Therefore, the critical conditions are only getting worse. Fortunately, in the last years, humankind has become aware of the possible actions that should be taken in order to restore a livable environmental situation. This has led to creation of more eco-friendly products and ideas. Nevertheless, these products, once consumed, will become wastes and they will have to be managed in some way. For this reason, the way each part of the entire *life-cycle* of a product is performed, becomes fundamental, from the production to the disposal.

The chemical product that brought great innovation but has contributed enormously to the environmental pollution, is the family of polymers. In fact, without them, for example, the weight of the cars and air resistance cannot be reduced. Supply and demand for this type of product are increasing. This is also determined by the fact that engineering tends to increase the use of these materials for more efficient solutions. In fact, in Mac Arthur et al. 2016, has been asserted that in 2014 the annual world production of plastic has reached 310 million tons.

The huge amount of these products on the market indicates that there must be more efficient ways to dispose of them. The further problem is that plastics are not all of the same types and only a few of them can be recycled while others cannot. During the rubbish collection, the different types of products are merged between them. Firstly, different plastics must be separated and only then, recycling can begin.

1.1 Recycling and partition

With the recycling process, the wastes can be considered as a resource and they can become an alternative to virgin material or traditional fuels. In fact, the recycling and the energy recover is preferable to land-filling. These processes allow replacing of raw material and traditional fuel. However, they are feasible only when strict risk control is guaranteed.

One of the best considered solutions to recycle is a mechanical process. It can produce high-quality products that can substitute virgin polymers or other types of materials as wood, and this reduces environmental impact and resource depletion. In fact, with these actions it is possible to save around $60 - 1600 \text{ kg } CO_2 - eq \text{ ton}$. In order to implement a mechanical process, several steps have to be made. Usually, they are: *cutting/shredding* to be able to reduce the products in small pieces for the subsequent processes, *separation in dry condition* to eliminate impurities, *polymer separation* to split the products into the different types of plastic, *milling* to make homogeneous each polymer group. Besides these main steps, there are other boundary processes that must prepare the end-product, according to the market standards. These can be washing/drying to clean the wastes and then to remove the washing liquid, agglutination and extrusion.

In addition to mechanical processes, the most common solutions, to perform these steps, are based on flotation processes, density differences, electrostatic forces, optical properties, and some others.

Despite the several existing processes, new ones can innovate the treatment of plastic waste, making the process cheaper or faster. At the Sapienza University of Rome, a device to separate different types of plastic was designed. This is a new wet technology to separate polymer particles, that can be employed in the separation process into the mechanical recycling plants. This device has the purpose to separate useful and useless polymers of an agglomeration of waste. It is able to split these materials although they have little difference in density from one another. The transport flow, within which plastic particles are immersed, is simply water without the use of chemical additives. Each element of the solid phase must have a density greater than $1000 \frac{\text{kg}}{\text{m}^3}$. This is an extra point since they cannot be separated in traditional density separation processes. This device is born from the idea of a previous apparatus: *Multidune*, in La Marca et al. 2012 and in Moroni, La Marca, et al. 2013. The Multidune is a hydraulic channel that makes a separation of the solid particles, based on the differential transport mechanism. Its shape is a serpentine, a series of repeated curves. The new device differs from the previous one for different geometric dimensions, which will be described in chapter 2. In particular it is greater and for example, this permits the use of

particles with a larger diameter.

The serpentine shape of the duct generates peculiar fluid dynamics conditions, for which a particle can settle inside the device or it can be expelled outside. Which of the two behaviour it assumes, depends on its physical properties: density, size, and shape.

First of all, in chapter 2, all the characteristics of the device will be analysed and its real dimensions will be described. Then, the attention will go on the flow that pass inside the apparatus, that is a multiphase flow. So, both fluid and solid phase will be characterized and their behaviour will be explained. Two fundamental dimensionless number will be introduced: *Reynolds number*, both for fluid and for solid phase, and *Stokes number*.

The kinematic investigation of the flow have been made with the use of image analysis, called *Hybrid Lagrangian Particle Tracking (HLPT)*. With this method the reconstruction of the velocity field of both phases is allowed. Furthermore, inside the fluid, some tracers are immersed, but they don't influence the motion of the flow. On the other hand, *Lagrangian Particle Tracking (LPT)* is used to obtain velocities and acceleration of the tracers. Finally, the results of the real experiments will be presented. All the informations, presented in that chapter, are taken from Moroni, Lupo, et al. 2017 and reworked for the purpose of this work.

1.2 The numerical model

Despite the real device worked perfectly in the real world, the purpose of this thesis is another. In particular, starting from the work in Moroni, Lupo, et al. 2017, in this work a numerical model of this experiment will be created and tested. This serves to give a numerical characterization of the device and to create a numerical model that allows doing several tests, changing every possible aspect, from the particles to the geometric characteristics of the serpentine. This will allow to understand more aspects of this phenomenon and eventually to increase the performances of the device.

This phenomenon has been modelled through an existent code, that is very efficient and performing. It has been developed with cooperation between the *University of Padova*, the *KTH mechanics* of Stockholm and *TU-Delft*, which started in 2011. It is a parallel software and it is able to use efficiently until 10 000 processors. It allows accurate simulations of solid-liquid two-phase flows, in which particles are transported. This detailed description is possible with the use of the *Immersed Boundary Method (IBM)*, whose initial idea is due to Peskin 1972. With this method, the fluid is described with the *Navier-Stokes equations*, discretized with a *Eulerian grid*, while the solid

phase is developed with the *Newton-Eulero equations*, that are implemented with a *Lagrangian grid*. The actual code implements the *Direct Numerical Simulation*, resolved for particles, (*PR-DNS*), Ardekani 2019.

The program can simulate fluid-solid, solid-solid, and solid-wall interactions with and without friction and complex geometries. This tool has been used in the last five years in a *ERC grant* project (TRITOS), and its results underlie over 50 articles in international journals.

The geometry implemented in the numerical model has been adapted to the phenomenon of interest.

In chapter 3, the implementation of this model will be described, and, furthermore, the criteria on which the model is based and the assumed hypotheses, will be specified. In the first part, an introduction to the computational fluid dynamics will be given. To analyse a certain phenomenon, there are different points of view, that differ from each other in the accuracy of the results and the computational cost. The main three methodologies that can be used are: *RANS*, *DNS* and *LES*. Then, there are variants of these methods that differ from each other for specific applications. As mentioned above, the flow of this experiment is a multiphase flow. This type of flow consists of two distinct phases which, for this case, are a fluid one and the other one is made of solid particles. The interaction between the two phases is very complex. In fact, in this treatise, for example, the behaviour of the flow depends on the interaction between the two phases and the collisions particle-particle and particle-wall. In the preliminary phase of analysis, some parameters have to be used to understand under which conditions the model falls and eventually, which simplifications can be assumed. This will be treated in depth, always in chapter 3.

However, this is just one of the two phenomena involving the flow in question. In fact, regarding the shape of the duct and the not so low Reynolds numbers used, that will be examined in the next chapters, the flow is in a transitional/turbulent regime. this condition implies the arising of certain behaviour that complicates the use of the constituent equations.

Now, a brief description of the turbulence will be made. In fact, since it is not an object of study in this work, for the sake of brevity, it is treated in the following section.

1.3 Turbulence in multiphase flows

The simplest way to analyse a fluid dynamic phenomenon is to treat it as incompressible and irrotational. These hypotheses can be used when the Reynolds number is very large and so two assumptions can be made:

- viscous forces and rotational flow are spatially confined to a small part of the domain;
- the accelerations of the flow caused by fluid inertia, are much larger than those caused by viscosity.

Another condition to be verified is that the boundary layer must stay attached to the boundary surfaces. However, when Reynolds number is smaller, these flow conditions are no longer correct. In this case, the flow may be influenced by viscosity. When a flow is assumed as viscous flow, it can evolve in two regimes: *laminar* and *turbulent*. The passage between these two states is not well defined and it is called *transitional regime*. The two main regimes determine the behaviour of the fluid, how it flows and how it should be analysed. Mainly, the way it evolves depends on three factors:

- *boundary conditions*: these define where conditions of slip, no-slip, and no-penetration have to be applied, and how the pressure gradient acts on the contours of the domain;
- *velocity*: the averaged value of this quantity influences which regime incurs;
- *cinematic viscosity*: it defines the propensity of vorticity to diffuse through the fluid.

Laminar flow is characterized to evolve in a well-defined straight path. This means that the fluid moves in parallel layers, without unsteady macroscopic mixing. This happens when the flow rate, and consequently the velocity, is low. In this condition, there are no eddies or swirls and neither cross-currents perpendicular to the flow direction.

On the other hand, when the velocity increases, the flow begins to become more irregular and it develops eddies and unsteady behaviour. In this case, the flow enters a turbulent regime and, as anticipated, this is the case of interest for this work.

In figure 1.1, the two different regimes and the unsteady behaviour of the turbulent flow downstream the obstacle can be observed.

Turbulence is an unsteady three-dimensional phenomenon and the quantities, of a turbulent flow, vary randomly in space and time coordinates. The quantities of a turbulent flow have a random variation in time and space. In figure 1.2 is showed the velocity trend of a fixed point in space.

The turbulent energy is generated by the large-scale structures and they transfer the energy in cascade to smaller scales up to the smallest ones. From there, the energy is transformed into heat. This transfer of energy, from the

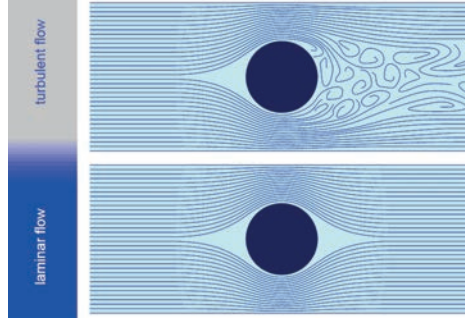


Figure 1.1: The two different regimes of a flow, turbulent and laminar, are represented. In the turbulent case is possible to observe the eddies behind the body.

biggest scales to the smallest one, is denominated as *energy cascade*. This concept of different size eddies and transfer of energy was introduced by Richardson 1922.

In this process, two main mechanisms occur. The first one consists in the generation of the eddies and it is associated to the gradients of the mean properties. The second one instead is referred to the destruction of these vortexes at the smallest scale by the viscous properties of the flow. While the large-scale are referred to *Richardson*, the small-scale has been studied by Kolmogorov 1941. The hypotheses of his development are fundamental to the study of turbulence. They are based on the fact that the small scale turbulent quantities are statically isotropic for high Reynolds number. Also, small scale motions are universal, this implies that the small scales can be determined by the viscosity and dissipation of the fluid.

To the base of the *RANS* method, there is the *Reynolds decomposition* that decomposes the velocity in two components: an average and a floating value. So, the results of this implementation are the average values of the flow. However, to model the turbulence is preferable to use another method, the *DNS* simulation. This method solve the Navier-Stokes equations directly and they provide the instantaneous values. The key to model the flow in the most appropriate way, is to have the size of the grid smaller than the Kolmogorov length scale. At this scale, the viscous effect dissipates the smallest eddies. But this algorithm has a very high computational effect. In fact, it is limited to low numbers and the search field. For this thesis, the use of a *DNS* model is perfect to give a precise description of the phenomenon. If the study of turbulence is already quite complex, when there is a multiphase flow, the complexity of the model augments even more.

Turbulence modulation is the effect of the *dispersed phase* on the *continuous phase*. The presence of particles or droplets can increase or reduce

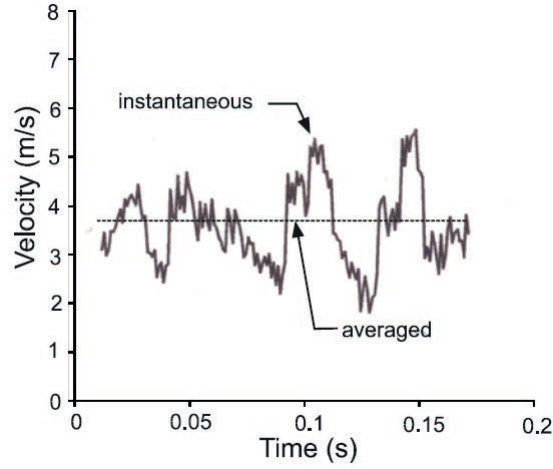


Figure 1.2: Assuming a fixed point in space, the turbulent velocity shows a very chaotic variation in time, with an average value and fluctuating values around it.

the turbulence. Furthermore, the combination of particles and turbulence greatly affects the rates of heat transfer and chemical reaction. Many studies have been carried out to understand in a better way this coupling. The first problem in this analysis is to obtain data from real experiments. In the past years, many tests have been made. Initially, to measure the turbulence, hot-wire or hot-film anemometry was used to measure turbulence. G. Hetsroni et al. 1971 attempted to use a hot-wire probe in a gas-droplet free jet in the study of a two-fluid atomizer. The invention of *Laser Doppler Velocimetry (LDV)* has had a large impact on turbulence research in multi-phase flows. Gore et al. 1989 and Hetsroni 1989 summarized the available data on turbulence modulation. These papers suggest criteria for the suppression and enhancement of turbulence. Given L_e the characteristic length of the most energetic turbulent eddy and D the particle size, it was observed that the turbulence is attenuated for value of $\frac{D}{L_e} < 0.1$. Another criterion, to establish the turbulence is given by the *particle Reynolds number*. For low values, the particles tend to suppress the fluid turbulence. Varaskin et al. 1998 showed that in *turbulence kinetic energy (TKE)* there is attenuation for low particle Reynolds number and varying concentration. From all the works done, five key factors arise that contribute to turbulence modulation: surface effects, loading effects, inertial effects, response effects, and interaction effects.

Therefore, it is obvious that turbulence and multiphase flow joined together, are very complex to implement into a model and to analyse. In fact, in the subsequent part of the chapter 3, the numerical model used, will be explained.

1.4 Analyses

Finally, in chapter 4, the several analyses, that have been made in this work, will be explained and some considerations will be exposed. The parameters which have been examined in this work, are mainly two: the geometry of the chamber and the density of the particles. Going to change the combination between these two parameters, different behaviours can be shown. In particular, the quantities that have been studied are the trend of the mean flow, the trajectories of all the particles and some other statistical quantities, that are useful to do quick comparisons.

At this point, that the structure of the work has been outlined, it can be explained in detail in all its aspects.

Chapter 2

Plastic separation

Before proceeding with the description of the work done, this chapter wants to make a premise. Its purpose is to give the basis for the next chapters. All the descriptions and the analysis made explicit in this chapter, have been taken from the paper Moroni, Lupo, et al. 2017. They have only been re-worked for the aim of this work.

First of all, the purpose of this chapter is to outline the real experiment. In fact, on this, the numerical model was created and analysed for the development of this thesis. After that, it serves also to define up to where the analysis and the deductions made have arrived. Finally, to explain the unknown behaviours of the experiment, that can be specified with the analysis of the subsequently numerical simulations.

2.1 The duty to separate

Among the several problems existing in this era, one of the biggest challenges to face is the management of plastic life. Daily, this common name refers to all the products that are part of the family of synthetic polymer. In their more general definition, polymers consist of macromolecules, that are long chains where there are small repeated groups of atoms or molecules: monomers. This molecular chains can mainly vary in length or in the chemical elements that constitute them. Based on these different characteristics, plastic materials can be divided into various categories, whose main and interesting ones for the purposes of this work, are the following:

- **polyethylene (PE):** packaging, tubes, and toys;
- **polypropylene (PP):** furnishing objects, food containers, and bottles;

- **polyvinyl chloride (PVC)**: piping e insulating films, that they are used for walls, windows or tiles;
- **polyethylene terephthalate (PET)**: classical plastic bottles and synthetic fibres;
- **polystyrene (PS)**
- **polycarbonate (PC)**.

The list that has just been shown represents only the most common plastics that are used in commerce. However, many other variants are used for the most diversified uses, and each of these polymers has its chemical-physical features.

Their life cycle begins with the production of useful products to sell and buy, and they are made up of virgin plastic. After being used, they are thrown away, and from this point, the regenerative phase begins. The largest possible amount of plastic is tried to recycle, to then create new products made from *regenerated plastic*. This serves to reduce the consumption of raw materials and the resulting wastes.

At the beginning of this paragraph, the most relevant categories of polymers have been shown. From this so great diversification, the problem arises that every type of plastic must, as far as possible, be separated from one another to then be recycled. Indeed, the recycling of this material can only be done for products manufactured with the same chemical compound. Therefore, the purpose is to obtain homogeneous agglomerates constituted by the same type of plastic, to be able to carry out the subsequent phases of the process. Since the daily amount of plastic to be handled is enormous, the regeneration process is not easy to manage. In addition to this difficulty, there is also the fact that some products cannot even be recycled, for example, polycarbonate. However, plastic products are gathered together indistinctly. Hence, in the machining center, there will be a heterogeneous mass of different types of plastic to be managed, which will have to be subjected to a whole series of processes, before each type of plastic can become a final regenerated product. First of all, the material is washed to remove all the traces of undesired grime. After that, within the recycling plant, to split out the different types of plastic, some or all of the following processes will have to be performed:

- *mechanical process*: through some rotating sieves, the different families are separated in terms of size;

- *flotation process*: the principle at its base is that the surface properties of different materials could be altered selectively by surfactant adsorption and this allows the separation of different materials. Initially, a pulp (made of the solid particles and water) enters in contact with gaseous bubbles that make certain materials hydrophobic, while others are hydrophilic. Then, through a flotation machine it's possible to separate these types of materials;
- *blowers*: some optical readers identify polymer variants and unsuitable types are wiped out;
- *electrostatic process*: through the use of the electrostatic effect, a certain type of product is attracted away from the group. This method is considered to be of high efficiency, so there are many configurations, which are explained in Inculet et al. 1998.
- *human activity*: to remove further undesirable objects, which are not detected by the machines.

From this sequence of processes, it can be deduced the number of activities that are needed to realize the recycling of plastic and the related great cost that derives from the simple partition in the different types.

In such situations, innovative ideas born to reduce costs and to increase the efficiency of a given process. For example, other materials can be separated from each other by decantation. This method exploits a substantial difference between the two densities, one of the decantation liquid and the other one of the material of interest, to obtain the partition. This process would be less expensive, but with plastic, it is not so easy for three main reasons:

- since the considered fluid, due to its inert characteristic, is water, the difference between its density and the density of the plastic is very low;
- the types of considered plastics vary very little between them in density;
- the last problem to make the use of this technique more complicated is that all these polymers are generally denser than the simple water. So, some additives have to be used, to create a halfway fluid density between the density of two plastics. But this creates a process that is not rapid, repetitive in the case of more than two polymers and it adds unnecessary components to the fluid, which can reduce the quality of the regenerated products.

This solution, due to the complications described above, is therefore not feasible. The innovation that allows us to always use water, as a means of separation for the different plastic materials, was to create a dynamic process inside a duct.

2.2 The separation device

At the University La Sapienza of Rome, a device was created, in Moroni, Lupo, et al. 2017, with a simple functioning, that using a fluid of water, in which plastic particles are immersed, it can carry out a separation between different types of plastic. However, this equipment has been developed and tested only for polymers with a density greater than those of water.

In figure 2.1 the device created and used for the various tests is represented. It is a serpentine that is assembled with the union of two halves. Each part is a sequence of eight half cylinders parallel to each other. The size of each channel, which constitutes the block, has an internal radius of $R_t = 0.026\text{ m}$ and a longitudinal length of $W_t = 0.48\text{ m}$. Every cylinder ($C1, \dots, C8$), created by the connection of the two parts, is called *chamber*. The two sections are joined together with an offset between them. This causes the horizontal dimension at the inlet to be different from the output size. In fact, with reference to the figure 2.1(b), the two values are $L_1 = 0.032\text{ m}$ and $L_2 = 0.017\text{ m}$. With the experiments carried out, using these values for the respective parameters, good results were obtained for the separation. However, this configuration will be discussed during this work with several simulations

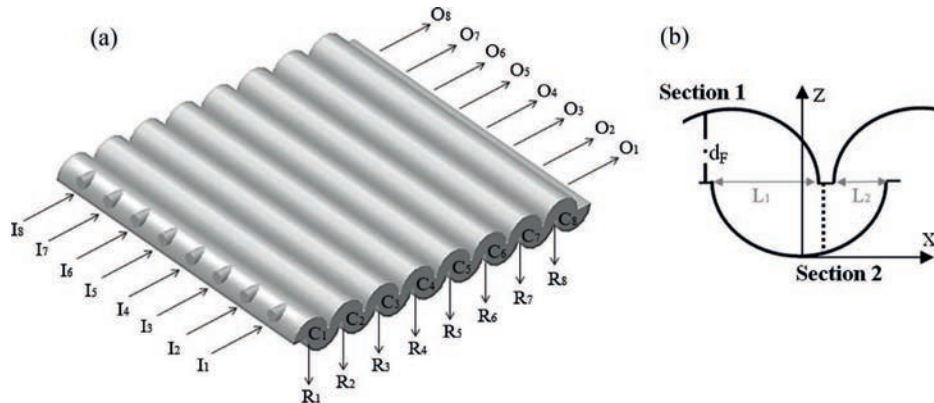


Figure 2.1: (a) Three-dimensional view of the separation device. (b) A sectional view of the device. Figure adapted from Moroni, Lupo, et al. 2017.

to tests the different parameters. The geometric quantity d_f , visible in the figure 2.1(b), represents the height of the section and it assumes the value of $d_f=0.0249\text{ m}$. This parameter will be taken as the reference quantity to determine the Reynolds number. The material of which the ducts are made is transparent *perspex* but the choice of this type of material does not affect the test results. The purpose of this material used to create the device will be explained subsequently, explaining how the analysis was performed.

2.3 Functioning

The physical dimensions of the experimental device were defined in the last paragraph. At this point, the two phases, that constitute the operating fluid which flows in the chambers, have to be outlined. As anticipated, it is a biphasic fluid and there may be mutual interactions between the two different phases.

The solid phase is formed by particles of different types of plastic and they differ each other in some aspects:

- *polymer*: PC, PET, and PVC are mixed;
- *nature*: from every type of polymer, the particles are taken in different states of their life cycle. So virgin plastic V , wastes W and regenerated plastic R are used;
- *shape*: the considered elements can be granular G , flakes F or pieces P ;
- *size*: since a single constant dimension for all the particles cannot be defined, with the use of sieves these have been separated into two classes based on the diameter of the element:
 - *Class I*: $0.002\text{ m} < d_p < 0.00336\text{ m}$
 - *Class II*: $0.00336\text{ m} < d_p < 0.00476\text{ m}$

In this way, the test was performed with particles of one class or another.

The acronyms exhibited for the different particle parameters will be used, in combination with each other, for all subsequent treatise to shorten the considered type of particle. For virgin plastics, the shape of the particles can be attributed to known geometries but it depends on the type of polymer considered. Indeed, for example, the shape of the element *PVC_VG* can

be compared to a semi-sphere, instead of *PC_VG* and *PET_VG* that can be compared to cylinders with elliptical section. Then, the plastic resulting from the wastes or the regeneration process, cannot be related to known geometries. However, the shape factor can be used to refer the shapes to known analytical form. At this point, the solid phase has been completely defined with all its variants that it can assume for a generic recycling process. Now, the liquid phase has to be described.

The fluid used is simply water, the different operating conditions and the different behaviour that it can assume into the duct must be defined. Along the lateral surface of the first cylinder and parallel to its longitudinal axis, eight entry holes have been created. Thanks to these, the fluid enters into the serpentine, with horizontal direction respect to the figure 2.1(b). These eight inputs are named I_i with $i = 1 \dots 8$. On the opposite side there are eight other holes that are used as output and named O_i with $i = 1 \dots 8$, as can be seen in the figure 2.1. Each of these is equipped with a stopper to change the number of outlet holes.

The flow rate that flows inside the device can be changed in two ways. The first one is to open or close the outlet hole caps. If the total cross-sectional area increases, consequently also the flow rate raises. The second way to change the flow rate is to act on the tank. This latter is used to supply the biphasic fluid to the device. The altitude of the serpentine is supposed to be the reference zero point. By changing the height of the tank, compared to that of the device, the flow rate is changed. As can be easily deduced, by increasing the difference in altitude between the two components, the flow rate will raise. The other way around, by decreasing the difference in height, there will be a lower flow rate. In table 2.1, the effects of the variations of the parameters just described, can be observed. By way of clarification, by acting on the flow rate, the flow speed will change and it influences some dimensionless parameters.

The first characteristic dimensionless number analysed is the *Reynolds number*. It is of fundamental importance, and it is widely used as a reference parameter in fluid dynamics problems. The values that it can assume, for each possible flow rate, are explained in the last column of table 2.1.

In this case, this number is attributed to the fluid, and it can be defined as follows:

$$Re = \left(\frac{Q}{W_t \cdot d_f} \right) \cdot \frac{d_f}{\nu} \quad (2.1)$$

In the equation 2.1, Q makes reference to the flow rate shown in the table 2.1, while the two geometric dimensions were defined in the paragraph 2.2. The only parameter still unknown is ν , which represents the kinematic viscosity of the considered fluid. In the case of water it assumes the value of

Table 2.1: In the following table, nine analysed cases are listed, in which the number of open outlet ducts and the height of the tank change. The values of this latter are to be intended respect to the plane where the device is located.

Hydraulic head	Opened outlet ducts	Case	Flow rate Q $10^{-3} \frac{m^3}{s}$	Re
$H_1=1.0$	O_3, O_6	1	0.72	1800
	O_2, O_4, O_6	2	0.92	2300
	O_2, O_4, O_6, O_8	3	1.08	2700
$H_2=1.5$	O_3, O_6	4	0.84	2100
	O_2, O_4, O_6	5	1.08	2700
	O_2, O_4, O_6, O_8	6	1.24	3100
$H_3=1.0$	O_3, O_6	7	0.92	2300
	O_2, O_4, O_6	8	1.22	3050
	O_2, O_4, O_6, O_8	9	1.36	3400

$\nu = 8.9 \cdot 10^{-7} \frac{m^2}{s}$. Given the generic dimensionless formula of the Reynolds number, it is deductible that the flow speed corresponds precisely with the term in brackets. Therefore, the flow speed depends on both the flow rate and geometric characteristics.

Preliminarily, based on the Reynolds number, what kind of flow develops, can be defined. In fact, the fluid can evolve in three different ways: *laminar*, *transitional* and *turbulent*. For the case in question, a simplified comparison with the case of a flow into a linear duct can be made. For this type of behaviour the three types of evolution can be divided, according to the Reynolds number, in this way:

- laminar flow for $Re < 2300$
- transitional flow for $Re > 2300$ e $Re < 4000$
- turbulent flow for $Re > 4000$

The Reynolds numbers defined above are useful to provide an approximate indication of the type of flow that develops. Indeed, the flow in a serpentine will have a different Reynolds number for which there will be the passage between two states of the fluid. This last one cannot flow in a straight direction as in a simple linear duct, so the curves will affect the reshuffles and the passages between the states. Despite the approximation, this comparison is useful for defining the hypotheses with which the numeric model will be expressed, in order to analyse the flow. In fact, regarding table 2.1, it's clear

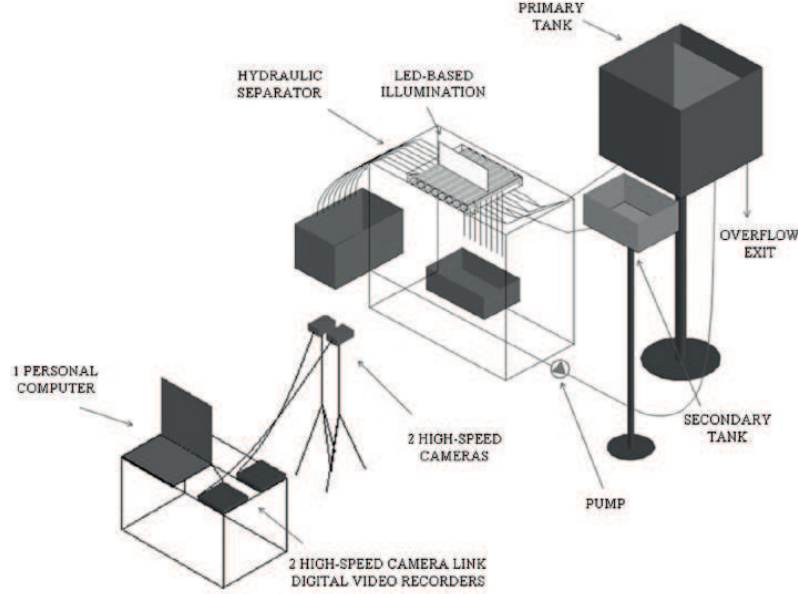


Figure 2.2: Schematic representation of the configuration for the experiment. Figure adapted from Moroni, Lupo, et al. 2017.

that fluid falls mainly into the transitional state, or in any case, tending to the turbulent one.

In figure 2.2, the predisposition of the separation device and all the surrounding instruments, to power, observe and describe the phenomenon, can be observed. The main objects to paying more attention, are the device, the tank, and the two high-resolution cameras. The more detailed use of these last two will be described later.

At this point, both phases of the operating fluid are defined and now, the multiphase flow can be considered.

In the real experiment, three of the nine cases assumed in table 2.1 have been tested, and they can be observed in table 2.2. For the considered particles, besides defining their geometric characteristics, two very useful dimensionless numbers have been determined. The first one, that has already been defined for the fluid, is the *particle Reynolds number* Re_p . In fact, it is referred to the particle with the following expression:

$$Re_p = \frac{d_p |U_p - U_f|}{\nu} \quad (2.2)$$

This time, the Reynolds number is calculated as the difference between the particle velocity U_p and the fluid velocity U_f , thus this dimensionless number is expressed as a function of the relative velocity between the phases. Then,

the quantity d_p refers to the average diameter of a particle. For further details, regarding this last parameter, see below. The meaning ν is known.

The second number is the *Stokes number* and it is defined as:

$$St = \frac{\tau \cdot U_0}{d_f} \quad (2.3)$$

This dimensionless number is useful for characterizing the behavior of suspended particles in a fluid. In fact, it represents the ratio between the *relaxation time* of the particle and the characteristic time of the fluid. U_0 indicates the average velocity of the undisturbed fluid, while d_f is known. The parameter τ represents the particles relaxation time and with the hypothesis of spherical particles, it can be expressed by:

$$\tau = \frac{\rho_p \cdot d_p^2}{18 \cdot \mu_g} \quad (2.4)$$

where ρ_p is the density of the considered particle and μ_g is instead the dynamic viscosity of the fluid:

$$\mu_g = \nu \cdot \rho \quad (2.5)$$

and for water, that it has a density of around $\rho = 1000 \frac{kg}{m^3}$, μ_g simply takes the value of $\mu_g = 8.9 \cdot 10^{-4} Pa \cdot s$, at the reference temperature of $T = 25^\circ C$.

In table 2.2, the different types of samples used in the experiment can be observed. For the particle Reynolds number, the velocity is a relative velocity, so, changing the flow rate, the number doesn't change for the same

Table 2.2: List of the different types of materials used with the geometric parameters and the characteristics of the fluid for the three cases examined: #1, #7, #9.

Name	Density $\frac{kg}{m^3}$	Size Class	d_p $10^{-3} \cdot m$	Shape factor	Re_p	St		
						Case 1	Case 7	Case 9
PC_VG	1180	II	3.17	0.85	270	0.24	0.30	0.45
PC_RF	1200	I	2.98	0.53	260	0.22	0.28	0.41
		II	3.59	0.51	350	0.27	0.34	0.51
PVC_VG	1300	II	3.19	0.84	360	0.23	0.29	0.43
PVC_WP	1610	I	3.39	0.81	560	0.24	0.31	0.46
		II	4.41	0.74	830	0.32	0.41	0.61
PET_VG	1310	I	2.64	0.83	270	0.18	0.23	0.35
PET_WF	1350	I	3.31	0.60	400	0.23	0.30	0.44
		II	3.93	0.49	510	0.28	0.36	0.53

particle. Instead, this Reynolds number varies only for different values of the diameter. It's a different story for Stokes number, where it is a function also of the fluid. So, depending on the case considered and on the properties of the particle, the Stokes number changes. One thing to consider is that for all the cases considered, this dimensionless number assumes values lower than the unit. Therefore, the relaxation time for the solid phase is less than the characteristic time for the fluid. This means that the difference between the two velocities, U_p and U_f , is small and so there is a strong coupling between the phases.

The particles used are completely generic, so they have different shapes and sizes from one another. In order to attribute values of some parameters to the two classes of particles, a certain average diameter must be used. The diameter of ten particles, of the same type and shape, was measured using a calibre. In this way, it was possible to associate a specific average value to an entire typology of elements. Thus, these values don't change for every particle.

Having defined all the parameters that determine the biphasic fluid trend, now, the analysis of the real behaviour can be analysed. To do this, two high-speed and high-resolution cameras were used to shoot some snap-shots of the flow. Exactly for this reason, as mentioned above, the device was built in *perspex*, to perform visual observations of the interior of the duct. To determine the flow field of the fluid phase, some tracers were released into the flow. They have neutral buoyancy so they can continue to flow into the ducts together with the water. The tracer material is *Vestosint2157*, a polyamide 12 derivative and it is in a powder state. Moreover, it has a density of $1016 \frac{kg}{m^3}$ and an average diameter of $56 \cdot 10^{-6} m$. Finally, through the predisposition of the optical apparatus, some acquisitions of the mixture of tracers and plastic particles have been taken.

2.4 Analysis

By obtaining the snapshots of the fluid through the optical instrumentation, it was possible to obtain sequential images of the progress of fluid and particles. First of all, this made possible the graphic representations of the phenomenon. After that, all the subsequent analysis, that will be shown in this and the next section, have been obtained with an *image analysis*. In figure 2.3, the behaviour of tracers and polymeric materials inside a chamber can be observed.

The image (a) is a real snapshot of the experiment, and there are both plastic particles and tracers. Subsequently to the acquisition, the other two

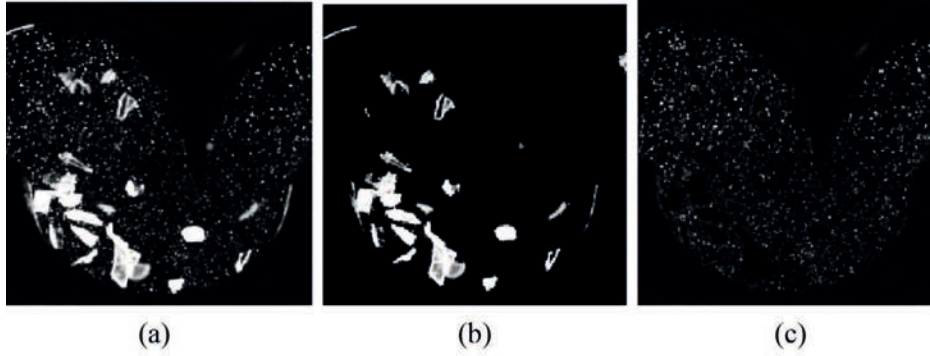


Figure 2.3: (a) Real image of the fluid. (b) Computer image processed, with only particles of plastic. (c) Computer image processed, with only tracers. Figure adapted from Moroni, Lupo, et al. 2017.

images (b) and (c), shown in figure 2.3, were processed through a binarization procedure. In this way, they show the presence of only polymeric materials or tracers only. This was possible due to the great size difference between the particles and the tracers. Therefore, they are easily distinguishable from one another.

Going to take two successive images, through the use of software, it is possible to obtain the movement of a single particle. Moreover, knowing the temporal distance between the two images, its moving velocity can be determined. To be able to do this, the *Particle-Tracking-Velocimetry* algorithm has been implemented. To obtain a solution to the *optical flow equation*, the *sum of squared difference* method was used.

The equation of continuity for optical flow, also known as *Brightness Constancy Constrain (BBC)*, is defined as:

$$\frac{D\bar{\mathbf{I}}}{Dt} = \frac{\partial \bar{\mathbf{I}}}{\partial t} + u \frac{\partial \bar{\mathbf{I}}}{\partial x} + v \frac{\partial \bar{\mathbf{I}}}{\partial y} = 0 \quad (2.6)$$

where $\bar{\mathbf{I}}(\mathbf{x}, t)$ is a matrix that contains the intensity values of the image considered at the time t , $\bar{\mathbf{x}} = (x, y)$ are the coordinates of a generic pixel and $\bar{\mathbf{U}} = (u, v)$ are the unknown velocities in the point $\bar{\mathbf{x}}$. But there is one equation in two unknown quantities and it cannot be solved. The solution is to compute this equation in a reduced two-dimensional window, centered on the pixel of interest. A least square optimization, with the use of the cost function SSD (sum of squared difference), is implemented to determine the displacement vector of the window in question between two subsequently snapshots. The implementation is precise since, for a small time difference, the reference window remains almost unchanged.

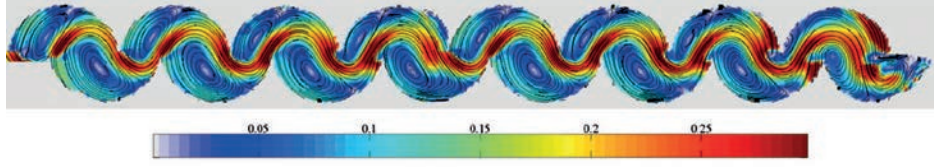


Figure 2.4: It is possible to observe a simulation of the behaviour of the only fluid, within the entire serpentine. This figure shows the velocity module for case 5. Figure adapted from Moroni, Lupo, et al. 2017.

Once the unknown velocities have been obtained, it is possible to represent the flow behaviour, but only a graphical representation of the fluid phase is known. In fact, as anticipated, until the beginning of this thesis work, it was not possible to represent the solid phase. To be more precise, it was possible to represent only the tendency of the fluid in a graphic way. However, it is affected by the presence of certain polymer particles, but these latter were not possible to be represented with a model.

In the work performed in Moroni, Lupo, et al. 2017, it is assumed that the flow is in a steady-state and that the different averages represented, have been calculated in a time interval of 40 s. In figure 2.4, the simulation of the behaviour of the single fluid phase of the flow in all the ducts can be observed. Moreover, there is a steady-state and periodic tendency after the first chamber and before the last two. To perform a more in-depth analysis, a more detailed zoom was performed inside chamber 3. It is possible to distinguish the different areas of the fluid and its behaviour mediated over time, in figure 2.5.

In fact, it is possible to observe the trends of the different velocities, horizontal and vertical, and of the turbulent kinetic energy for the two extreme cases, the case 1 with the minimum flow rate and the case 9 with the maximum flow rate. The velocities represented are statistical quantities and they are not instantaneous values. Indeed, the two velocities mentioned above are averaged over time, while the turbulent kinetic energy $TKE2D$ is calculated as follows:

$$TKE2D = \frac{\bar{u'^2} + \bar{w'^2}}{2} \quad (2.7)$$

with $\bar{u'^2}$ and $\bar{w'^2}$ the variances of the two velocities.

With these representations, it's noted that in each chamber two recirculation zone are created, one upper and lower, and this second one is greater than the first one. Instead, the transport current continues to flow from one chamber to the other until to the output, and it can also transport materials without separating them.

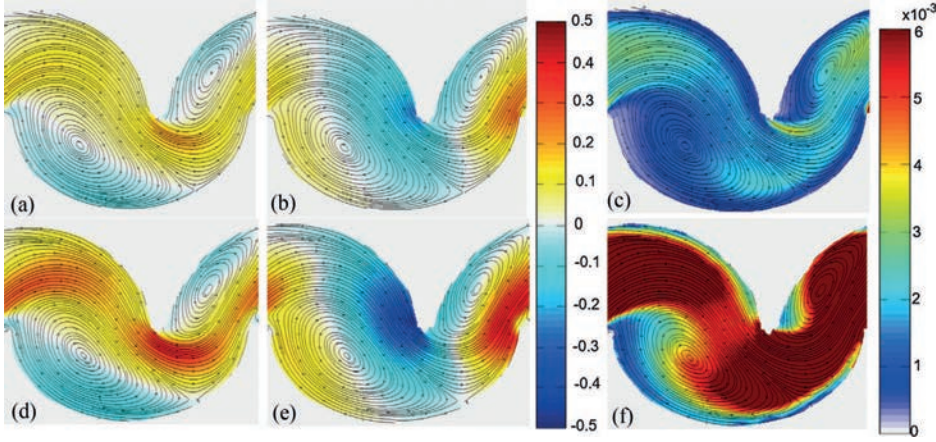


Figure 2.5: The flow in chamber C3 is shown. The sequence of images of the first line represents case 1 while the second line reproduces the case 9; (a) and (d) show the horizontal velocity; (b) and (e) show the vertical velocity; (c) and (f) show the two-dimensional turbulent kinetic energy. Figure adapted from Moroni, Lupo, et al. 2017.

The lower recirculation zone is positioned under the transport current in the left side of the chamber. It rotates clockwise and it is suitable for capturing particles, removing them from the main transport current. These captured pieces can behave in one of the following three ways:

- settle within the chamber;
- they can follow the ascending part of the rotating motion, but the current doesn't have enough effect to get them back into the flow;
- they can execute an entire rotation for be recaptured by the transport current and then settle in one of the next chambers or be expelled from the device.

Instead, the upper recirculation zone, located above the transport current in the right side of a chamber, rotates counter-clockwise. This zone can capture particles, but they must move across the current and settle in the lower recirculation zone to be separated from each other.

2.5 Results

Once the various characteristics of the biphasic flow are known and its behaviour assumed in the different chambers is defined, finally, the results that

the device can obtain can be quantified.

As better specified in the paragraph 2.3, the particles have been divided into two different classes *I* and *II*. This partition was performed based on a specific diameter value used as a threshold. For real experiments, the same two classes were used to execute separate tests. Each class includes different types of polymeric materials, and for any of these, very different percentages were obtained for each of them. In figure 2.6, for each type of polymer, the percentages of settled particles in each chamber and the percentage of how many particles are not trapped in the device, are shown. In particular, always referring to the two graphs of the same figure:

- **Class I:** a full expulsion of PC_RF can be noted. Instead, there is almost full sedimentation of PVC_WP, of which the 80.9% is settled only in the second chamber. An intermediate situation is had with the two types of PET where there is a partial separation with the opposite behaviour.
- **Class II:** even with larger diameter particles, the behaviour of PC and PVC is practically unchanged. What changes significantly is the percentage of PET_WF. It can, in fact, be noticed that there is a much greater quantity of this material that remains stuck in the different chambers.

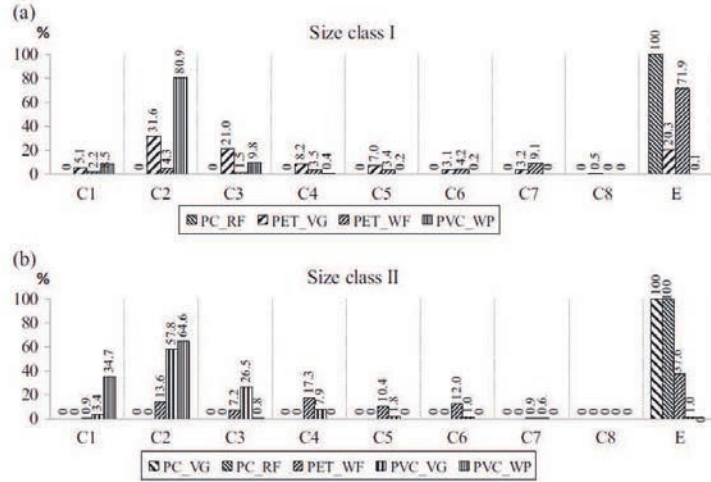


Figure 2.6: Representation of the percentages of settled particles along the 8 chambers and of the percentage of particles expelled from the duct. In the legend, the different types of polymers can be distinguished. The acronyms to define the materials refer to the explanation of the paragraph 2.3. Figure adapted from Moroni, Lupo, et al. 2017.

With these analyses, it is shown that there is a perfect separation in the case of PC and PVC. Along the input section of chamber C2, the tendency of the two usual velocities, horizontal and vertical, can be compared as a function of the vertical coordinate, as shown in figure 2.7. In particular, by changing the considered case of the flow rate, these trends don't change and they collapse in a common trend. This suggests that the solid phase does not exercise a consistent influence on the fluid one. Furthermore, it can be seen how the two extremes of the velocity profiles are negative. This highlights that with these profiles, the recirculation zones are intersected: the upper one of the previous chamber and the lower one of the same chamber examined.

Through the study of the carried out analyses, the reciprocal influence between the shape factor and the recirculation zones was observed. In fact, particles like PC_VG, with a high shape factor, interact more easily with the lower recirculation zone, and the latter tends to settle these elements. Instead, the particles with a low shape factor, such as PC_RF, are influenced by the upper recirculation zone and are only occasionally captured in the lower one. However, due to the size and density of these polymers, they are taken up by the transport current. In this way, they are transported to the output of the duct, as shown in the figure 2.6.

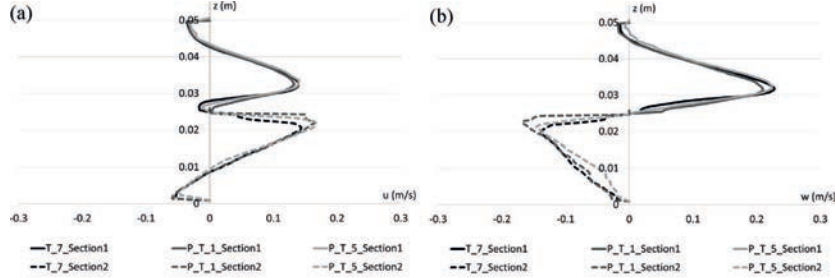


Figure 2.7: Trend of horizontal (a) and vertical (b) velocities inside chamber C2, varying the case examined. Figure adapted from Moroni, Lupo, et al. 2017.

2.6 Conclusions

The images represented during this chapter were taken through the *Particle-Tracking* method, which allows excellent reconstructions of real phenomena. With these representations, the behaviour of the real flow was observed, in particular, the development of a transport current and two recirculation zones, one upper and one lower.

Regarding the behaviour of the liquid phase, it can be said that with the same flow rate, the material expelled from the device is greater when there is

a greater turbulent kinetic energy. Moreover, a reciprocal influence between the two phases of the flow happens. This is also highlighted by the fact that the Stokes number assumes values less than unity.

Instead, concerning the solid phase, it was possible to observe how the variation in density, diameter, and shape-factor greatly affects the separation performance of the device.

For example with the same density and shape factor, particles with a larger diameter, exerting greater interaction on the liquid phase. If instead the shape factor changes, it is noted that when it is smaller than the unit and therefore the shape of the particles is far from the sphericity, the particles are more easily expelled from the apparatus.

2.7 Next works

Through the various considerations presented in this chapter, with the work done in Moroni, Lupo, et al. 2017, from the point of view of the real phenomenon, it was possible to define what happens in the device. From the next chapter onwards, the idea developed with the work of this thesis will be described in each aspect. First of all, the working hypotheses of the experiment and the equations on which the created numerical model is based will be defined. Thus, the *IBM* method will be explained since it is a fundamental technique for obtaining very good results. Then, the principles on which the simulation domain is based will be described. And so, all the different tests performed will be examined. Initially, the simulation will use a laminar flow, then with the introduction of a temporary disturbance, it will become a turbulent flow. Once the motion of the single-phase fluid will be developed, also the solid phase will be introduced in the duct with the placement of a certain quantity of particles. Moreover, to observe the changes in the behaviour of the particles, their density will have changed.

Parallel to the execution of the various simulations, the velocities will also be examined from a statistical point of view. In this way, it will be possible to have average values to make more concrete judgments. Therefore, the average quantity that will be observed will be for example the spatial and temporal average or even the variance to evaluate the turbulent kinetic energy.

At this point, the bases of the phenomenon under examination were founded. With the next chapter, more detailed considerations by defining the numerical model will be made.

Chapter 3

IBM and the numerical model

In this chapter, all the numerical aspects of the problem are presented. First of all, the main aspects of the experiment are explained to give a clear idea of the problem. Then, the different problems that occur in the computational fluid dynamics are shown. In fact, the numerical model has been developed to simulate several different situations from the collision between particles until heat transfer, or both. To can model these different cases, many factors must be kept in mind, above all, to have the convergence of the program. So, both equations and hypotheses of the simulation done, are highlighted. Finally, considerations on the current implementation will be clarified to understand with which criteria the results have been obtained.

3.1 The complexity of fluid dynamics

Fluid dynamic phenomena can be simulated with the creation of a more or less complex numerical model. The fundamental equations for describing every type of phenomena are the *Navier-Stokes equations*. Practically, in all the cases, they must be resolved through the implementation with a computer. Thus, computational fluid dynamics comes into play.

In general, these equations are a cornerstone of the fluid dynamics and they can solve every possible fluid dynamic phenomenon. Starting from the determination of simple flow fields and coming up to the interaction between different phases of an operating flow such in this case. The problems that arise can be solved by these equations in a very precise and accurate way, but this depends on the way in which they are implemented and with which hypotheses. However, their use is considerably more complicated by two main problems. The first of these two ones, is that only in very few and extremely simple cases these equations have analytical solutions. This complication

makes very high the computational cost. Due to this, the equations have to be solved on a discretized domain. This latter will be sufficiently refined depending on both the resolution model and the quality and reliability of the requested solution. The second problem is that these equations are not a *closed-form expressions*, in fact the system of equations to implement consists of five partial differential equations containing twenty unknowns. To obtain a system of closed-form expressions, the number of unknowns can be reduced with some simplifying hypotheses. Then, we have to use some physical models to add other equations to the system and so make it closed.

This is precisely what has been done and it is defined in the following paragraphs.

3.2 Numerical approaches

The first level to manage the Navier-Stokes equations is based on the quality required by the results, and therefore on how much to simplify them. Obviously, more the equations are simplified, less detailed will be the results of the model of the phenomenon. More the equations are simplified, smaller is the computational cost. However, the right compromise depends on the purpose of the model, whether it is better to give all the details of the problem, in a very onerous way or just the general trend of the phenomenon, but with a small use of resources. The three main alternatives, on which the computational fluid dynamics is divided, are the following:

- **RANS - *Reynolds Average Navier-Stokes*:** this model uses time-averaged Navier-Stokes equations. The main idea is to use the *Reynolds decomposition* to simplify them. This method consists of expressing the velocities, such a sum of their time-averaged and fluctuating quantities. However, this assumption produces a new set of unknowns called *Reynolds Stresses*. Since this stress matrix is symmetrical, there are six unknowns. Therefore, to have a closed system of solvable equations, it is necessary to use a turbulence model. The simplest and most used methods are for example the *k- ϵ method* or *k- ω method*. With these, two additional transport equations are added and a turbulent viscosity is introduced to compute the Reynold stresses. More complex models, instead, solve an equation for each of the six unknown stresses plus a scale equation, ϵ -equation or ω -equation. The choice of which of these turbulence models should be used depends on some preliminary hypotheses on the specific problem to be solved. An improvement of the RANS method is the *URANS-model* which produces less averaged and more representative results of the unsteady characteristic.

The advantages of this model are considerable, such a very low computational cost compared to other methods, and the average flow velocity is calculated as a direct result. However, the problem with this type of solution is the requirement of a turbulence model that is typically tuned to empirical tests;

- DNS - *Direct Numerical Simulation*: this approach solves the Navier-Stokes equations numerically, without the use of any turbulence model. In this way, the model will have to solve the whole range of spatial and temporal scales to be accurate. Here, the discretization is very significant and fine since the model should represent the vortices from the biggest scale until to the smallest dissipative scale, the *Kolmogorov micro-scale*. The computational cost can be roughly defined as the number of operation that have to be done, in order to solve the model. This number results to be proportional to Re^3 . So, it easily deducible that also for low Reynolds numbers the computational cost is very high. In fact, for the main industrial application, the Reynolds number are too high to be able to use a DNS. So, for these purposes is better to use a RANS, the approach implemented by the commercial CFD software programs. Instead, the direct numerical simulation is used by research centre. This method is really precise and it permits to extract from the numerical experiments, some informations impossible to obtain with a real experiments. Moreover, this method help to understand better the physics of the turbulence. Finally, it is useful to create some turbulence models to use to solve RANS o LES.
- LES - *Large Eddy Simulation*: nowadays, this third implementation is having large development and use for its great possibilities. The most extensive applications are for example acoustic and combustion. The criterion on which it is based, is a combination of the approaches just described. The larger scales of the flow are solved in a direct way with Navier-Stokes equations. Contrariwise, the smallest scales, which are the most computationally expensive to solve, are filtered out by the use of a low-pass filter criterion. The informations of the sub-grid scales are not lost but are modelled by a turbulence model. The filter can perform a spatial or a temporal filtering operation, or both. From this, it is easy to understand that the computational costs are much less than a DNS, and the precision is greater than RANS.

With this comparison, pros and cons of each methodology have been highlighted. The model that has been created previously, having to simulate accurately the fluid dynamics problems, has been implemented with the use

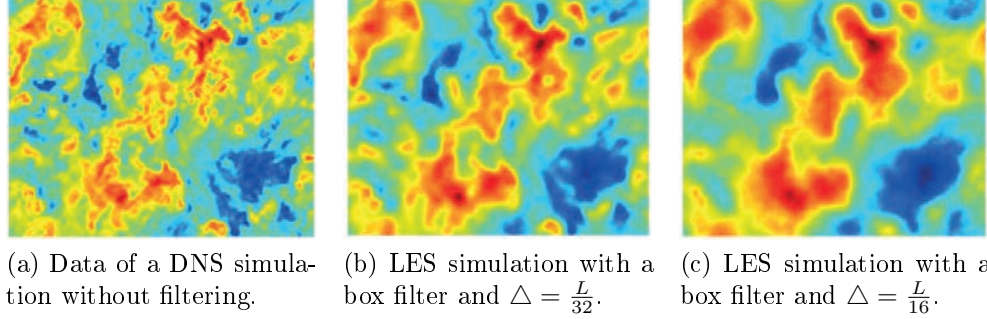


Figure 3.1: In these figures are represented the data of a DNS simulation without filtering and then with two different filtering to show the results of a LES simulation. Figure obtained from the data of Lu 2007.

of DNS. So, the computational cost is high but for the research purposes, reliability and precision are more important.

3.3 Multiphase flows

3.3.1 Preliminary introductions

The fluid dynamics can be implemented in more or less complex ways. This depends on many point of views concerning the characteristics of the problem. How to make a trade-off between accuracy and computational cost has just been described, with the appropriate simulation method. Another aspect, to manage the equations, is the number of components of the flow and how they are mixed.

A single-phase flow is an homogeneous flow, consisting of one or more mixed components and its characteristics are the same in all the domain. A typical very clear example of this, is the air. It consists of different gases such oxygen and nitrogen, but they constitute a single mixture with average values of the characteristics of each gas. The result is a *multicomponent single-phase flow*. But this is true, until some conditions are met. Until the different components have similar molecular weight, this approach is right and practical. But when the molecular weights are significantly different from each other, this is no longer true. In this case, the momentum, that is associated to the diffusional velocities, may be considerable. Another problem, that can make this criterion unreliable, is the variation of the temperature. In fact, when this last one is very high, some dissociation processes may occur and the multicomponent nature can become relevant. On the other hand, when

the temperature is too low, some species may condense and the multiphase condition becomes evident.

In addition to these phenomena, also in more evident cases, there is presence of a multiphase flow. For example, when solid particles are immersed inside a liquid phase. In fact, a multiphase flow may occur in very different situations, that are listed in table 3.1.

Two main components of the flow can be identified. The first one is the *continuous phase* that is represented by the transport fluid. The second component is the *dispersed phase* that is immersed in the other phase. For the purpose of this work, the combination of interest is the *liquid-solid flow*. This type consists of a flow in which solid particles, those represent the solid phase, are carried out by the transport current, that in this work it is water. These flows are referred to as *slurry flows*. Moreover, particle-particle and particle-wall interactions are much more important than the forces due to the interstitial liquid.

There are two possible behaviour of the solid phase. The first one is when the particles can move inside a liquid, so they are the dispersed phase immersed in a liquid phase. The second one, instead, is when the particles are motionless. In this case, the problem reduces to flow through a porous medium. Here, the viscous force on the particle surfaces is the first and most important mechanism affecting the liquid flow. However, it is not appropriate to refer to this case as a liquid-solid flow, since the solid phase is not in motion.

Table 3.1: The different situation of when a multiphase flow can occur.

Gas - Liquid flows	Bubbly flows
	Separated flows
	Gas - droplet flows
Gas - solid flows	Gas - particle flows
	Pneumatic transport
	Fluidized beds
Liquid - solid flows	Slurry flows
	Hydro-transport
	Sediment transport
Three - phase flows	Bubbles in a slurry flow
	Droplets/particles in gaseous flows

3.3.2 Slurry transport

This type of multiphase flow consists of a liquid fluid that transports a solid phase. It can represent many situations, such as a flow of mud or coal-water flows, that can be substituted for fuel oils. Moreover, this flow can be subdivided into four categories:

- *homogeneous*: is when small particles are kept in suspension by the turbulence of the carrier fluid. In these situations, it can be easier to treat the fluid as a single-phase flow with average properties between those of the two phases;
- *heterogeneous*: is when the particles are greater and they tend to settle on the bottom of the duct. This is the case for the following discussion;
- *moving bed*: it occurs when the particles settle on the bottom of the duct and they move along as a bed;
- *stationary bed*: this last regime happens when the particles fill the pipe and they can't move anymore. This case is analogous to the flow through a porous medium.

The fluid mechanics for this multiphase flow is complex because of the two main interactions: particle-particle and fluid-particle. This type of flow is part of the *dispersed phase flows*, where the dispersed phase is not materially connected.

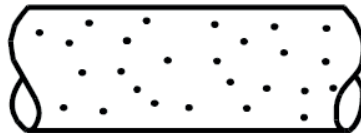


Figure 3.2: In this figure is represented a schematic example of a homogeneous liquid-solid flow inside a linear channel. Figure adapted from Crowe et al. 2012.

3.3.3 Properties of the phases

The dispersed phase flows include, in addition to the liquid-particle flows mentioned above, also gas-droplet, gas-particle and bubbly flows.

The first part to analyze, is the continuum phase of the flow. The fluid consists of continuous matter for which the different properties, such as density and velocity, vary continuously in all the domain. The density of the

liquid, can be defined as the ratio between the mass and the volume:

$$\rho = \lim_{\Delta V \rightarrow \Delta V_0} \frac{\Delta M}{\Delta V} \quad (3.1)$$

Starting from a small volume, increasing the number of molecules, the density will increase but less and less. Finally, a *point volume* ΔV_0 will be reached and the variations of density will become insignificant. According with the Poisson distribution of the probability theory, this limit is reached for a volume containing 10^5 molecules, and the fluctuations of density are less than 1%. If the dimension of this point volume is much less of the volume of flow considered, the continuum assumption is valid. For the case in question, a volume of water, that contains this amount of molecules, has the size of $10^{-2} \mu m$. Thus, the concept of a continuum is perfectly applicable to this situation.

Since that the Navier-Stokes equations were developed for a continuum, to analyze the domain around a particle, the condition $V_0^{\frac{1}{3}} \ll D$ with D the particle diameter, must be respected. Another quantity, very important to check the applicability of the Navier-Stokes equations for the continuum, is the *Knudsen number*. This number is defined as follows:

$$K_n = \frac{\lambda}{D} \quad (3.2)$$

where D is the particle diameter and λ is the mean free path:

$$\lambda = \frac{K_B T}{\sqrt{2} \pi \sigma^2 P} \quad (3.3)$$

with K_B the Boltzmann constant, T the temperature of the system in Kelvin, σ the diameter of the molecules and P the pressure of the system. When the Knudsen number is much less than unity, the continuum approximation is valid. Since here, temperature and pressure are the environment ones, that are $298.15^\circ K$ and $101\,325\,Pa$, the Knudsen number is close to zero and it confirms the continuum hypothesis again.

Now, the dispersed phase must be defined. As above, with the probability theory, a volume ΔV_{m0} must be considered, where there aren't significant variations. Therefore, the *number density* can be defined as:

$$n = \lim_{\Delta V \rightarrow \Delta V_{m0}} \frac{\Delta N}{\Delta V} \quad (3.4)$$

where ΔN is the number of particles in the volume ΔV . Moreover, the *volume fraction* can be expressed as:

$$\alpha_d = \lim_{\Delta V \rightarrow \Delta V_{m0}} \frac{\Delta V_d}{\Delta V} \quad (3.5)$$

with ΔV_d the volume of the dispersed phase in the volume. For this phase, the *bulk density* is the mass of the dispersed phase ΔM_d per unit volume of mixture and is defined as:

$$\bar{\rho}_d = \lim_{\Delta V \rightarrow \Delta V_{m0}} \frac{\Delta M_d}{\Delta V} \quad (3.6)$$

If all the particles have the same mass m , then the expression 3.6 become:

$$\bar{\rho}_d = n m \quad (3.7)$$

In the same manner, the bulk density for the continuum phase can be defined. From these, the *mass concentration* can be defined:

$$C = \frac{\bar{\rho}_d}{\bar{\rho}_c} \quad (3.8)$$

It is the ratio between the mass of the dispersed phase and that of the continuum.

Now, the focus goes to the different aspects of the interactions between the particles. Firstly, it must be defined if there is enough space between the particles, so they can be treated as isolated elements. Considering spherical particles, the volume fraction become:

$$\alpha_d = \frac{\pi D^3}{6l^3} \quad (3.9)$$

Making explicit the equation 3.9 respect to $\frac{l}{D}$, this gives an idea if the particles are too close between them. This happens when the diameter, D , is too great or the size, l , of the domain is too small. When this ratio is enough great, the particles can be treated as isolated and they have little influence of the neighbouring elements. However, since this ratio depends from the ratio of densities, for slurry flows, as in this case, the space cannot be sufficient to treat the particles as isolated elements.

Another important aspect is the response time, referred to the changes in flow velocity or temperature of the particles. It is useful to establish which dimensionless parameters are important to characterize the flow. For the next dissertation, spherical particles will be assumed, and they are the same that have been assumed for this work. The equation of motion is given by:

$$m \frac{dv}{dt} = \frac{1}{2} C_D \frac{\pi D^2}{4} \rho_c (u - v) |u - v| \quad (3.10)$$

where m is the mass, C_D the drag coefficient, u and v are the velocities of particle and flow, respectively. Here, the expression 2.2 of the chapter 2

returns, that identify the Reynolds number for a dispersed phase:

$$Re_r = \frac{\rho_c D |u - v|}{\mu_c} \quad (3.11)$$

where μ_c is the kinematic viscosity of the liquid. Combining the equation 3.10 with the equation 3.11, it is possible to obtain:

$$\frac{dv}{dt} = \frac{18\mu_c C_D Re_r}{\rho_d D^2} \frac{24}{24} (u - v) \quad (3.12)$$

From this, the *momentum (velocity) response time* can result as follows:

$$\tau_V = \frac{(u - v)}{\frac{dv}{dt}} = \frac{\rho_d D^2}{18\mu_c C_D Re_r} \frac{24}{24} \quad (3.13)$$

Going to integrate this equation over time, the momentum response time is obtained. This gives the time required for a particle to achieve 63% of the free stream velocity. The value of this quantity, depends, in a very sensitive way, on the particle size.

The other fundamental dimensionless parameter, for fluid-particle flows, is the *Stokes number*. With reference to the particles, this number is defined as:

$$St_V = \frac{\tau_V}{\tau_F} \quad (3.14)$$

where τ_V is the relaxation time of the particles and τ_F is a characteristic time of the flow. This last can be reformulated in the following way:

$$St_V = \frac{\tau_V U}{D_T} \quad (3.15)$$

where U is the undisturbed velocity flow and D_T the throat diameter of the duct. As described in section 2.3 of chapter 2, when $St_V \ll 1$ there is a coupling between the two phases. In particular, the response time of the particles is much less than the characteristic time of the flow. Therefore, the velocities of particles and flow are nearly equal between them. With this consideration, the affirmation, at the end of the section 2.3 of chapter 2, can be confirmed. In fact, as just mentioned, since Stokes number is less than unity, the two velocities are close to each other and there is a reciprocal coupling. So, the Reynolds number for particles doesn't depend on the flow velocity but only on the particle diameter. Varying the velocity of the fluid, also the velocity of the particles will change.

Another estimate to make, concerns the behaviour of the particles with references to collisions. To do this, the following ratio can be used:

$$\frac{\tau_V}{\tau_C} \quad (3.16)$$

where τ_C is the average time between particle-particle collisions and τ_V is defined with equation 3.13. When this ratio is less than unity, the flow can be considered dilute, and the particles have sufficient time to react to local fluid dynamics forces before the next collision. On the other hand, if this ratio is greater than one, the flow is dense and the particle-particle collisions prevail.

To determine the *characteristic collision time* τ_C , the classic equations for collision frequency can be used. Let's take a group of particles with diameter D , one of these is travelling with relative velocity v_r compared to that one of the other particles. Considering a tube of radius $2 \cdot D$ and length $v_r \cdot \delta t$, this particle will intercept all the other particles in a time δt . The number of these particles is:

$$\delta N = n\pi D^2 v_r \delta t \quad (3.17)$$

where n is the number density of the particles, defined above. The *frequency collision* is:

$$f_c = n\pi D^2 v_r \quad (3.18)$$

and, finally, the characteristic collision time is:

$$\tau_C = \frac{1}{f_c} = \frac{1}{n\pi D^2 v_r} \quad (3.19)$$

In figure 3.3, the different conditions of when a flow can be considered dilute or dense, are represented. The particles used for the representation are made of glass and the continuum phase is air.

Many mechanism can affect on the collisions between particles. Among these there are for example local turbulence, transport flow velocity changes, particle-wall collisions and so on. Caused by this, is difficult to determine the behaviour of the flow, if it is dilute or dense. A parameter that can give a rough idea, is the particle volume fraction α_d . The dense zone of the flow is further divide in two parts: a *collision-dominated* and a *contact-dominated* regime. In the first type of flow, the particles collide between them and they change their trajectory. This zone can be identified with a range of values of the indicator of $0.001 < \alpha_d < 0.1$. For this work, as it will be specified later, with 100 particles, this parameter takes the value of $\alpha_d = 0.03$. Therefore, this first type is the regime that occurs in the considered phenomenon. Instead, the second condition occurs when the particles are in continuous

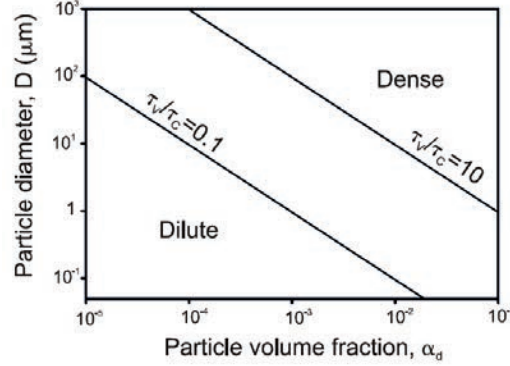


Figure 3.3: Graph of zones of dilute and dense flow, and the transition slot. The particles considered are made of glass and the flow is air with a fluctuating velocity magnitude of $1 \frac{m}{s}$. Figure adapted from Crowe et al. 2012.

contact and this is the main reason that causes the motion. For this case the range worth $0.1 < \alpha_d$. Finally, when $\alpha_d < 0.001$ the flow is in a dilute regime.

Another main aspect to control is the coupling between the two phases. This phenomenon can be reciprocal or not. If one phase influence the other one, without any reverse effect, the flow is said *one-way coupled*. Otherwise, if there are mutual effects, it is called *two-way coupled*. The coupling is possible through three type of exchange:

- *mass coupling*: it can occur with condensation or evaporation between the phases. Let's consider a gas flow, with n droplets per unit volume, in a box with side L . If each droplet evaporate with a given mass rate \dot{m} , the mass produced per unit time by the dispersed phase and added to the continuum phase is:

$$\dot{M}_d = nL^3\dot{m} \quad (3.20)$$

The flow rate of the continuum phase is:

$$\dot{M}_c \sim \bar{\rho}_c u L^2 \quad (3.21)$$

Now a *mass coupling parameter* can be defined:

$$\Pi_{\text{mass}} = \frac{\dot{M}_d}{\dot{M}_c} \quad (3.22)$$

If this parameter is much less than unity, the mass transfer may be neglected. There can be defined a Stokes number for the mass transfer:

$$St_{\text{mass}} = \frac{\tau_m u}{L} \quad (3.23)$$

where τ_m is a characteristic evaporation, burning or condensation time and the other parameters are known. Finally, remembering the definition of the mass concentration, the mass coupling parameter can be rewritten as:

$$\Pi_{\text{mass}} = \frac{C}{St_{\text{mass}}} \quad (3.24)$$

- *momentum coupling*: it is the result of the combination of the drag force of the dispersed phase with the momentum flux of the continuous phase. The *momentum coupling parameter* can be determined as:

$$\Pi_{\text{mom}} = \frac{F_D}{Mom_c} \quad (3.25)$$

with F_D the drag force of the particles and Mom_c is the momentum flux. For spherical particles, the first one can be defined as:

$$F_D = nL^3 3\pi\mu_c D(u - v) \quad (3.26)$$

while the second takes the form of:

$$Mom_c = \bar{\rho}_c u^2 L^2 \quad (3.27)$$

As before, considering a mass concentration C , a characteristic time of the flow τ_v and a Stokes number for the momentum transfer can be related as follows:

$$St_{\text{mom}} = \frac{\tau_v u}{L} \quad (3.28)$$

Therefore, the momentum coupling can be expressed as follows:

$$Mom_c = \frac{C}{St_{\text{mom}}} \left(1 - \frac{v}{u}\right) \quad (3.29)$$

If, as in this work, the Stokes number can approach to zero, this parameter become:

$$Mom_c = \frac{C}{1 + St_{\text{mom}}} \quad (3.30)$$

- *energy coupling*: this coupling can be assessed by comparing the heat transfer of the dispersed phase with the energy flux of the continuous phase. For this third condition, the *energy coupling parameter* worth:

$$\Pi_{\text{ener}} = \frac{\dot{Q}_d}{\dot{E}_c} \quad (3.31)$$

Also for the other two parameters, if it assumes values much less than unity, the energy coupling can be neglected. The heat transfer can have the form of:

$$\dot{Q}_d = nL^3\pi N_u k'_c D(T_d - T_c) \quad (3.32)$$

where N_u is the *Nusselt number*, k'_c is the thermal conductivity of the continuum and T_i are the temperatures of the two phases. The energy flux of the continuous phase is defined as:

$$\dot{E}_c = \bar{\rho}_c u c_p T_c L^2 \quad (3.33)$$

where c_p is the specific heat at constant pressure of the continuum. A Stokes number can be defined as:

$$St_T = \frac{u\tau_T}{L} \quad (3.34)$$

with τ_T a thermal response time. Taking account, as usually, of the mass concentration C , the energy coupling can be expressed as:

$$\Pi_{\text{ener}} \sim \frac{C}{St_T} \left(1 - \frac{T_c}{T_d}\right) \quad (3.35)$$

If the Stokes number approaches to zero, the expression becomes:

$$\Pi_{\text{ener}} = \frac{C}{1 + St_T} \quad (3.36)$$

These three aspects are just explained singularly, but often they can occur simultaneously and they can also be coupled to each other. For example thermal and kinetic energy can be transferred due to the mass transfer. However, for the model considered in this work, the possible coupling is only one, the momentum coupling, since that there are no mass or heat transfers.

In this section, the main aspects of a multiphase flow have been treated. The fundamental parameters have been shown, to understand which particular assumptions have to be made depending on which characteristics are more or less relevant. Besides all this, turbulence plays a fundamental role because it influences the way to analyse the equations, which further assumptions have to be made and it changes the behaviour of both the particles and the fluid. In fact, the implemented numerical model takes into account of all the aspects described above. In the following part, the crucial point on which all the work is based, is finally examined, that is the *IBM method*.

3.4 IBM

Once the conditions of the flow have been explained, the methodology, used to implement the numerical model, remains to be examined. Direct numerical simulations (DNS) of *particle-laden flows* can be performed with different numerical approaches proposed in literature. For example, some methods are *Physalis* in Sierakowski et al. 2016, *force coupling* in Lomholt et al. 2003 and *front-tracking* in Unverdi et al. 1992. A tool becomes popular in recent years is the *Immersed Boundary Method (IBM)*. It can provide a very accurate modelling of several models. Furthermore, it exploits efficient computational algorithms to solve the Navier-Stokes equations on a Cartesian grid. The introduction of this method is attributed to Peskin 1972, who first developed it. In his paper, he modelled the blood flow joined with a variable boundary geometry, as the flexible leaflet of a human heart valve. The discretized domain is a rectangular Cartesian grid, and the boundaries are replaced by a force introduced in the Navier-Stokes equation. This permits to have a simple discretization of the domain. In fact, it does not fit the boundary shape of particles and walls.

There are multiple advantages to treat the boundaries immersed in a rectangular domain:

- referring to the main argument of Peskin 1972, an heart-valve leaflet, this method is the only reasonable method to model this phenomenon. But the same discussion can be made for several other problems, whose implementation, with other techniques, would be impracticable;
- the discrete equations of motion of the fluid can be taken in an identical way at all the mesh points of the rectangular domain. There isn't distinction between points inside, outside, or near the edge of the region of interest;
- availability of very fast stable direct methods for solving Poisson's equation on rectangular domain.

The discretization grid, in an IBM, uses two types of coordinate systems. The first one is associated to the fluid and it is an *Eulerian coordinate system*. The flow is represented as function of time and space. The observer is in solidarity with a fixed reference point and he photographs the velocity field at each instant of time. The second type is the *Lagrangian coordinate system* and it is associated to the structure and particles. The attention is not focused on the fluid, but on a single fluid particle. So, the properties of the flow are functions of the specific fluid element and time. Considering

a function \bar{f} , the relationship between these two coordinate systems is the following:

$$\frac{Df}{Dt} = \frac{\partial f}{\partial t} + \langle \bar{\mathbf{v}} \rangle \cdot \nabla f \quad (3.37)$$

where $\frac{D}{Dt}$ is the *Lagrangian derivative*, called also *material derivative*, $\frac{\partial}{\partial t}$ is the *Eulerian derivative* and $\langle \bar{\mathbf{v}} \rangle \cdot \nabla f$ is the advection term.

The use of IBM becomes very useful with complex geometries, variable boundaries and fluid-solid interactions. From these explained aspects, this method results to be an excellent solution also for the purpose of this thesis. After this preliminary introduction to the IBM implementation, now, the specific model, used in this work, is treated in all its aspects.

3.4.1 The Navier-Stokes equations

In the introduction and in the previous chapters, the *Navier-Stokes equations* have been mentioned many times, but only in a qualitative way. Now, the physical principles on which they are based and their final form will be described.

Generally, the *Navier-Stokes equations* are a system of partial differential equations and they describe the behaviour of a fluid from a macroscopic point of view. The first principle, which must be respected, is that the flow can be modelled as a continuous deformable mean. This means that they are not applicable to rarefied gas. The flow is considered a viscous flow in the three-dimensional space. These equations can be expressed in two forms: an integral one and a differential one. However, for the sake of brevity, here, only the differential form will be obtained.

Let's consider a three-dimensional infinitesimally small moving fluid element of fixed mass. To this portion of the fluid, the Newton's second law have to be applied:

$$\bar{\mathbf{F}} = m \cdot \bar{\mathbf{a}} \quad (3.38)$$

The three-dimensional vector $\bar{\mathbf{F}}$ represents the resultant of all the body and surfaces forces acting on the fluid element in all three directions. For the moment the body force is ignored, but it will be reintroduced later for the equations of the IBM model. Now, the acting force are due to the pressure and viscous stress distributions over the surface of the element, as in figure 3.4. The viscous stresses are referable to shear stress τ_{ij} con $i, j = x, y, z$.

Then, the mass of the element can be described as:

$$m = \rho dx dy dz \quad (3.39)$$

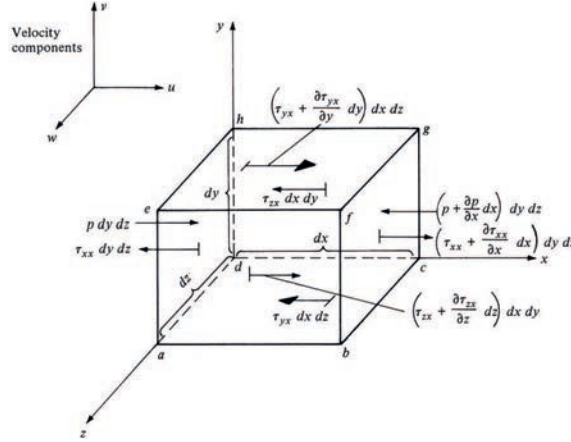


Figure 3.4: Considering an infinitesimally small moving fluid element, pressure and surfaces forces can be outlined. They act along all the surfaces of the element. Figure adapted from Anderson 2009.

where ρ is the density of the fluid. Accelerations, in the equation 3.38, are given in the following differential forms for the three directions:

$$a_x = \frac{Du}{Dt} \quad a_y = \frac{Dv}{Dt} \quad a_z = \frac{Dw}{Dt} \quad (3.40)$$

Where $\frac{D}{Dt}$ represents the total derivative. Finally, combining the different terms and adding the body forces $\bar{\mathbf{f}}$, the *momentum equation* in the differential form is obtained as follows:

$$\rho \frac{D\bar{\mathbf{U}}}{Dt} = -\bar{\nabla} p + \bar{\nabla} \cdot \bar{\mathbf{T}} + \bar{\mathbf{f}} \quad (3.41)$$

where $\bar{\mathbf{U}}$ is the three-dimensional vector of the velocities (u, v, w), p is the pressure and $\bar{\mathbf{T}}$ is the stress tensor. This equation is valid for an unsteady, compressible, three-dimensional viscous flow.

The second one of the Navier-Stokes equations is the *continuity equation*. Starting from the physical principle that the mass can be neither destroyed nor created, and considering the mass that flows in the unit of area in the time dt , this equation in the partial differential form can be written as:

$$\frac{\partial \rho}{\partial t} + \bar{\nabla} \cdot (\rho \bar{\mathbf{U}}) = 0 \quad (3.42)$$

This equation is true for every type of fluid or condition and it is independent whether the flow is viscous or inviscid. The only assumption to be respected is that the fluid must be a continuum. Obviously, remembering the purpose of this work, since the fluid is water, this assumption is respected.

The last main equation is the *energy equation* and it works when there is an heat transfer to or from the fluid. This equation derives from the first law of thermodynamics, which is outlined in the following way:

$$A = B + C \quad (3.43)$$

where the three capital letters have the meaning of:

- **A**: rate of change of energy inside the element;
- **B**: net flux of heat into element;
- **C**: rate of work done on element due to pressure and stress forces on surface.

transforming these three concepts in formulas, the energy equation becomes:

$$\frac{\partial}{\partial t}[\rho(e + \frac{\bar{\mathbf{V}}^2}{2})] + \bar{\nabla} \cdot [\rho \bar{\mathbf{V}}(e + \frac{\bar{\mathbf{V}}^2}{2})] = \rho Q + \bar{\nabla} \cdot (k \bar{\nabla} T) + \bar{\mathbf{V}} \cdot \rho \bar{\mathbf{f}} + \bar{\nabla} \cdot (\bar{\mathbf{V}} \cdot \bar{\bar{\mathbf{T}}}) \quad (3.44)$$

Also in this case, it is valid for an unsteady, compressible, three-dimensional, viscous flow.

These equations, just mentioned, are the general dimensional Navier-Stokes equations. Regarding to the characteristics of the multiphase flow of this dissertation, some simplifications can be done. First of all, both in this work and in the model developed, the flow is assumed incompressible. With this consideration the continuity equation is not linked to the pressure. So, the mass conservation is a constraint on the only velocity field. Since, in this work, heat transfers are not considered and the flow is incompressible, the energy equation is useless. Therefore, only the continuity and momentum equations have been implemented to solve the duct.

Finally, these equations have to be changed in another form to be more useful to use. In fact, to ensure the dynamic similarity between different flows, it is better to treat the equations in a dimensionless form.

3.4.2 The equations of the model

Now that the Navier-Stokes equations have been shown, the numerical model created and analysed in Ardekani 2019 and used for this thesis, can be exposed here. In fact, as affirmed in the introduction of this chapter, the computational fluid dynamics is complex to implement, due to specific methods and convergence criteria that must be used to obtain a solution.

The resolution method, on which the model is based, is a *particle-resolved direct numerical simulation (PR-DNS)*. In fact, given the research purposes, this is the most suitable approach to solve the considered fluid domains, in order to get as much data as possible. The created program is applicable to a very large range of conditions. Particles can have a spherical/non-spherical shape. As already said, it is implemented with the IBM for the fluid-solid interactions with lubrication, friction and collision models for the close range particle-particle or particle-walls interactions. Moreover, the fluid can be both Newtonian and non-Newtonian and it may be subject to heat transfer, though this condition is unnecessary in the application for this work.

What makes the IBM so powerful, is the possibility to simulate the effects of the boundaries of particles or walls, through the addition of an extra force $\bar{\mathbf{f}}$. It is added to the right-hand side (hereinafter it will be shortened with *RHS*) of the momentum equation, creating virtual boundaries in the model.

With this consideration, the two Navier-Stokes equations become:

$$\frac{\partial \bar{\mathbf{u}}}{\partial t} + \bar{\nabla} \cdot \bar{\mathbf{u}} \otimes \bar{\mathbf{u}} = -\bar{\nabla} p + \frac{1}{Re} \bar{\nabla}^2 \bar{\mathbf{u}} + \bar{\mathbf{f}} \quad (3.45)$$

$$\bar{\nabla} \cdot \bar{\mathbf{u}} = 0 \quad (3.46)$$

where $\bar{\mathbf{u}}$ is the three-dimensional vector of the velocities and Re is the Reynolds number, and it is expressed in the general form as:

$$Re = \frac{u \cdot L}{\nu} \quad (3.47)$$

with u the velocity of the flow respect to the object, L a characteristic linear dimension and ν the kinematic viscosity of the fluid.

The force $\bar{\mathbf{f}}$ is the IBM force distribution, close to a solid surface, to impose the *no-slip (ns)* or *no-penetration (np)* boundary condition. This force doesn't have an unique formulation but it can be formulated in different ways, depending on the method chosen. Obviously, the first way of calculating an expression of $\bar{\mathbf{f}}$ is attributed to Peskin 1972. Then, many modifications and improvements have been developed, in Mittal et al. 2005. The determination of $\bar{\mathbf{f}}$ can be made in two ways:

- *continuous forcing*: $\bar{\mathbf{f}}$ is calculated based on the fluid velocity of a point at the interface and the desired velocity at that point. In this way, the force is added to the RHS of the momentum equation before discretization and it doesn't depend on the numerical scheme used to solve Navier-Stokes equations. This approach is commonly used to simulate elastic boundaries. In fact, Peskin applied this method to simulate blood flow in a beating heart, through the use of elastic fibers joined with the *Hooke's law*.

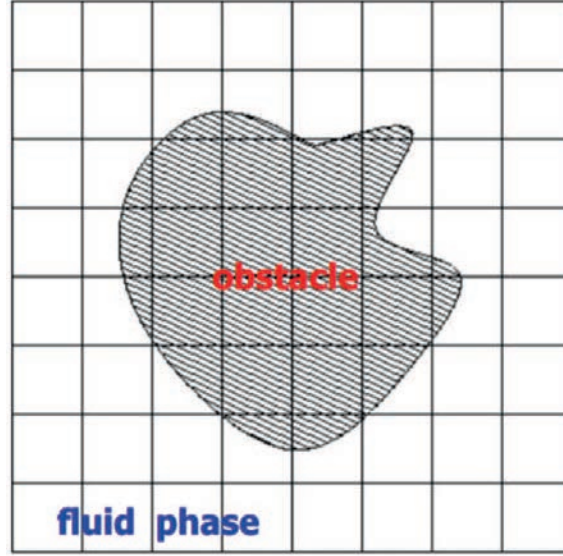


Figure 3.5: Schematic representation of a multiphase flow, with a rectangular cartesian grid, indifferently if there is the obstacle or not. Figure adapted from Ardekani 2019.

- *discrete forcing*: this method is, instead, used for rigid boundaries. Here, the force $\bar{\mathbf{f}}$ is added after the discretization and it depends on the numerical scheme. This approach allows a better control over the numerical accuracy, stability and conservation of the forces.

In the study made in Ardekani 2019, to develop the numerical model, different approaches have been used to obtain different results. The equations are always the same, but they are implemented in different ways, depending on the geometries or conditions. For this work, since the geometry is curvilinear and the boundaries are rigid, the discrete forcing approach is used and it is explained in the following parts.

3.4.3 Volume penalization

When discretized equations have to be solved on a grid, they are applied node by node. The choice, of how it have to be implemented and how to move on the grid, influences the convergence of the program and how to obtain the solution. There are two types of discretization grids. The simplest is a *collocate grid*. It solves all the variables (u, v, w, p) at the same point, but the Navier-Stokes equations have to be modified in order to stabilize them. The other one, that has been used for this model, is the *staggered grid*. In figure 3.6, this type of grid is shown, including a solid boundary. It is a

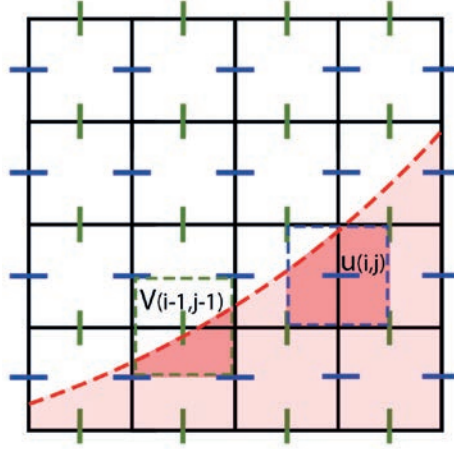


Figure 3.6: Schematic representation of a staggered grid with a curvilinear geometric boundary. Figure adapted from Ardekani 2019.

two-dimensional grid, but in the model, it have been implemented as a three-dimensional grid. It computes the different variables at different points of the grid. Considering a cell, the pressure is calculated at the centre of it, while the velocities are computed at the edges of every face. This implementation allows to avoid checkerboarding oscillatory solutions and a coupling between pressure and velocity.

The method underlying the implementation considered, is the *finite-volume/pressure-correction scheme*. It consists to solve the momentum equation for a provisional velocity, obtained by velocity and pressure of the previous step. Then, through the continuity equation and using the provisional velocity, a correction is obtained.

The *volume penalization method* was proposed by Breugem et al. 2014 and Kajishima et al. 2001. The integration in time is based on different schemes for equation terms, but both are second-order accurate in time. A Crank-Nicolson scheme is used for the pressure-gradient term, while the other terms are implemented with an Adams-Bashforth scheme. The first prediction velocity is computed as follows:

$$\bar{\mathbf{u}}^* = \bar{\mathbf{u}}^n + \frac{\Delta t}{\rho_f} \left(-\nabla p^{n-\frac{1}{2}} + \frac{3}{2} \mathbf{rhs}^n - \frac{1}{2} \mathbf{rhs}^{n-1} \right) \quad (3.48)$$

where Δt is the delta time used in the simulation and it is variable between the different iterations. From the determination of this velocity, the IBM force $\bar{\mathbf{f}}$ is obtained with:

$$\bar{\mathbf{f}}_{ijk} = a_{ijk} \frac{(\bar{\mathbf{u}}_s - \bar{\mathbf{u}}^*)_{ijk}}{\Delta t} \quad (3.49)$$

where a_{ijk} is the solid volume fraction in the grid cell with index (i, j, k) and it varies between 0 (the cell is located entirely in the fluid phase) and 1 (entirely in the solid phase), $\bar{\mathbf{u}}_s$ is the velocity at the interface between solid and liquid phase, within this grid cell.

Now, the second prediction velocity is given by:

$$\bar{\mathbf{u}}^{**}_{ijk} = \bar{\mathbf{u}}^*_{ijk} + \Delta t \bar{\mathbf{f}}^*_{ijk} \quad (3.50)$$

Using this velocity, the velocities and pressures are updated with the following equations:

$$\nabla^2 \hat{p} = \frac{\rho_f}{(\alpha_q + \beta_q) \Delta t} \nabla \cdot \bar{\mathbf{u}}^{**} \quad (3.51)$$

$$\bar{\mathbf{u}}^q = \bar{\mathbf{u}}^{**} - \frac{(\alpha_q + \beta_q) \Delta t}{\rho_f} \nabla \hat{p} \quad (3.52)$$

$$p^{q-\frac{1}{2}} = p^{q-\frac{3}{2}} + \hat{p} \quad (3.53)$$

where $\bar{\mathbf{u}}^q$ is the velocity at the Runge-Kutta sub-step q and α_q and β_q are two coefficient whose values are adjusted with the simulation.

In case of an uniform Eulerian grid, where $\Delta x = \Delta y = \Delta z$, and the central-differencing scheme is used, time step Δt must respect a criterion for von Neumann stability:

$$\Delta t \leq \min \left(\frac{1.65 \Delta x^2}{12\nu_f}, \frac{\sqrt{3} \Delta x}{\sum_{i=1}^3 |u_i^q|} \right) \quad (3.54)$$

The volume penalization IBM is very efficient, and it permits to represent in an accurate way the walls, using a simple Cartesian grid. Since, it is a multiphase flow, also the equations for the particles have to be clarified.

3.4.4 Discrete forcing method for moving particles

To describe the motion of the particles, Breugem 2012 improved the method to fully resolve particle-laden flows, making it second order accurate in space. This is possible, by applying a multi-direct forcing scheme (Luo et al. 2007) to better approximate the no-slip/no-penetration (*ns/np*) boundary condition on the surface of the particles and by introducing a slight retraction of the grid points on the surface towards the interior. Such in this work, when the mass density ratio (particle over fluid density ratio) is near unity, there can be some instabilities of the code. The numerical stability was improved by a direct accounting of the inertia of the fluid contained within particles (Kempe et al. 2012).

In this thesis, the examined plastic particles are considered spherical, so, the next treatment will be referred to the shape of a sphere. The velocity $\bar{\mathbf{U}}_p$ of an infinitesimal particle segment at position $\bar{\mathbf{X}}$ can be expressed as a sum between a translational and a rotational velocity:

$$\bar{\mathbf{U}}_p = \bar{\mathbf{u}}_c + \omega_c \times \bar{\mathbf{r}} \quad (3.55)$$

where $\bar{\mathbf{r}} = \bar{\mathbf{X}} - \bar{\mathbf{x}}_c$ is the position vector relative to the particle centroid at $\bar{\mathbf{X}} = \bar{\mathbf{x}}_c$, $\bar{\mathbf{u}}_c$ is the translational velocity of the particle centroid and ω_c is the angular velocity of the particle. These two components of the velocity are described by the *Newton-Euler equations*:

$$\rho_p V_p \frac{d\bar{\mathbf{u}}_c}{dt} = \oint_{\partial V} \bar{\bar{\tau}} \cdot \bar{\mathbf{n}} dA + (\rho_p - \rho_f) V_p \bar{\mathbf{g}} - V_p \nabla p_e + \bar{\mathbf{F}}_C \quad (3.56)$$

$$I_p \frac{d\omega_c}{dt} = \oint_{\partial V} \bar{\mathbf{r}} \times (\bar{\bar{\tau}} \cdot \bar{\mathbf{n}}) dA + \bar{\mathbf{T}}_c \quad (3.57)$$

where ρ_p and ρ_f indicate the particle and liquid densities, respectively, V_p is the volume of the particle and it is equal to $V_p = (\frac{4}{3})\pi R^3$, $\bar{\mathbf{n}}$ is the outward-pointing unit normal at the surface ∂V of the particle, $\bar{\mathbf{g}}$ is the gravitational acceleration and I_p is the moment of inertia of the particle and equal to $I_p = (\frac{2}{5})\rho_p V_p R^2$. $\bar{\mathbf{F}}_c$ and $\bar{\mathbf{T}}_c$ represent, respectively, the force and the torque acting on the particle as a result of collisions/physical contact with other particles or solid walls. The symbol $\bar{\bar{\tau}}$ represents the stress tensor for a Newtonian fluid:

$$\bar{\bar{\tau}} = -p\bar{\bar{\mathbf{I}}} + \mu_f(\nabla \bar{\mathbf{u}} + \nabla \bar{\mathbf{u}}^T) \quad (3.58)$$

with $\bar{\bar{\mathbf{I}}}$ the unit tensor.

The equations 3.45 and 3.46 are coupled with the equations 3.56 and 3.57 through the *ns/np* condition on the surface of the particle:

$$\bar{\mathbf{u}} = \bar{\mathbf{U}}_p(\bar{\mathbf{X}}) \quad \forall \quad \bar{\mathbf{X}} \in \partial V \quad (3.59)$$

All these equations are the main ones to implement the numerical model. The IBM is based on the definition of a force that simulates the boundaries. The schematic procedure to determine it, is the following:

- interpolation of the first prediction velocity $\bar{\mathbf{u}}^*$ from the Eulerian to the Lagrangian grid;
- computation of the IBM force on the Lagrangian grid based on the difference between the interpolated first prediction velocity and the particle velocity;

- spreading of this force from the Lagrangian to the Eulerian grid.

At this point, the treatment of the numerical model has been completed. In the next chapter, it will be adapted to the project of this work, and several simulations will be analysed and shown, in order to examine the numerical results of the serpentine.

Chapter 4

Analyses

Finally, in this chapter, the simulations done will be examined, in order to show the veracity of the numerical model and some aspects that can be hidden in the real experiments. First of all, the setup of the simulations and the criteria used will be described. Then, the behaviour of the only fluid phase will be analysed. Finally, the particles will be added and the behaviour of the multiphase flow can be exposed. This last part will be the greatest since different aspects of particles must be defined.

4.1 Setup of the model

4.1.1 Configuration model

The problem considered in this thesis has been implemented through the numerical model created in Ardekani 2019. However, this latter can't be used directly, but different adjustments have to be made, to ensure stability and truthfulness to the specific model. The first thing is to define the geometry into the code, by defining which areas are solid and on which there may be the flow. Once this is fixed, the model can solve the equations depending on whether that point is occupied by fluid or solid.

Now, the model is ready to carry out several simulations, changing the specific parameters, that have to be tested in this work. Before starting the simulations, the case, that has to be tested, must be defined. The first differentiation between the different simulations is to change the geometry of the duct. More specifically, the ratio $\frac{L_1}{L_2}$, specified in figure 2.1(b) of section 2.2, is changed, in the different sets of simulations. The three types of geometries, that have been supposed, are shown in figure 4.1. With these different geometries, the change in the behaviour of the flow and the particles,

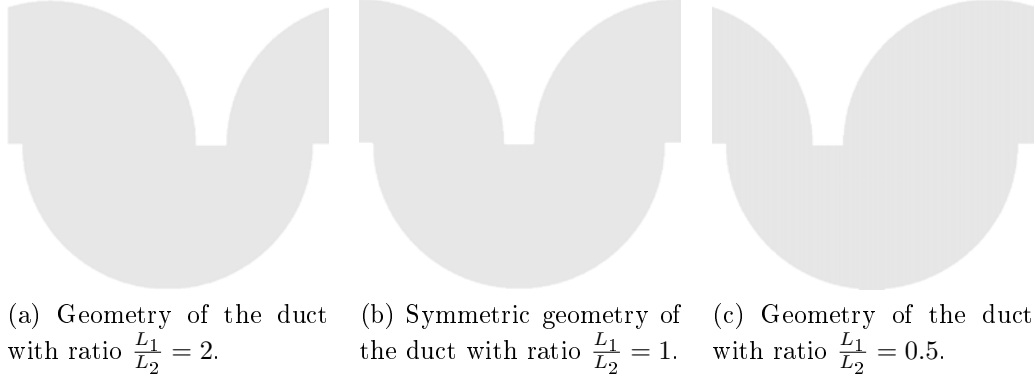


Figure 4.1: Representation of the three geometries used in simulations, with different ratio $\frac{L_1}{L_2}$. With grey colour it is highlighted the part of the domain where the flow can pass.

wants to be observed. With the geometries shown, it's good to precise the orientation of the reference axes, right away. Then, in all the subsequent treatise, the orientation of the coordinate system will be the same. With reference to one of the three images in figure 4.1, the point $\langle 0, 0, 0 \rangle$ is the lower-left corner. The horizontal axis is the y -axis and it goes from left to right, the velocity is v . The vertical axis is the z -axis and it goes from the bottom to the top, with the velocity w . Finally, the x -axis completes the *right-handed coordinate system*, with the velocity u .

The real device is a serpentine composed of eight double curves. The domain results to be very expensive, from the computational point of view. However, one of the strengths of this model is the periodicity. In fact, to make lighter the simulations there are two periodicity conditions. The first one is on x -direction, so the first and the last velocity, in this direction, is the same. The second one is on the y -direction. In this case, the flow that go-out on the right side, it enters again in the duct from left. The particles will behave in the same way. These impositions permit to solve a phenomenon, with a smaller model in a faster way.

The numerical model can solve problems, starting from different types of elementary flow. In these cases, it is assumed as a laminar flow of an incompressible Newtonian fluid. In particular, the two main possible flows can be:

- *Couette flow*: it is a drag-induced flow between parallel flat plates or between concentric rotating cylinders.
- *Poiseuille flow*: it is a pressure-induced flow. This is the initial flow

used in these simulations. The turbulent regime is achieved through the insertion of some initial noise, that allows the flow to evolve in this regime.

The implemented Navier-Stokes equations are in a dimensionless form. As specified in the previous chapter, for the simulations carried out in this work, the particles are considered all as spheres. Therefore, the diameter of the spheres is the unit of measurement for the dimensions. Further considerations, on the dimensions of the particles, will be made in subsection 4.1.2. For the moment is sufficient to know that, based on the choice of the particle diameter, the domain has a length along the y -axis of 17.6, while along the z -axis the size is 16. The radius of the curvature of the curves is 8.

The size of the domain has been defined in relation to the particle diameter. However, equations are solved in a discretized domain. So, each of the three directions has to be divided into an appropriate number of nodes, obtaining a 3D-matrix of points. To chose the number of nodes, the *resolution* is used. It refers to how many points the unit diameter is divided. Fewer of them are chosen, less precise the results will be. On the contrary, more nodes are used, much more the computational cost will be high. Based on Picano et al. 2015, a good number of points per unit of diameter is 16. To have better accuracy in modelling the flow, in these simulations, a resolution of thirty points per unit of measurement has been chosen. Consequently, the domain will have, in the two specified directions y and z , a number of nodes equal to 528 and 480, respectively.

To choose the dimension of the domain along the x -axis, the situation is different. In fact, the real dimension of the device is much larger compared to a single chamber. Choosing the real dimension rescaled for the x -direction, the computational cost will be enormous. Since, in the model there is a condition of periodicity, this length could be chosen arbitrarily. That's not entirely true, in fact, the x -dimension must satisfy two lower limits. In the simulations with particles, that have been carried out, one hundred particles have been located in the fluid domain. In x -direction, there are groups of five particles that are aligned with each other. The first limit is that the x -dimension must be able to contain the particles, with a small distance between one another, 0.5. The second lower limit is more complex, and it is based on *correlation*.

Correlation is a statistical property and it represents a relationship between two different variables and for each value of the first one, corresponds a value of the second one. The degree of association is measured by a *correlation coefficient*. It can assume a variable real value between -1 (*inverse correlation*) and +1 (*direct correlation*). Obviously, when the coefficient is

zero, there is no correlation. The general formula to determine this index is expressed through the *Pearson's correlation coefficient*:

$$l = \frac{\sigma_{xy}}{\sigma_y \sigma_x} = \frac{\sum_{i=1}^n (x_i - \mu_x)(y_i - \mu_y)}{\sqrt{\sum_{i=1}^n (x_i - \mu_x)^2} \cdot \sqrt{\sum_{i=1}^n (y_i - \mu_y)^2}} \quad (4.1)$$

In particular, it is the ratio between the covariance of the two variables σ_{xy} and the product of the standard deviation, σ_x and σ_y .

Turbulence is a chaotic and randomly phenomenon. This means, that there must not be a correlation between the v velocities along the x -direction. Therefore, the x -length must be great enough to obtain a low correlation coefficient, close to zero. The opposite problem is that the longer the domain, the greater the computational cost. Therefore, a trade-off must be found.

At this point, to be able to determine if there is a correlation and for which length the correlation is negligible, some simulations, with different x -length and without particles, have been launched. The correlation coefficient has been computed for three different points of each geometry. The three selected points have been taken near the entrance of the duct, evenly spaced each other and with the walls. For each point, a certain number of velocities, variable in time, have been used. In fact, the created algorithm computes, for each point of the domain, the correlation coefficient mediated over time. Taking all the velocities fields, the correlation coefficient would be misrepresented. In fact, there is an initial transition phase where the fluid begins to flow. Therefore, the velocity fields have been considered after about thirty seconds of simulated time¹. After these analyses, an x -length of eight has been fixed and therefore it consists of 240 nodes.

In the three graphs in figure 4.2, the trend of the correlation coefficient is represented for the three different geometries with the chosen depth of eight. Each line shows how the coefficient of every point varies along the x -axis. The graph is developed for half of the conduct since the condition of periodicity results in the fact that the remaining part is specular. From these graphs, can be noticed that the correlation coefficient is small. Considering the interval $[0, 1]$, three slots can be identified:

- $0 < l < 0.3$: weak correlation;
- $0.3 < l < 0.7$: moderate correlation;
- $0.7 < l < 1$: strong correlation.

¹The simulated time, during which the fluid flows, is, obviously, different from the time required to simulate it.

Oppositely, it's true also for the interval $[-1, 0]$. Therefore, with the choice of this length in the x -direction, the correlation falls into the lowest category. Practically, the velocities result to be uncorrelated to each other. Turbulence can evolve in the duct without any deterministic behaviour.

At this point, the simulation domain has been analysed and defined. After that, which simulations have to be carried out, have been selected.

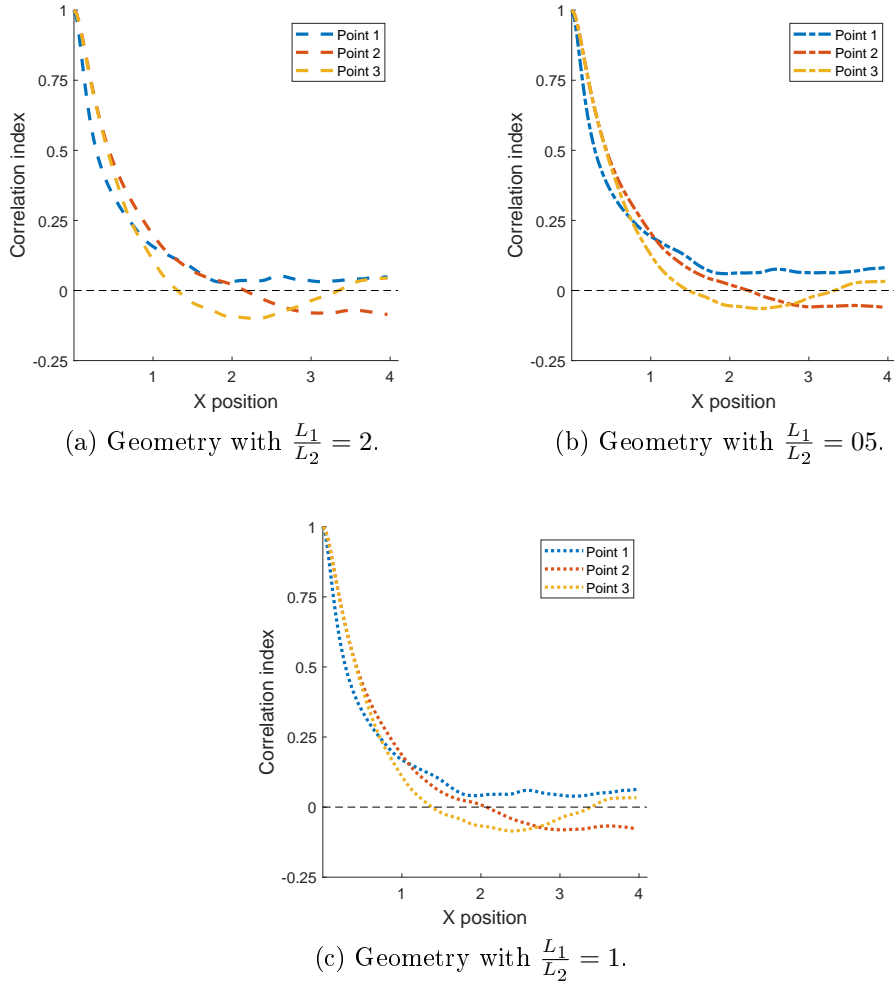


Figure 4.2: Trend of the correlation coefficient, in the x -direction, for the three chosen points in each geometry. The depth of the domain is eight.

4.1.2 Simulations parameters

Different types of simulations have been prepared and launched. An initial subdivision has already been defined, and it is based on the geometry. Two sets of simulations have been designed. The first one consists to simulate a single-phase flow, consisting of only water. Then, particles are added to this flow.

To be able to validate the model and to can affirm the correctness of the results, a similar case to those explained in Moroni, Lupo, et al. 2017, has been modelled. The model accepts as input, some parameters that outline the specific flow. For this problem, the Stokes number is less than unity, so the velocity of the particles is very similar to that of the fluid. Therefore, for the two Reynolds numbers, for the fluid and the particle, the velocity used is the same. The DNS simulations need low Reynolds numbers, in order to have not too great computational time. This because, the higher the Reynolds number, the more refined the grid must be, to simulate even the smallest eddies. Therefore, its value for the particles and the diameter of a real particle, are 270 and 0.003 m , respectively. To make a comparison of the model with the real experiment, the values shall be expressed in a dimensionless form. As has been said before, the diameter of the particle is the unit of measurement, so its dimensionless diameter is one. Exactly, for this reason, the domain has the dimensions specified in subsection 4.1.1. The Reynolds number remains the same since it is dimensionless. To make all dimensionless, an appropriate viscosity has to be inserted. At each step, a certain flow rate is set, so that the mean velocity is one. Referring to the equation 3.47, with these values, the dimensionless viscosity is expressed as:

$$\nu = \frac{1}{Re_p} \quad (4.2)$$

In this way, the flow of the model has the same characteristics as the real flow. At this point, the parameters of the fluid phase have been defined. The great part of simulations is though constituted by the presence of particles.

The idea is to simulate light plastic particles, which have a density near that of water, such as PC. When particles are immersed in a transport fluid, they are subjected to a resultant acceleration. It can be determined by the *Archimedes number* that is explained by the following expression:

$$Ar = \frac{a L^3 \left(\frac{\rho_p}{\rho_l} - 1 \right)}{\nu^2} \quad (4.3)$$

where L is a characteristic length, that in this case it is the particle diameter, a is the acceleration and ρ_l and ρ_p are the fluid and particles density,

Table 4.1: In this table are listed the ratio between the densities and the resulting number. The values with which the Archimedes numbers have been obtained are: $\nu = 8.9 \cdot 10^{-7} \frac{m^2}{s}$ for a temperature of $25^\circ C$, $L = 0.003 m$ and $a = g = 9.81 \frac{m}{s^2}$.

ρ_p $\frac{kg}{m^3}$	$\frac{\rho_p}{\rho_l}$	Ar
1050	1.05	16719
1100	1.10	33439
1150	1.15	50158
1200	1.20	66878
1250	1.25	83597

respectively. Regarding the acceleration, a clarification must be made. The value of the Archimedes number is computed using the gravity acceleration and the dimensional values.

Then, using that number, the acceleration in the numerical model is obtained, inserting the dimensionless quantity in the turned equation. The density and kinematic viscosity of the water are known. The particle densities and the other dimensionless parameters are listed in table 4.1.

These parameters just described are the values with which the simulations have been set. Therefore, there are three simulations with only a single-phase flow plus another five for each geometry with the presence of particles, for a total of 18 simulations. Finally, once the starting parameters have been defined, the results can be explained.

4.2 Single-phase flow

With the insertion of the right parameters and correcting properly² a coefficient that regulates the Δt^3 , the simulations, with the presence of the liquid phase only, can be started.

For each geometry, a simulation has been launched. The initial starting condition consists of a flow with a zero velocity. Through the imposition on the flow rate, specified above, the fluid begins to flow inside the duct. To ensure that it evolves in a turbulent regime, an interference in the initial velocities has been applied. This permits to obtain turbulent velocities,

²This was possible only after that the simulations started. With the advancement of them, the coefficient has been adjusted to the best value.

³At each step of the simulation, a Δt_{\max} is computed. The coefficient set the actual time step as a percentage of this latter, to avoid the divergence of the results.

progressing over time. From the classic definition of turbulence, it is an unsteady phenomenon but that has a constant mean velocity for every point. Therefore, there is an initial phase of transition, that tends to a steady field of the mean velocities. Obviously, the longer the simulation time, the more the mean field will tend to reach the final value of the steady velocities.

4.2.1 Mean velocities

Now, the mean velocities of the fluid phase are represented, in order to outline the movements of the flow.

The average of the u velocity, for the periodicity condition, tends to zero. So, the only two components that matter, are the v and w velocities. These last that are computed in the numerical model, varies both in time and space. To be able to manipulate easily the results, firstly an average over time has been made. Then, also an average in space has been executed. However, a clarification has to be explained. Because of the geometry, the velocities can't be summed to each other along the y - or z - direction. The average in space has to be made on the x -direction, and it is done for all the velocities. At this point, the mean velocities fields are available, and they can be represented graphically, as can be observed in figure 4.4. To be able to make a comparison with the numerical results, in figure 4.3 are brought again the velocities field of Moroni, Lupo, et al. 2017. Those images refer to the two extreme cases of flow rate. The flow, numerically simulated, is an intermediate case between those two.

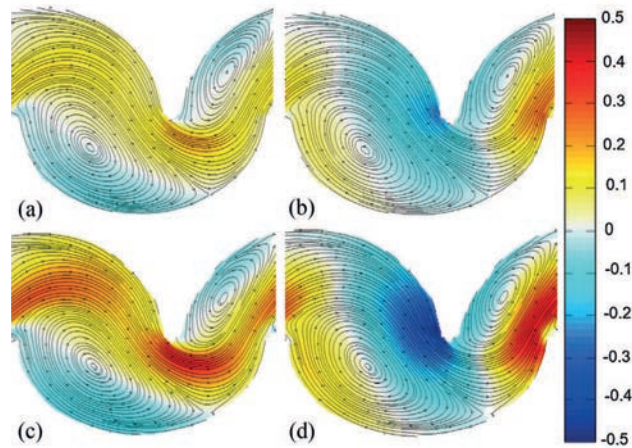
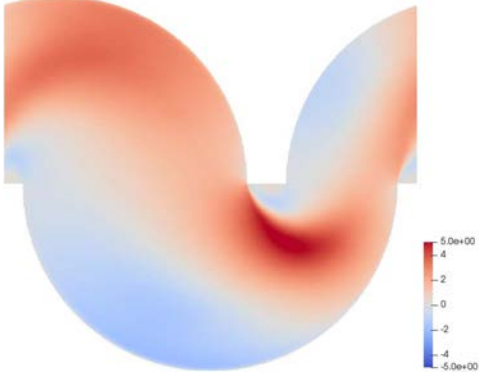
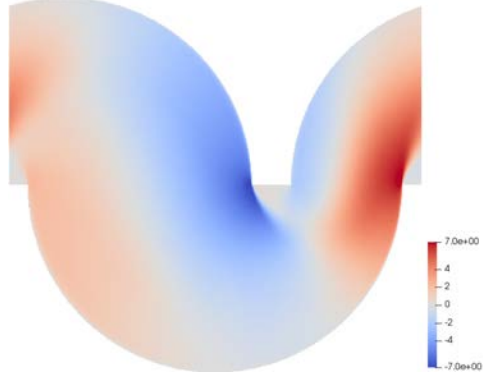


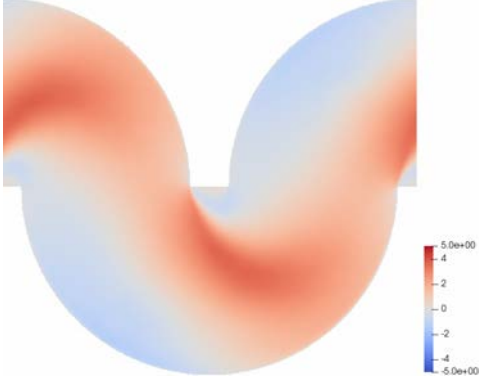
Figure 4.3: The flow in chamber C3 is shown. Images of the first line represent case 1 while the second line reproduces the case 9; (a) and (c) show the velocity v ; (b) and (d) show the velocity w . Figure adapted from Moroni, Lupo, et al. 2017.



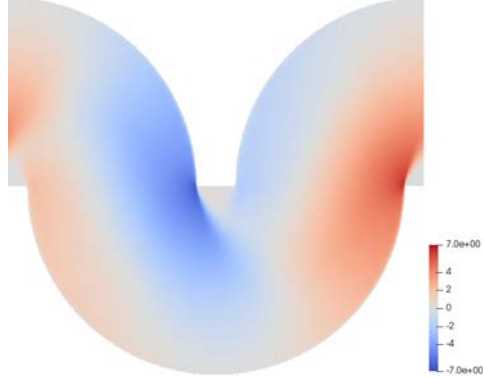
(a) Mean field of the velocity v , for the geometry with $\frac{L_1}{L_2} = 2$.



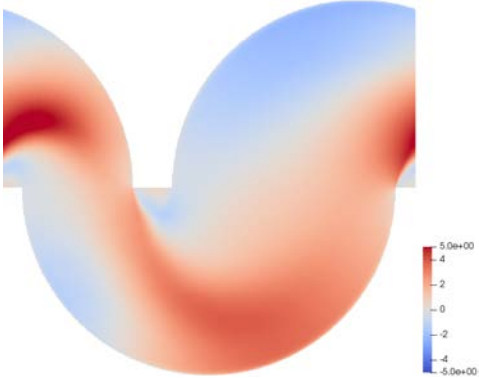
(b) Mean field of the velocity w , for the geometry with $\frac{L_1}{L_2} = 2$.



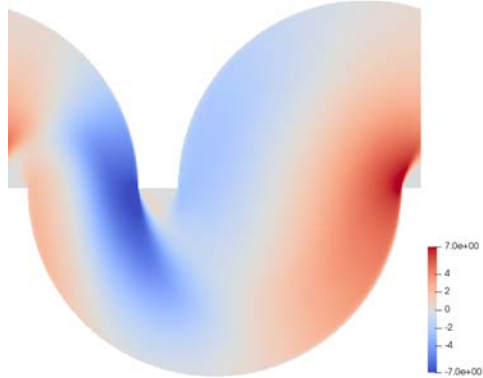
(c) Mean field of the velocity v , for the geometry with $\frac{L_1}{L_2} = 1$.



(d) Mean field of the velocity w , for the geometry with $\frac{L_1}{L_2} = 1$.



(e) Mean field of the velocity v , for the geometry with $\frac{L_1}{L_2} = 0.5$.



(f) Mean field of the velocity w , for the geometry with $\frac{L_1}{L_2} = 0.5$.

Figure 4.4: The mean fields of the velocities v and w for the single-phase flow are represented for each considered geometry. The velocities have been mediated over time and space, along the x-direction. The scale is dimensionless.

Paying more attention to the velocity v , a main transport current is observed. Obviously, it follows the shape of the duct. Due to curves, boundary layer separations are formed and the flow creates two recirculation zones, more or less large, depending on the geometry. The first one, in the lower left corner, observing the signs of the velocities, rotates clockwise. Instead, the second one rotates in the opposite way.

In particular:

- Geometry with $\frac{L_1}{L_2} = 2$: this is the geometry, where the ratio is almost the same of Moroni, Lupo, et al. 2017. It is represented in figures 4.4a and 4.4b. The flow goes in from the left with a direction to the upper right side and then it flows downward. On the bottom, it changes direction, moving upwards, and it accelerates, as a result of the narrowing of the section. Finally, it goes out with an almost vertical direction. As already mentioned, the simulated case is a middle way between the two cases in figure 4.3. However, comparing the colours, the same behaviour and the same areas are identifiable. So, can be affirmed that the model reproduces the real phenomenon well. In the left side of the inferior curve, a great recirculation area is visible.
- Geometry with $\frac{L_1}{L_2} = 0.5$: this geometry is the mirror image of the previous one. It is represented in figures 4.4e and 4.4f. The fluid goes in, always on the left side, with maximum velocity. Then, it gets slower due to the widening of the duct. This time, the greatest recirculation zone is located in the upper right side. It could be a good area to make the particles settle. In zero gravity, the effect of this geometry would be the same of the previous case. However, there is the influence of gravity that could change the behaviour of the particles. In fact, they could return more easily to the transport current, and they may have more difficulty to settle. In addition to this, the difficulty is increased by the small size of the lower recirculation zone.
- Geometry with $\frac{L_1}{L_2} = 1$: finally, this geometry is symmetrical with respect to the vertical axis with coordinate $y = 8.8$. It is represented in figures 4.4c and 4.4d. The effect of the symmetry also acts both on the velocities and on the behaviour of the flow. The two recirculation zones have the same area but less than other cases. So, the available space that the particles have, is the same for the two zones. The only difference between them is that they rotate in opposite directions to each other, as in the other two configurations.

In the two opposite geometries, there are two velocity v peaks. In the symmetric geometry, instead, the trend is more homogeneous and it is due to

the equal distribution of energy in the curves. In the same way, the two peaks of the velocity w , one positive and the other one negative, are mitigated for the symmetrical case.

4.2.2 Reynolds stress and kinetic energy

The mean velocities fields have just been explained. However, in the study of the flow, other important quantities can be extracted from the knowledge of instantaneous and mean velocities fields. One of these main quantities is *Reynolds Stress tensor*. Analytically, it is obtained from the averaging operation over the Navier-Stokes equations. With the *Einstein notation*, each component of the tensor can be expressed as follows:

$$\tau_{ij}' = \overline{u_i' u_j'} \quad (4.4)$$

where u_i' and u_j' are the fluctuating velocities of the Reynolds decomposition. Assuming an incompressible flow with a known density, stresses can be determined through only the velocities fields. In this work, the velocities have been obtained with the numerical model, so the Reynolds stress tensor can be computed and represented. Once the average velocities are known, they can be subtracted from the instantaneous values at different time steps, to obtain the fluctuating velocities and consequently the stress values. Finally, these instantaneous stresses are mediated over time and space, along the x -direction, as before. In this context, the results that depend on the velocity u , lose interest. In fact, this velocity is across the main direction of the flow. Therefore, it hasn't a precise trend, and it is chaotic. Below, only the stresses, depending on the other two velocities, will be treated. Therefore, the components that have to be analysed are three, because the tensor is also symmetrical.

The first stresses, those of the diagonal of the tensor, are shown in the figures 4.6. Some considerations on these stresses:

- τ_{22} : generally, the stress field is, in all the domain, near to zero. There are only two zones where this stress reaches a peak, and it is in the proximity of the edges. Furthermore, also the stripe between these two peaks has high values of the stress component, but its intensity depends on the geometry. It is noted, that the stresses of the biggest recirculation zone are practically null. This effect could be a parameter that influences the settlement of particles.
- τ_{33} : for these stresses, the behaviour is a little different. Considering the two geometries with $\frac{L_1}{L_2} \neq 1$, the zone where there is the narrowing

of the section, a strong increase of the stresses happens. This time, in the larger area, the stress is not zero but around one. Instead, for the symmetrical case, there is repetitiveness of the behaviour in each curve, and the intensities are generally lower. Considering zero gravity, for this geometry there is no distinction between descent and ascent of the flow, while the other two geometries behave identically. But, of course, with the presence of gravity, the effect on the particles is different.

After these comparisons, the last component of the stress tensor has to be analysed: τ_{32} . It is computed in the same way as before. To the product of the instantaneous values, the product between the mean velocities \bar{v} and \bar{w} is subtracted. Then, the average over time and space is performed. This stress is shown in the first column of the figure 4.7. Instead, in the second one, the behaviour of the *turbulent kinetic energy* is represented. It is the mean kinetic energy associated with eddies. It is computed as half of the sum of the variances of the velocity components, as follows:

$$TKE = \frac{v'^2 + w'^2}{2} \quad (4.5)$$

where v'^2 and w'^2 are the variances of the velocities v and w .

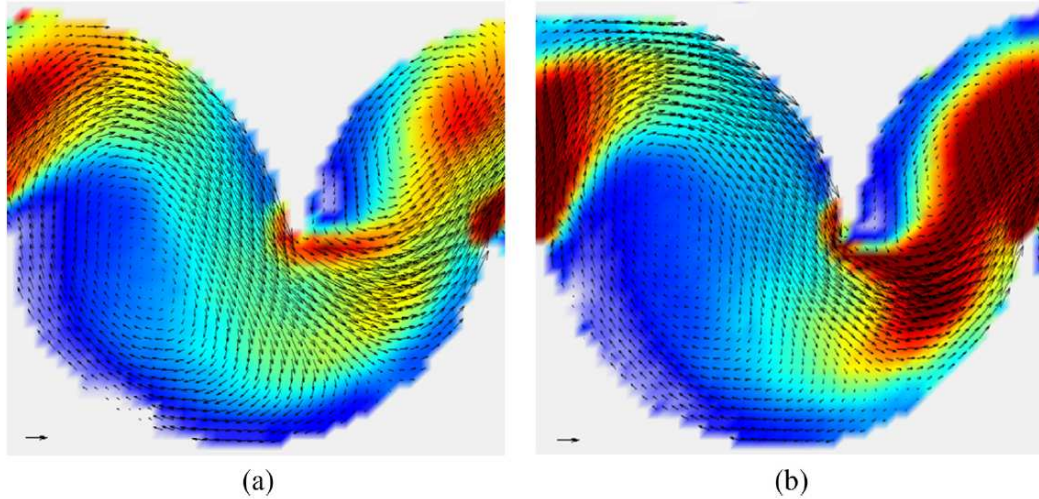
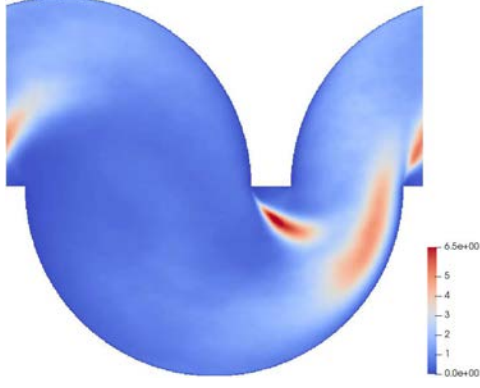
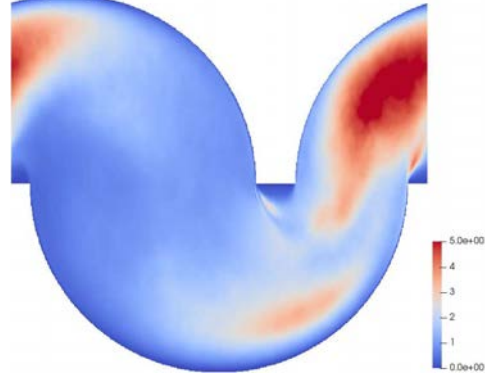


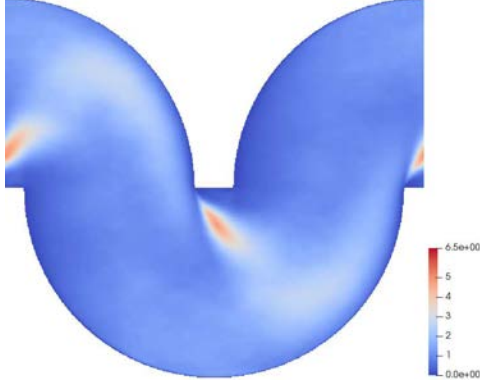
Figure 4.5: In these figures, the turbulent kinetic energy, computed in Moroni, Lupo, et al. 2017 is shown. (a) case #7. (b) case #2. Figure adapted from Moroni, Lupo, et al. 2017.



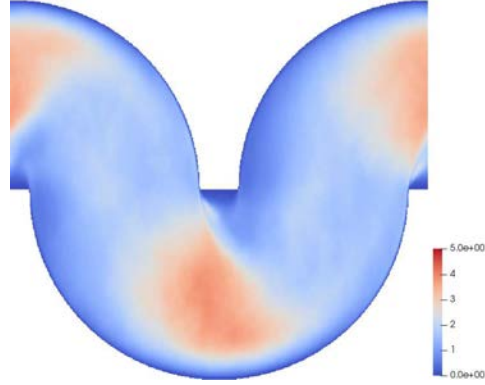
(a) Stress component τ_{22} , for the geometry with $\frac{L_1}{L_2} = 2$.



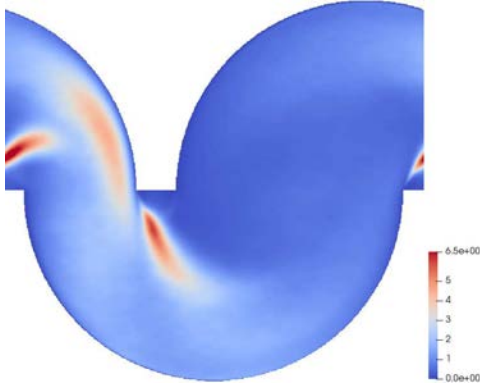
(b) Stress component τ_{33} , for the geometry with $\frac{L_1}{L_2} = 2$.



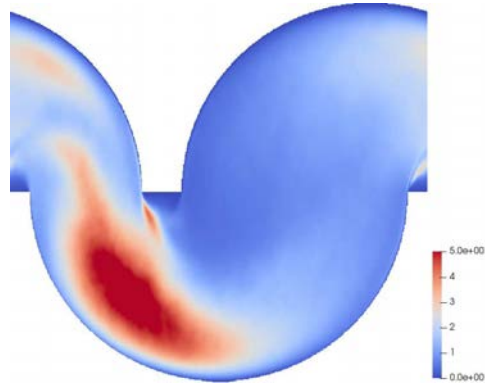
(c) Stress component τ_{22} , for the geometry with $\frac{L_1}{L_2} = 1$.



(d) Stress component τ_{33} , for the geometry with $\frac{L_1}{L_2} = 1$.

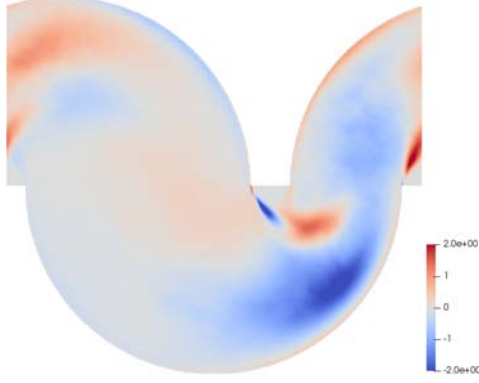


(e) Stress component τ_{22} , for the geometry with $\frac{L_1}{L_2} = 0.5$.

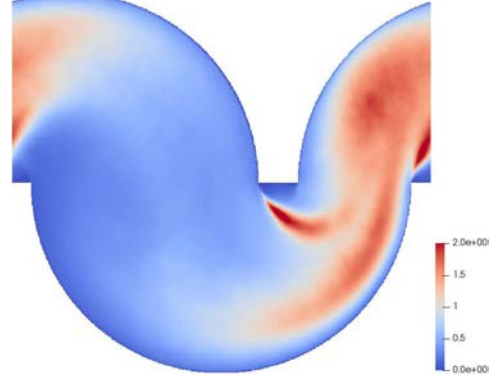


(f) Stress component τ_{33} , for the geometry with $\frac{L_1}{L_2} = 0.5$.

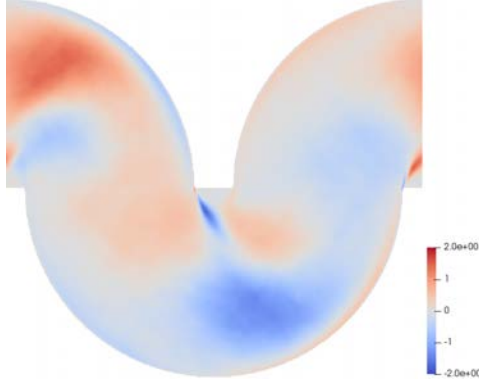
Figure 4.6: In these figures the components τ_{22} and τ_{33} of the Reynolds stress tensor, divided by the fluid density, are represented for each considered geometry. The fluctuating velocities, that make up stresses, have been first squared and then mediated in time e in space, along the x-direction. The scale is dimensionless.



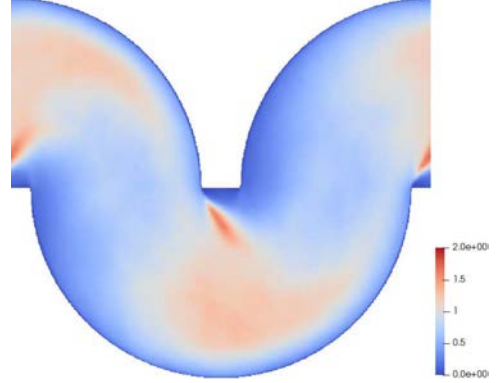
(a) Stress component τ_{32} , for the geometry with $\frac{L_1}{L_2} = 2$.



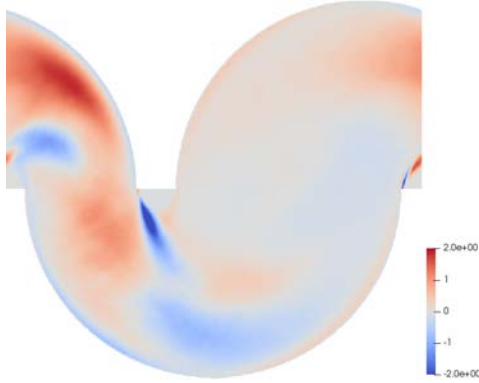
(b) Turbulent kinetic energy, for the geometry with $\frac{L_1}{L_2} = 2$.



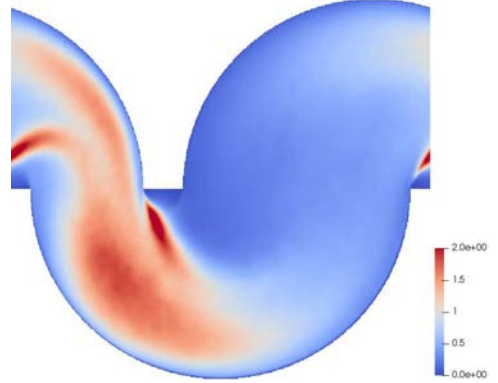
(c) Stress component τ_{32} , for the geometry with $\frac{L_1}{L_2} = 1$.



(d) Turbulent kinetic energy, for the geometry with $\frac{L_1}{L_2} = 1$.



(e) Stress component τ_{32} , for the geometry with $\frac{L_1}{L_2} = 0.5$.



(f) Turbulent kinetic energy, for the geometry with $\frac{L_1}{L_2} = 0.5$.

Figure 4.7: In the first column the component τ_{32} of the Reynolds stress tensor is represented. It is computed subtracting from the instantaneous velocities, the product between \bar{v} and \bar{w} . In the second column, with the use of the variance, the turbulent kinetic energy is shown. These components are represented for each geometry.

Physically, the quantities v' and w' are the fluctuation components of the velocity, compared to the mean value. The general formula, to calculate the variance, is the following:

$$\sigma_x^2 = \frac{\sum_i (x_i - \mu_x)^2}{n} \quad (4.6)$$

where μ_x is the mean value, and n the number of samples.

In figure 4.5, the trend of the turbulent kinetic energy, computed in Moroni, Lupo, et al. 2017, is shown. The figure 4.5(a), explain the turbulent kinetic energy for the case #7 of the same paper, while the figure 4.5(b) shows the case #2. The first one has the conditions closest to those of the simulations performed here. From the figures, it is noted that there are some peaks both positive and negative, of stresses and kinetic energy, where the section is narrower and when the flow passes around the edges. Instead, in the wider zone, both stresses τ_{32} and turbulent kinetic energy are near to zero. This means that the behaviour is less turbulent, with values closer to the averages ones. Considering the geometry with $\frac{L_1}{L_2} = 2$, the turbulent kinetic energy can be compared, through the figures 4.5, with the reference paper, in particular for the case #7. The colours of the different zones are practically the same, with a very similar variation of red and blue.

The geometry with $\frac{L_1}{L_2} = 0.5$, has the same behaviour of the previous one, but in a mirror image, and this is due to both geometry and direction. In fact, the intensity is the same, but the directions are opposite. For the stress τ_{32} , this results in two opposite colours: red and blue, for the same zones. In the case of the turbulent kinetic energy, the colours are the same, since the velocity is squared.

The symmetrical case, both for the stress and for the energy, is more homogeneous with less strong and more distributed variations. In fact, in all the domain, the values are around the average ones. The only exception is for the two peaks near the edges, that, however, are less intense than those of the other two configurations. Comparing the first half of the section, of these three geometries, it is noted that narrower is it, stronger are the values in this zone.

With these observations of velocities, stress, and kinetic energy, some peculiarities have been highlighted. In particular, some common characteristics have been explained, for which favourable areas for particles sedimentation can be defined. Their stresses and kinetic energy are near zero, this means that the velocities are around the average ones and recirculation zones are formed.

The behaviour of the single-phase flow has been completely defined, in all its aspects. Now, simulations with the insertion of the solid phase can be

launched.

4.3 Multiphase flow

Simulations with only the fluid phase, have been run and analysed, first. Now, the multiphase flow has to be analysed, in such a way that, considerations on how the particles are separated, can be made. When particles are added to the flow in simulations, the computational cost increases considerably. If these are launched with the presence of particles and zero flow velocities of the fluid, the simulation time becomes too long, before having analysable results. There is another solution that shortens this duration, and give the possibility to run much more simulation in less time.

4.3.1 Pressure gradient

A better way to run multiphase simulations is to add the particles when the flow has achieved a mean steady-state. The flow is turbulent, so it doesn't have a steady behaviour. However, its mean fields become steady when the flow is *fully developed*. To be able to understand when it is possible to add the particles, the trend over time of the pressure gradient is to observe. There is a transitory phase, but after a certain time, it settles down fluctuating around a mean value. When this happens, the flow is developed and therefore the particles can be located inside the domain. At each time step, the pressure gradient has an average value, which ensures that the mean velocity in the domain is unitary. In figure 4.8 can be observed this behaviour for the three different geometries.

There is an initial transitory phase where the pressure gradient has a very variable trend. After this first part, the gradient settles around an average value, with some oscillations. Here, the flow can be assumed as a *developed flow* and the particles can be added in simulations. This time is similar for all the three geometries and the chosen value is around 35 seconds of simulated time. The same duration of time is used to simulate even all cases with particles.

For these simulations, the density variation of the particles is chosen. The possible cases are five and light polymers have been simulated. These ones can have more difficult to settle in the different chambers because their density is near to that of water. The used densities are: $1050 \frac{kg}{m^3}$, $1100 \frac{kg}{m^3}$, $1150 \frac{kg}{m^3}$, $1200 \frac{kg}{m^3}$, $1250 \frac{kg}{m^3}$.

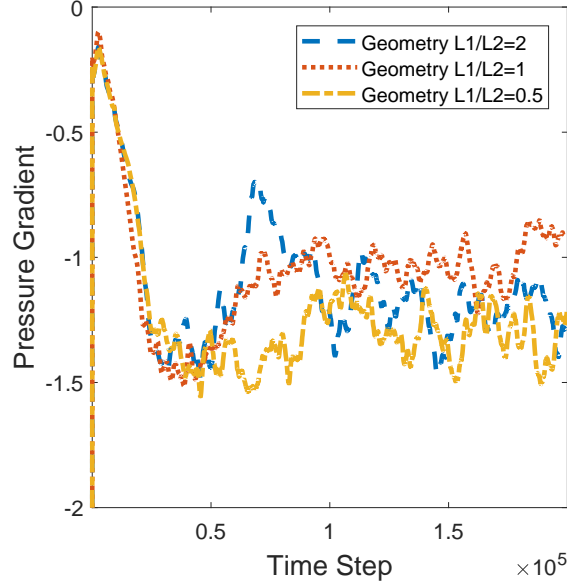
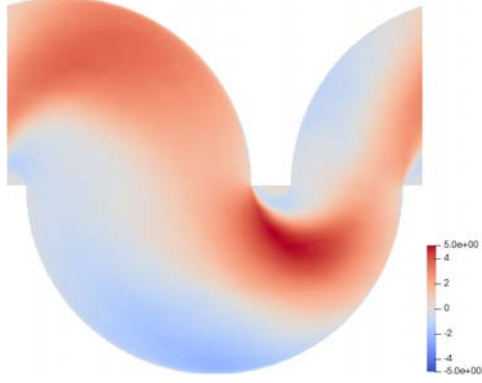


Figure 4.8: Variation related to the time steps, of the mean pressure gradient of the domain. There is an initial transitory phase, after which the gradient stabilizes around a mean value.

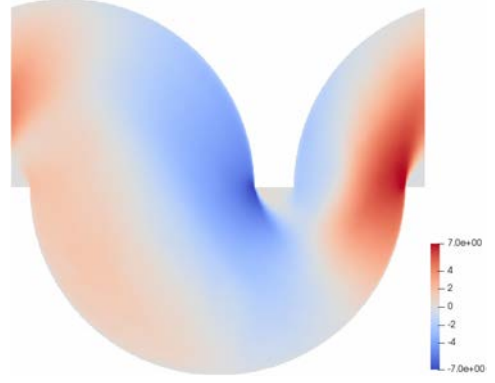
Once the parameters for the particles have been chosen, the positions of the particles in the domain must be assigned. There are two solutions to do this. The first one is randomly, so that the distribution of the particles is as real as possible. However, this may cause that the position of some particles falls over the solid domain. The other solution, that is less real but it doesn't have this problem, is to position the particles in an arbitrary way. The number of particles, that have been inserted in the domain, is 100. They have been distributed over four layers along the y -direction. Each layer is located on the plane x - z , and it is constituted of 25 particles, placed in a 5×5 grid. A minimum distance of 0.5 dimensionless units has been considered between one particle and another and between particle and walls. Now, simulations, with a zero initial velocity of the particles, can be launched.

4.3.2 Fluid phase

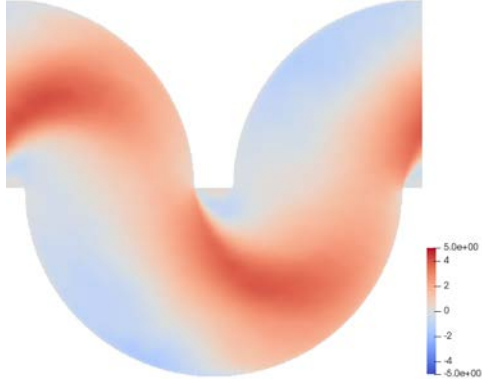
In the previous section, the motion of the single-phase flow was analysed in all its main features. Once that this one is developed, multiphase flow can be simulated, to get data on the behaviour of the particles. Now, the mean velocities for the only fluid phase are shown in figure 4.9. A comparison, between this case and the one in figure 4.4, want to be done.



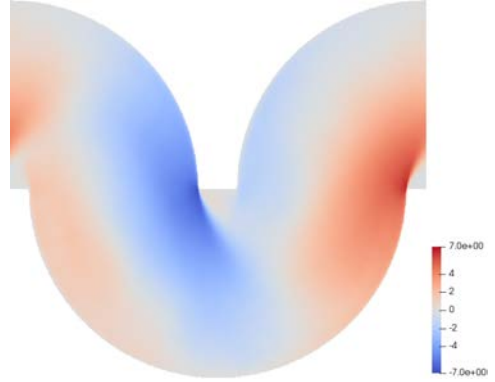
(a) Mean field of the velocity v , for the geometry with $\frac{L_1}{L_2} = 2$.



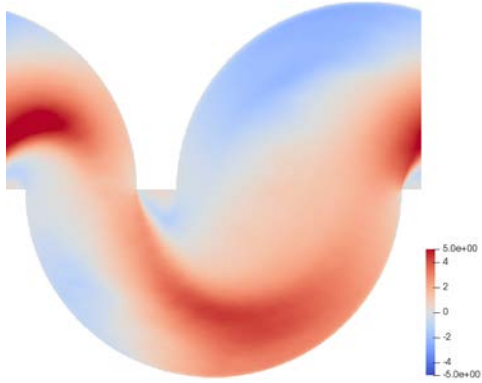
(b) Mean field of the velocity w , for the geometry with $\frac{L_1}{L_2} = 2$.



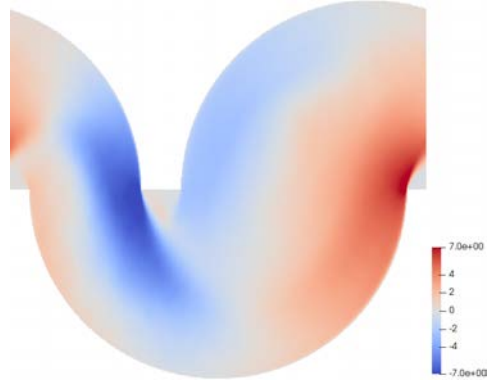
(c) Mean field of the velocity v , for the geometry with $\frac{L_1}{L_2} = 1$.



(d) Mean field of the velocity w , for the geometry with $\frac{L_1}{L_2} = 1$.



(e) Mean field of the velocity v , for the geometry with $\frac{L_1}{L_2} = 0.5$.



(f) Mean field of the velocity w , for the geometry with $\frac{L_1}{L_2} = 0.5$.

Figure 4.9: The mean fields of the velocities v and w , for the fluid phase, are represented for each considered geometry. The velocities have been mediated in time \bar{v} in space, along the x -direction. The scale is dimensionless.

When there is the presence of the particles, the velocities of the instantaneous fields must not be considered in the computation of averages. The average must, therefore, consider the nodes, only when they are covered by the fluid.

Comparing the averages of the velocities v and w , for the single-phase flow and for the multiphase flow, it is noted that the behaviour of the fluid is, practically, the same. Velocities have the same range of values and its distribution over the domain is equal. The only small observation that can be done, is that the velocities profiles are moved slightly to the right. Particles have certain inertia and being a multiphase flow, the two phases are influenced by each other. Therefore, the liquid phase has more difficulty to follow the trend of the geometry, but mainly it is hardly affected by particles, and it continues to flow undisturbed in the duct, as before.

4.3.3 Particles tracking

A comparison between the fluid phase of the single-phase and the multiphase flow has been done. Now, the solid phase has to be analysed in all its aspects, depending on the considered geometry and density. Once the particles are placed in the domain and simulations are launched, they move in the duct and they can assume certain behaviours.

The first aspect to analyse is their motion inside the different chambers of the device. The simulation consists of only one chamber and, as already mentioned, there is a periodicity condition on the y-direction. Particles that come out on one side of the domain, re-enter in the domain from the other. Precisely on this principle, the algorithm to generate the trajectories, shown in figures 4.10, 4.11, and 4.12, is based. The created algorithm, analyses for each particle every point that its centre covers and it plots the path for each one on the relative graph.

When in the y-coordinate of two consecutive points there is a difference greater than $\frac{L_y}{2}$, the algorithm adds or subtracts⁴ the length L_y from the current and the subsequent coordinates. In this way, it is possible to create continuous trajectories for the particles and to see their behaviour from one chamber to another. The three sets of images shown present the trajectories for all one hundred particles in five consecutive chambers. The particles are all initialised in the first chamber that is represented. There are general behaviours that are common to all combinations *geometry/density*. Some particles settle in the different chambers, while other ones continue to flow.

⁴depending on which side the particle has left the domain. If the particles go out on the left, the algorithm will subtract the length L_y of the domain, and vice versa

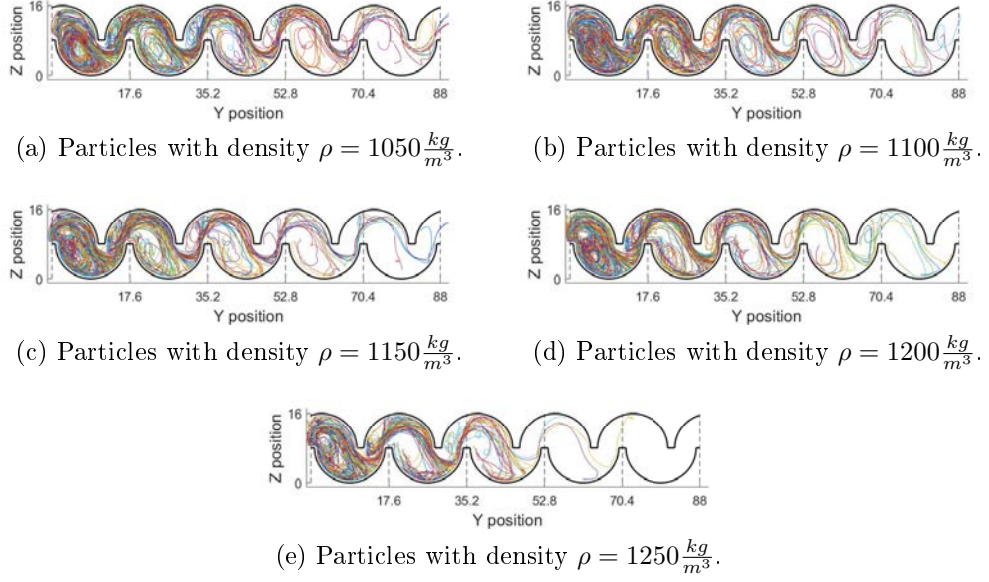


Figure 4.10: Particles trajectories with variable density. The considered geometry has $\frac{L_1}{L_2} = 2$.

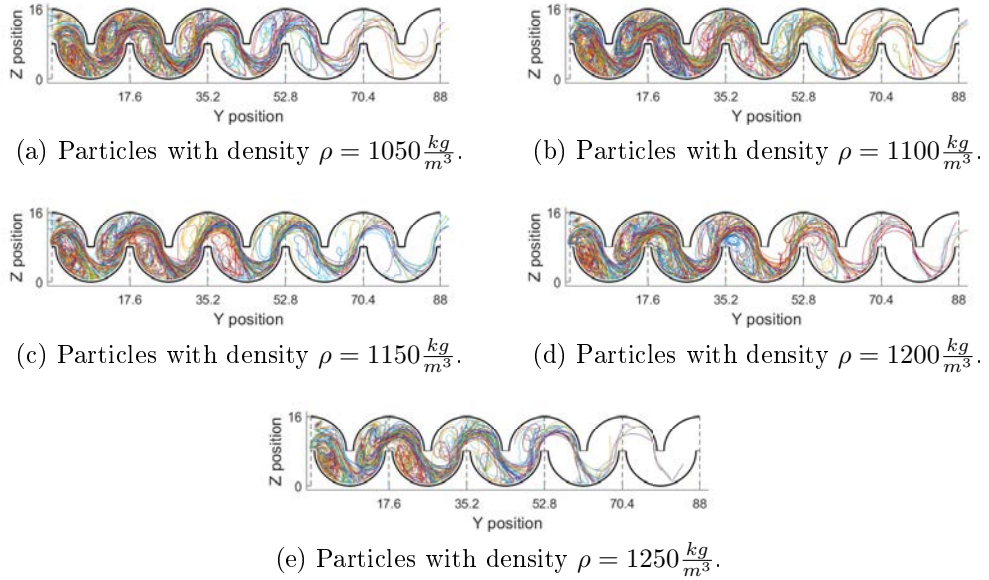


Figure 4.11: Particles trajectories with variable density. The considered geometry has $\frac{L_1}{L_2} = 1$.

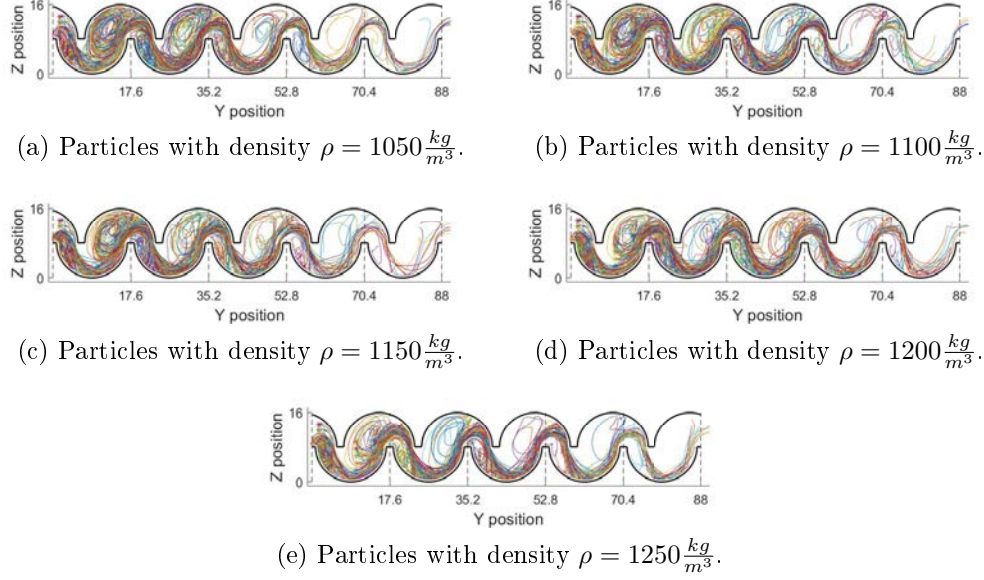


Figure 4.12: Particles trajectories with variable density. The considered geometry has $\frac{L_1}{L_2} = 0.5$.

The sudden changes of direction of the particles, in the domain, are caused by collisions between particle-particle or particle-wall. For each type of geometry, the flow is well defined by the motion of the particles, above all for the geometry in figure 4.12 where most of the particles continue to flow on all five chambers. Other more specific behaviours, instead, depending on the geometry and density considered:

- Geometry with $\frac{L_1}{L_2} = 2$: in the lower-left corner of each chamber, a great recirculation zone is clearly visible. Here, particles go around in circles and most of them get trapped in the first 2-3 chambers. The other ones continue to flow in the next chambers. Some of them end up in the smaller recirculation zone. However, they return almost immediately in the transport current and they are not trapped in this part. This is due to the small dimension of this portion of the fluid and to gravity. When the density changes, it is noted that the greater, the more particles settle in the first chambers.
- Geometry with $\frac{L_1}{L_2} = 1$: when the geometry is symmetrical, the two recirculation zones have the same dimension. Despite the lower one is smaller than the previous case, many particles are settled in the first chambers. Moreover, the behaviour of the particles, as the density changes, is like before. Lighter particles have more chance to continue

in the next chambers, immersed in the transport current. From a qualitative point of view, it seems that this geometry is less efficient to settle particles on the underside. However, in subsection 4.3.5 this affirmation can be discussed, when quantitative results, regarding the settling, will be presented.

- Geometry with $\frac{L_1}{L_2} = 0.5$: in this configuration the particles behaviour is different from before. A great recirculation zone is formed in the upper right corner of each chamber and some particles fall into it. However, most of the particles rest in the main current and they continue to flow from chamber to chamber. In fact, at the end of the last chamber, many particles are yet in the flow. These five trackings show that this geometry is quite inefficient.






In this subsection, it was possible to outline the position and dimension of the recirculation zones for each geometry and how the particles behave inside them. It's clearly visible, if only graphically, that with the decrease of the ratio $\frac{L_1}{L_2}$, less and less particles settle in each chamber.

In the next subsection, the motion of only one particle will be observed, in order to understand the specific behaviour that it assumes.

4.3.4 Tracking of one particle

The motion of all the particles has been shown and analysed. In this part, only one particle will be examined and its density will be changed. This has the purpose to understand the precise motion that the considered particle assumes.

First of all, a consideration has to be made. In the figures of this and the next subsections, each density will always be considered with the same colour. In order to represent all the quantities in a normalized way, the densities are expressed as a ratio between them and the density of the water. The associations *colour/density* are detailed below:

	$\frac{\rho_p}{\rho_l} = 1.05$		$\frac{\rho_p}{\rho_l} = 1.10$		$\frac{\rho_p}{\rho_l} = 1.15$
	$\frac{\rho_p}{\rho_l} = 1.20$		$\frac{\rho_p}{\rho_l} = 1.25$		

where ρ_p is the particle density and ρ_l is the fluid density which is that of water.

One particle at the begin of the first chamber was taken, and it is compared, for the same geometry, to all the other densities.

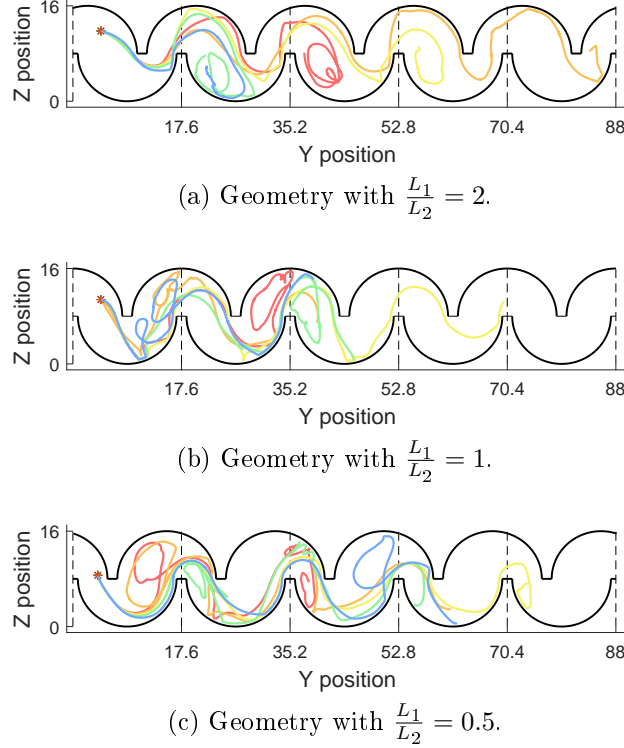


Figure 4.13: For each geometry, the trajectory of only one particle is tracked for all the five density.

Considering a specific geometry, for all the densities, the trajectories of this particle are overlapped on the same graph. The results of these comparisons are shown in figure 4.13. The behaviour of this particle is clear and it is different for each geometry:

- Geometry with $\frac{L_1}{L_2} = 2$: on the upper side the particle is dragged by the flow, following the geometry. Then it is trapped in the lower recirculation zone or it continues in the transport current. Nevertheless, for each density, sooner or later, the particle falls into a lower recirculation zone and it settles there, after one or more rounds. The particle, with the greatest densities, is immediately trapped in the second chamber. Heavier particles travel less space of the particle with lower densities.
- Geometry with $\frac{L_1}{L_2} = 1$: here, the particle rounds in the upper recirculation zone, that is mainly located on the left side of the upper curve. Then the particle falls into the next chamber. The lower recirculation zone does not appear to be involved by the multiphase flow. There isn't a clear distinction in the particle behaviour, varying the density. The

particle with the halfway density travels more than the particle with different density. The lightest particle settles before the other ones.

- Geometry with $\frac{L_1}{L_2} = 0.5$: the lower recirculation zone is located on the left side of the lower part, while the upper one involves all the upper curve. Here, for each density, the particle performs some rounds and then it continues in the next chamber, where it does one or no one round and finally it continues to flow in the transport current. The dependence on density is completely random, but also for this case, the particle that has $\frac{\rho_p}{\rho_l} = 1.15$ travel more than the particle with other density ratios.

In the way just presented, it is easy to highlight the path that a particle follows and its behaviour. Furthermore, further aspects of the change of density or geometry can be shown, with other methodologies.

4.3.5 Particles settling

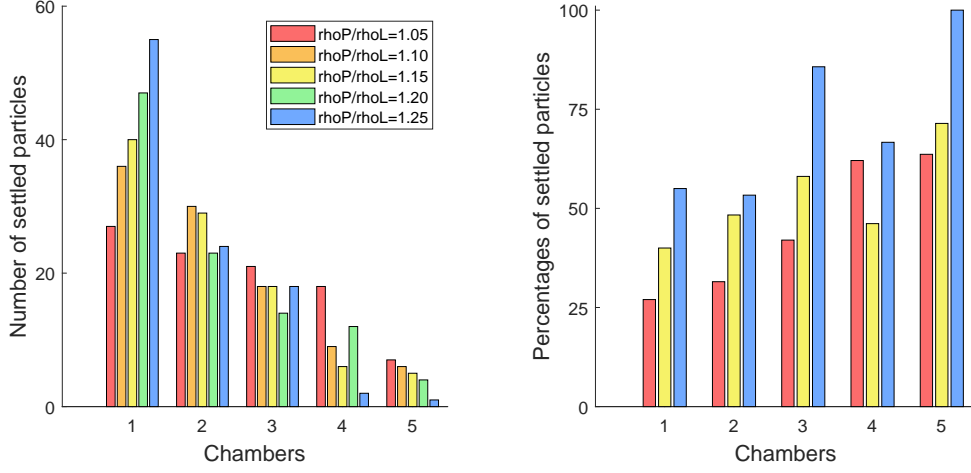
In the previous subsections, the behaviour of the particles from a qualitative point of view has been observed in different ways. Here, the particle settling is examined quantitatively.

In each chamber, a certain number of particles settle. In figures 4.14, 4.15, and 4.16, in histograms with the letter (a), the number of settled particles in each chamber is shown, bearing in mind that the total number of particles, used in simulations, is 100. In the other graphs with the letter (b), the percentage of how many particles settle in the chamber is shown.

This percentage is computed, comparing the settled particles in the chamber to how many particles enter in the related chamber. For this second type of histogram, only three densities are shown: the least, the largest and the middle way. This is made to highlight more clearly the differences in varying density. From the comparison of these values, the effects of geometry and density are clearly visible.

Regarding geometry, the larger the ratio $\frac{L_1}{L_2}$, the higher the efficiency in blocking particles. To parity of density, reducing the ratio, fewer particle settle in the considered chamber,. This is more marked when the density increases. When the ratio is 2, only the particles with density $\rho_p = 1250 \frac{kg}{m^3}$ settle completely in the portion of duct analysed. Some particles of other densities in this or other geometries can get out on the right side. With the lowest ratio $\frac{L_1}{L_2}$, many more particles come out of the serpentine.

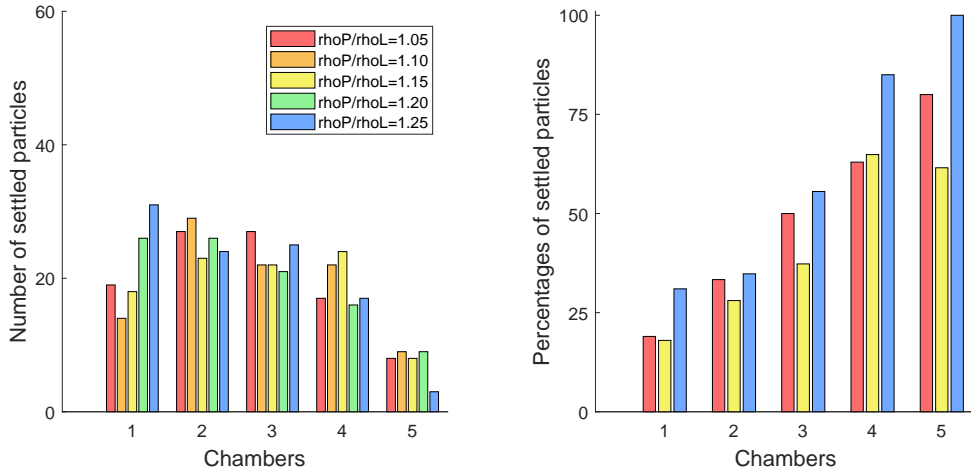
Paying attention to densities, the behaviour is a little more complicated. For the geometry with ratio $\frac{L_1}{L_2} = 2$, increasing the density, a larger number



(a) Numbers of settled particles in each chamber and for each density.

(b) Percentages of how many particles settle, compared to the total. The considered density ratios are: 1.05, 1.15, and 1.25.

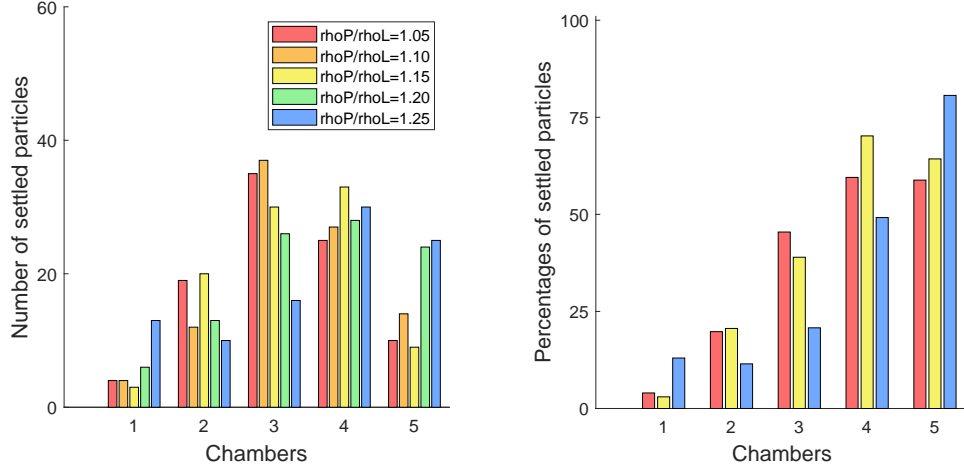
Figure 4.14: Number and percentages of settled particles in the geometry with $\frac{L_1}{L_2} = 2$.



(a) Numbers of settled particles in each chamber and for each density.

(b) Percentages of how many particles settle, compared to the total. The considered density ratios are: 1.05, 1.15, and 1.25.

Figure 4.15: Number and percentages of settled particles in the geometry with $\frac{L_1}{L_2} = 1$.



(a) Numbers of settled particles in each chamber and for each density.

(b) Percentages of how many particles settle, compared to the total. The considered density ratios are: 1.05, 1.15, and 1.25.

Figure 4.16: Number and percentages of settled particles in the geometry with $\frac{L_1}{L_2} = 0.5$.

of particles settle in each chamber. In the symmetrical case, the diversity between the density is attenuated but the behaviour is the same. Finally, when the ratio has a value of 0.5, there is no longer any distinction between densities in the settling. In this way, it is clear that the case with $\frac{L_1}{L_2} = 0.5$ has no effect on the partition of particles.

With this analysis, the interaction between density and geometry has been observed and analysed with the comparison of some data. It seems that for better particle separation, the dimension of the inlet section must be as large as possible than the outlet one. However, other analytical considerations can be made, using statistics.

4.3.6 Statistical comparisons

Analysis of the solid phase of the multiphase flow started with a qualitative comparison of the particles tracking. Then, the percentages of settled particles have been explained with the related histograms. Now, the quantitative analysis continues with other useful statistical parameters by which the comparison on the efficiency of the geometries is immediate.

For the discussion of this subsection, only the velocity v is considered, because it is the velocity of the main direction of the flow.

The *probability density function (PDF)* gives the probability distribution of a random continuous variable, which is the considered velocity. For a specific value, its probability is null. So, intervals of values have to be taken and the probabilities of how many values fall into these ranges are counted. Now, this method is applied to the instantaneous velocities v for all the particles and throughout the simulated time interval. This process can be made for each combination of *geometry-density*. However, the probability distribution is computed only for the least and the largest density. For this probabilistic function $p(x)$, two expressions are important. The first has the purpose to verify that the probability distribution refers to the whole set of values:

$$\int_{-\infty}^{+\infty} p(x) dx = 1 \quad (4.7)$$

The second equation, instead, is useful for obtaining the average value of the velocities distribution:

$$\langle x \rangle = \int_{-\infty}^{+\infty} x \cdot p(x) dx \quad (4.8)$$

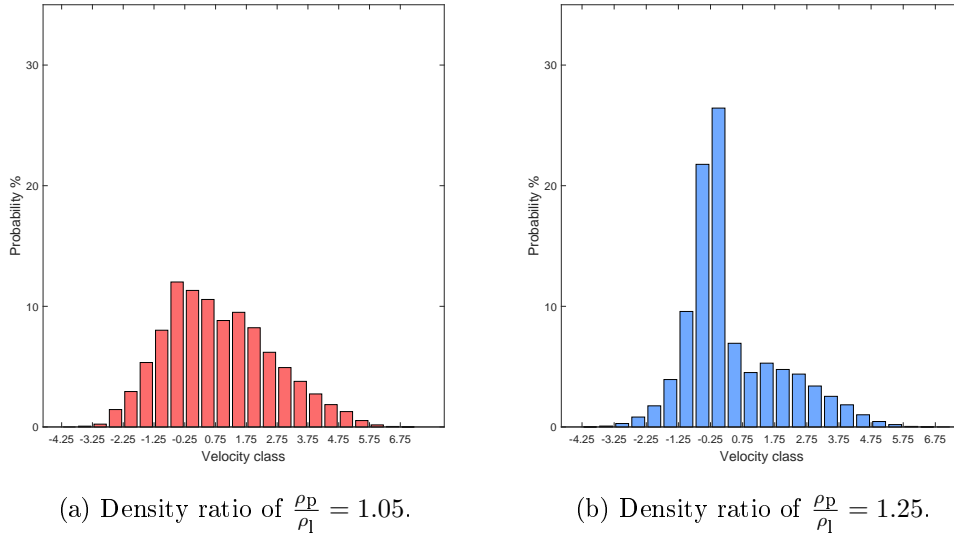


Figure 4.17: The PDF's for the particles velocities are shown with the use of an histogram for the geometry with $\frac{L_1}{L_2} = 2$, for two different geometries.

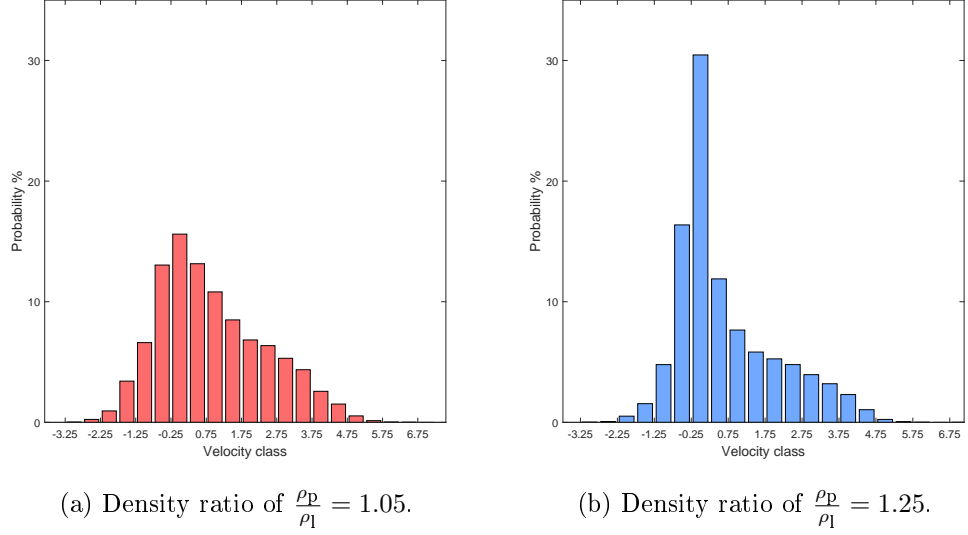


Figure 4.18: The PDF's for the particles velocities are shown with the use of an histogram for the geometry with $\frac{L_1}{L_2} = 1$, for two different geometries.

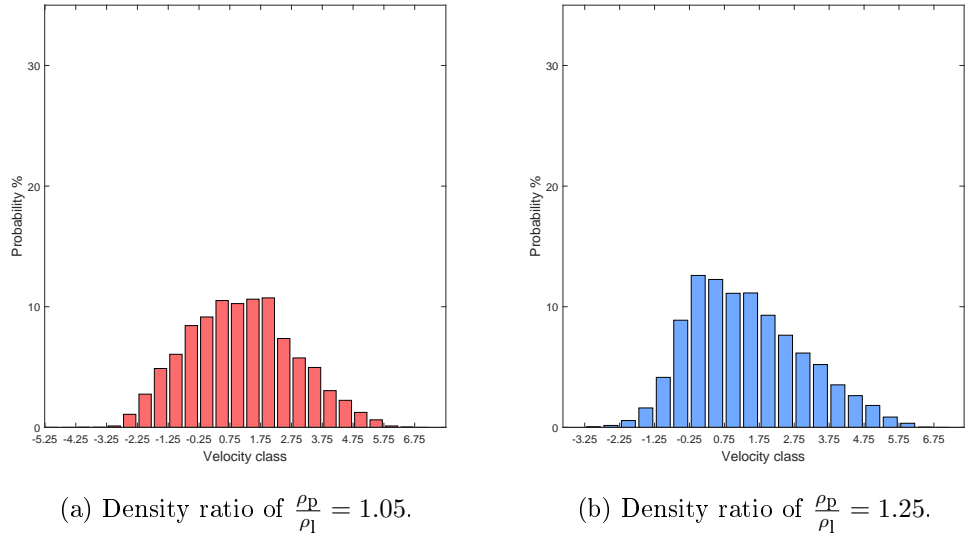
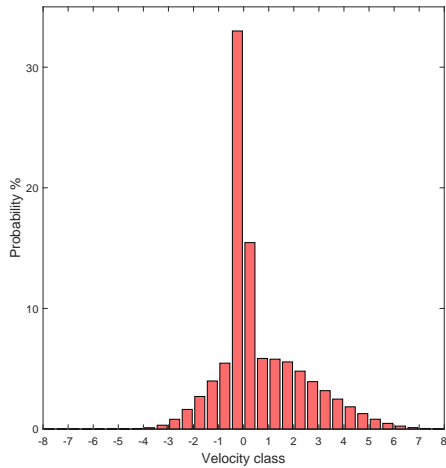


Figure 4.19: The PDF's for the particles velocities are shown with the use of an histogram for the geometry with $\frac{L_1}{L_2} = 0.5$, for two different geometries.

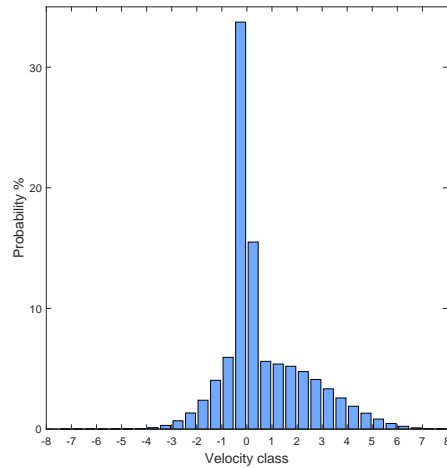
In the entire range of instantaneous velocities v , classes of amplitude of 0.5 are chosen. For each class, how many particles velocities fall into it are counted and the *PDFs* are shown in figures 4.17, 4.18, and 4.19.

This is another way to observe the same behaviours, that have been derived from the previous histograms. To parity of geometry, for the least density, the probability distribution is shifted to greater values than those of the largest density. This means that the average velocity is bigger for lighter particles and fewer of them settle in each chamber. When the density is larger, there is a peak of probability distribution around zero. Heavier particles have more difficulties to flow in the next chambers. This last statement loses its force when the ratio $\frac{L_1}{L_2}$ decreases. In fact, to parity of the density, when this ratio becomes smaller, most of the instantaneous velocities fall into greater classes for both densities. More particles continue to flow in the next chambers. However, as mentioned before, for the smallest ratio, there is no distinction in the settling of particles for different densities. In fact, the distribution tends to be symmetrical, above all for the lightest particles.

In order to make a complete investigation on the pdf's of the flow, in figures 4.20, 4.21, and 4.22, the *PDF'S* for the velocity v of the fluid phase are represented. The criterion with which these graphs are sketched is the same. It is clearly visible that there is almost no distinction in the different combinations of *geometry-density*.



(a) Density ratio of $\frac{\rho_p}{\rho_l} = 1.05$.



(b) Density ratio of $\frac{\rho_p}{\rho_l} = 1.25$.

Figure 4.20: The *PDF's* for the fluid velocities are shown with the use of an histogram for the geometry with $\frac{L_1}{L_2} = 2$, for two different geometries.

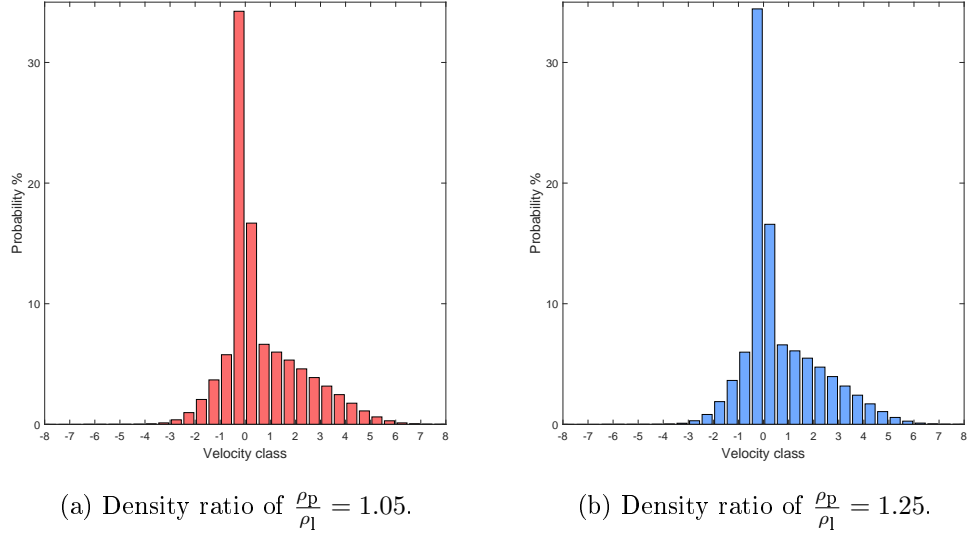


Figure 4.21: The PDF's for the fluid velocities are shown with the use of an histogram for the geometry with $\frac{L_1}{L_2} = 1$, for two different geometries.

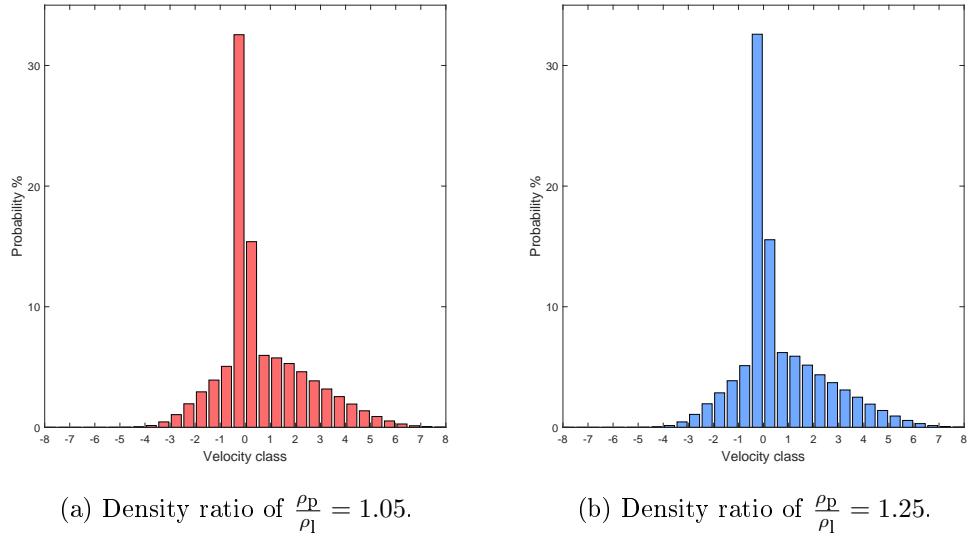


Figure 4.22: The PDF's for the fluid velocities are shown with the use of an histogram for the geometry with $\frac{L_1}{L_2} = 0.5$, for two different geometries.

Therefore, if the particles have a different density, they don't influence the fluid phase, which continues to flow in the same way. To be accurate, when the density is greater, the central peak it's a little higher. This means that the particles slow down slightly the fluid, but in a completely irrelevant way.

With the use of the *PDF*'s, the influence of the geometry on the separation of the particles is further highlighted. These techniques are useful to show these behaviours graphically.

To understand quickly which combination of *geometry-density* is more effective, to each of these combinations an average velocity is attributed. Each mean velocity is obtained by averaging the instantaneous velocities over time and over all the particles. This permits to assign, to each combination, a single scalar value, in order to subdivide which are the most efficient geometries and for which densities. With this method, the classification is shown in table 4.2. The mean velocities, for the geometry with $\frac{L_1}{L_2} = 2$, are the minors and they go down with the increase of the density. This is another way of presenting the same previous results where heavier particles settle more easily. Once again, the particles in the geometry with $\frac{L_1}{L_2} = 1$ behave like just said but in a less marked way. Finally, the particles behaviours in the last geometry are completely random and the values of the average velocities are much higher than the previous ones. This means that the particles flow quickly in the chambers and they don't get trapped.

To see the same aspects from another point of view, these average velocities can be converted into a *stationing time*. It can be expressed in the following way:

$$\tau = \frac{L_y}{\bar{v}} \quad (4.9)$$

where \bar{v} are the previous mean velocities and L_y is the length in the

Table 4.2: For each combination of geometry and density, a single scalar value is computed. It represents the particle mean velocity, obtained with the average over the time and all the particles.

$\frac{\rho_p}{\rho_l}$	$\frac{L_1}{L_2} = 2$	$\frac{L_1}{L_2} = 1$	$\frac{L_1}{L_2} = 0.5$
1.05	0.79	0.91	1.13
1.10	0.56	0.72	1.26
1.15	0.56	0.85	1.16
1.20	0.42	0.55	1.19
1.25	0.37	0.66	1.30

y -direction of a chamber and it assumes the value of 17.6.

If all the particles settle in the chambers, more the simulation time will increase, more the mean velocity will approach zero. In the opposite way, the stationing time will approach infinity.

Table 4.3: Using the average velocities of table 4.2, and knowing the length of a chamber, the stationing times in one chamber can be computed for each combination.

$\frac{\rho_p}{\rho_l}$	$\frac{L_1}{L_2} = 2$	$\frac{L_1}{L_2} = 1$	$\frac{L_1}{L_2} = 0.5$
1.05	22.23	19.34	15.63
1.10	31.22	24.54	13.91
1.15	31.53	20.82	15.14
1.20	41.91	31.87	14.74
1.25	47.67	26.70	13.53

4.3.7 Solid phase

At this point, several aspects of particles have been examined and explained, to outline the behaviour of the multiphase flow. In order to complete this sequence of analysis, now the average velocities v of the particles are represented on a single chamber. These velocities, are averaged over time and the x -direction, like in subsection 4.3.2, but this time only for the solid phase. In this and the previous statistical analyses, only the v -velocities were chosen to represent and to analyse. This is due to the fact, that this one is the direction of the mainstream.

In figures 4.23, for all three geometries, the trend of the v -velocities of the particles is shown. For this representation, only the least and the largest density has been chosen.

Both the transport current and the recirculation zones are easily identifiable in these figures. Along the transport current, particles have a great v -velocity and they follow the path of the main flow, as it has been identified in figures 4.9. In the recirculation zones, the particles v -velocities has the opposite direction, sign that the particles are turning in that zones. Under a qualitative point of view, for each geometry, the colours that identify the intensity of the velocities of the particles, are the same for the two densities. Therefore, these velocities have practically no dependence on density.

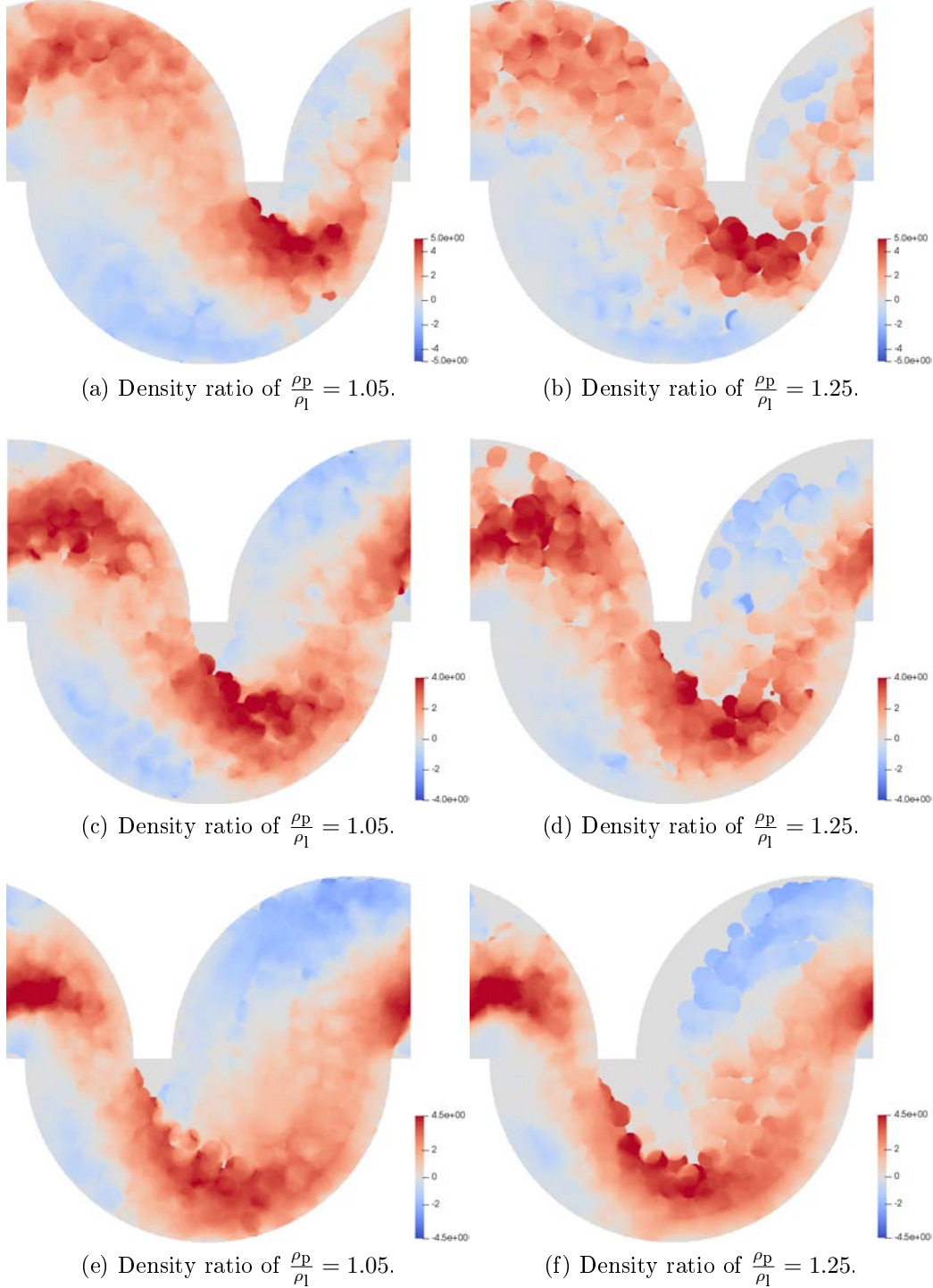


Figure 4.23: Average v -velocities of the solid phase for the three different geometries with $\frac{L_1}{L_2} = 2$ for (a) and (b), $\frac{L_1}{L_2} = 1$ for (c) and (d), and $\frac{L_1}{L_2} = 0.5$ for (e) and (f). Furthermore, the cases with the least and the largest density are shown.

It's clearly visible that the particles are distributed almost uniformly throughout the domain. However, in addition to these two large parts, there is a small zone where the average v -velocity is zero. This means that no one particles flow in this area, during all the simulation. For the least density, this zone is small and it is mainly located around the central edge of each geometry.

For low densities, it can be said that particles cover all the fluid domain. When the density assumes bigger values, the empty zone becomes larger. This behaviour may be associated with the greater particle weight and, therefore, the particles, in the second half of the chamber, are in lower positions. This trend depends also on geometry.

In fact, for the first two geometries, the empty zone is similar for both the densities, while for the last geometry, this zone also partially involves the first part of the upper curve. For this last configuration, the right half of the domain is larger, so the velocity of the flow is lower. In this way, the weight has a greater influence and the particles flow upward subsequently.

With these representations, the motion of the particles is well visible for all the three configurations. With this and the previous subsections, the behaviour of the particles was defined in all possible aspects. With these analyses, a classification of the geometries and the densities, based on the efficiency in plastic separation, was done. In this way, it was possible to define how the density influences the separation and which geometry has greater effectiveness.

4.4 Summary

In this chapter, the analytical phase of this work has been shown in all the examined aspects.

In the first part, the implementation of the numerical model has been explained. The aspects, that were faced, are the used geometries, the periodicity conditions, the size of the domain and which parameters are been chosen to be changed in the several simulations. Then, a single-phase flow has been analysed with attention to the average quantities as the velocities and the Reynolds stresses. Finally, the last part, with the study of the multi-phase flow, has been explained. Initially, the fluid phase has been compared to the single-phase flow. Then, with different approaches the behaviour of the particles in the different combinations of *geometry-density* was examined.

Chapter 5

Conclusions

This thesis project aims to improve a device for sorting plastic particles with different properties. Starting from a working physical device, the project was to model the real phenomenon with an existent code that uses a Direct Numerical Simulation resolving the particle interfaces. The efficiency and reliability of this code have been verified in several studies performed in the previous years. This model has been adapted to the geometry of the problem considered here, and some convergence parameters were adjusted.

Several geometrical and physical parameters of the device and of the plastics can be varied to optimize the sorting process. However, since the computational cost of a DNS is very high, it was possible to examine only some of these. The analyses focused on two main aspects: the effect of geometry and of the particle density. The shape of the particles was assumed spherical. The results of these cases gave a clear idea of the multiphase flow behaviours in the serpentine.

Whatever the geometry, two recirculation zones are formed in a chamber, and each one with the same direction of rotation. Changing the serpentine geometry with a longer down-flow chamber (higher L1) provides the best trapping performance.

If it is reduced, more and more particles continue to flow. These aspects are related to the form of the down-flow recirculation. It could be interesting for the future to enlarge even more this chamber. Regarding the density of the particles: Heavier they are, higher they settle. However, for less efficient geometries as the symmetric one this distinction is less marked, and the particles tend to continue to flow into the serpentine. This behaviour has been deeply discussed and analysed in this thesis using different tools and methods. Therefore, the density difference, even if of few percents, can be used to sort the different kind of plastics. Polymers with greater density are separated by lighter plastics that continue to flow until the end of the

conduct. More numerical simulations could be performed to optimize this geometry even changing the shape of the particles.

To conclude, this study demonstrated how important is DNS even for industrial applications since it allows to understand in details the aspects that control the process. Further insights on the studied phenomenon can make the device more efficient in order to achieve its industrial use helping the environment and life conditions.

Bibliography

- Anderson, John D. Jr. (2009). *Fundamental of Aerodynamics*. Fifth. McGraw-Hill.
- Ardekani, Mehdi Niazi (Jan. 2019). «Numerical transport phenomena in particle suspensions». Doctoral thesis in engineering mechanics. Stockholm, Sweden: KTH Royal Institute of Technology.
- Astrup, T., T. Fruergaard, and TH Christensen (2009). «Recycling of plastic: accounting of greenhouse gases and global warming contributions». In: *Waste Management & Research*.
- Breugem, W.-P. (2012). «A second-order accurate immersed boundary method for fully resolved simulations of particle-laden flows». In: *Journal of Computational Physics*.
- Breugem, W.-P., V. Van Dijk, and R. Delfos (2014). «Flows through real porous media: x-ray computed tomography, experiments, and numerical simulations». In: *Journal of Fluids Engineering*.
- Crowe, Clayton T. et al. (2012). *Multiphase flows with droplets and particles*. Second edition. CRC Press.
- Fadlun, E. A. et al. (2000). «Combined immersed-boundary finite difference methods for three-dimensional complex flow simulations». In: *Journal of Computational Physics*.
- Gore, R. A. and C. T. Crowe (1989). «The effect of particle size on modulating turbulent intensity». In: *International Journal of Multiphase Flow*.
- Hetsroni, G (1989). «Particles-turbulence interaction». In: *International Journal of Multiphase Flow*.
- Hetsroni, G. and M. Sokolov (1971). «Distribution of mass, velocity and intensity of turbulence in a two-phase turbulent jet». In: *Journal of applied Mechanics*.
- Inculet, I. I., G.s.P. Castle, and J. D. Brown (1998). «Electrostatic separation of plastics for recycling». In: *Particulate Science and Technology*.
- Kajishima, T. et al. (2001). «Turbulence structure of particle-laden flow in a vertical plane channel due to vortex shedding». In: *JSME International Journal Series B Fluids and Thermal Engineering*.

- Kempe, T. and J. Fröhlich (2012). «An improved immersed boundary method with direct forcing for the simulation of particle-laden flows». In: *Journal of Computational Physics*.
- Kolmogorov, A. (1941). *The local structure of turbulence in incompressible viscous fluid for very large Reynolds number*.
- Krähling, H. and I. Sartorius (2012). «Sustainable management of material and energy resources». In: *Materials Science and Materials Engineering*.
- Kundu, Pijush K. (2016). *Fluid Mechanics*. Academic Press.
- La Marca, F. et al. (2012). «Separation of plastic waste via the hydraulic separator Multidune under different geometric configuration». In: *Waste Management*.
- Lomholt, S. and M. Maxey (2003). «Force-coupling method for particulate two-phase flow: Stokes flow». In: *Journal of Computational Physics*.
- Lu, Hao (2007). *One-equation LES modeling of rotating turbulence*. Doctor of Philosophy (Mechanical Engineering. Madison, Wisconsin.
- Luo, K. et al. (2007). «Full-scale solutions to particle-laden flows: Multidirect forcing and immersed boundary method». In: *Physical Review E*.
- Mac Arthur, Dame Ellen, Dominic Waughray, and Martin R. Stuchtey (2016). *The New Plastic Economy: Rethinking the future of plastic*. URL: http://www3.weforum.org/docs/WEF_The_New_Plastics_Economy.pdf.
- Marques, Gisela Ablas and Jorge Alberto Soares Tenorio (2000). «Use of froth flotation to separate PVC/PET mixtures». In: *Waste Management*.
- Mittal, R. and G. Iaccarino (2005). «Immersed boundary method». In: *Annual Review of Fluid Mechanics*.
- Moroni, M., F. La Marca, et al. (2013). «Recovering plastics via the hydraulic separator Multidune: flow analysis and efficiency tests». In: *International Journal of Environmental Research*.
- Moroni, M., E. Lupo, and F. La Marca (May 2017). «Hydraulic separation of plastic wastes: Analysis of liquid-solid interaction». In: *Waste Management*.
- Peskin, Charles S. (Oct. 1972). «Flow patterns around heart valves: A numerical method». In: *Journal of Computational Physics*.
- Picano, Francesco, Wim-Paul Breugem, and Luca Brandt (Oct. 2015). «Turbulent channel flow of dense suspensions of neutrally-buoyant spheres». In: *Journal of Fluid Mechanics*.
- Richardson, Lewis F. (1922). *Weather prediction by numerical process*. Cambridge University Press.
- Sierakowski, A. and A. Prosperetti (2016). «Resolved-particle simulation by the physalis method: enhancements and new capabilities». In: *Journal of Computational Physics*.

- Unverdi, S. and G. Tryggvason (1992). «A front-tracking method for viscous, incompressible, multi-fluid flows». In: *Journal of Computational Physics*.
- Varaskin, A. Y. et al. (1998). «Experimental study of the direct influence of small particles on carrier air turbulence intensity for pipe flow». In: *3rd International Conference of Multiphase Flow*.